

Physics with neutrons

Michael Leitner

A	The neutron	1
A.1	On the neutron itself	1
A.1.1	History	1
A.1.2	Properties of the neutron	2
A.1.3	The neutron in nuclear physics	3
A.1.4	Quantitative properties of the neutron	4
A.1.5	Rules of thumb	5
A.2	The neutron's interaction with matter	6
A.2.1	Kinds of interaction	6
A.2.2	Concepts of neutron scattering	7
A.2.3	Absorption, activation and transmutation	9
A.2.4	Knock-on effects	12
B	Instrumentation and techniques	15
B.1	Neutron instrumentation	15
B.1.1	Neutron sources	15
B.1.1.1	Nuclear chain reactions in reactors	15
B.1.1.2	Spallation sources	18
B.1.2	Neutron moderation	18
B.1.2.1	Statistical distributions	19
B.1.2.2	Figures of merit	20
B.1.3	Components of neutron instruments	21
B.1.3.1	Neutron mirrors and guides	21
B.1.3.2	Crystal monochromators and analyzers	23
B.1.3.3	Mechanical velocity selectors and choppers	25
B.1.3.4	Collimators	26
B.1.3.5	Energy filters	27
B.1.3.6	Polarizers	28

B.1.3.7	Spin guiding and manipulation	29
B.1.3.8	Shielding	30
B.1.4	Neutron detectors	31
B.2	Neutron-based experimental techniques	33
B.2.1	Powder diffractometry	34
B.2.2	Single-crystal diffractometry	35
B.2.3	Small-angle scattering	37
B.2.4	Reflectometry	37
B.2.5	Triple-axis spectrometry	38
B.2.6	Time-of-flight spectrometry	39
B.2.7	Backscattering spectrometry	40
B.2.8	Spin-echo spectrometry	41
B.2.9	Incoherent spectrometry	42
B.2.10	Neutron radiography	43
B.2.11	Activation analysis	43
C	Theoretical descriptions of scattering	45
C.1	Theories of weak elastic scattering	45
C.1.1	Huygens-Young-Fresnel theory	45
C.1.2	A fixed point scatterer in an incident plane wave	46
C.1.3	Extended scatterers and the Born approximation	47
C.1.4	Kinematical diffraction from perfect crystals	48
C.1.5	Scattering with uncorrelated scattering length randomness	50
C.1.6	Scattering and pair correlations	51
C.2	Beyond kinematical scattering	52
C.2.1	Propagation through matter	53
C.2.2	Refraction	55
C.2.3	Reflectivity of a slab	57
C.2.4	Reflectivity of a multilayer structure	58
C.2.5	Dynamical diffraction from single crystals	59
C.3	Quantum-mechanical treatment of scattering	63
C.3.1	Basic expression for the differential cross section	63
C.3.2	The neutron spin during scattering	67

C.4	The van Hove formalism	69
C.4.1	Correlation functions	69
C.4.2	Properties of the correlation functions	71
C.4.3	Classical interpretation of the correlation functions	72
C.5	Fundamentals of magnetic scattering	74
C.5.1	The neutron-electron interaction	75
C.5.2	The partial differential scattering cross section due to electrons	76
C.5.3	The general double differential cross section	77
C.5.4	Spin-only scattering and the magnetic form factor	78
C.5.5	The magnetic case of van Hove theory	80
C.5.6	The fluctuation-dissipation theorem for magnetism	81
D	Applications	83
D.1	Diffraction	83
D.1.1	Single-crystal diffraction	83
D.1.2	Diffraction on polycrystals	85
D.1.3	Powder diffraction	87
D.1.4	Diffuse scattering	89
D.1.5	Small-angle scattering	91
D.1.6	Diffraction on magnetic structures	94
D.2	Quasi-elastic scattering	96
D.3	Inelastic scattering	98
D.3.1	Vibrational dynamics in crystals	98
D.3.2	Collective magnetic dynamics	102

Preamble

The ways in which physics as a scientific discipline has occupied itself with neutrons can be classified in three fields:

- the physics of the neutron itself — the properties of the particle
- the physics of the interaction of neutrons with matter and
- doing physics by employing neutrons as a tool.

The order of these points indicates roughly their temporal sequence. Indeed, at the present stage the first two problems are solved to a sufficient level to allow to tackle questions of (typically) condensed matter physics by doing neutron experiments, which constitute a large and active field. This sets the point of view of the present lecture: To show what can be learned by letting neutrons in more or less well-defined states interact with samples and observing the changes either in the outgoing neutrons or in the sample, and to explain how to do that. Of course, in order to accomplish this task, the physics of the neutron and of its interaction with matter are a prerequisite.

The presentation in this lecture will deviate from the sequential development that is often followed in textbooks of neutron scattering, which consists in starting with the quantum-mechanical treatment of the scattering process and applying it to specific processes in the samples. Instead, here we will start with the properties of the neutron, phenomenologically discuss its interaction with matter, and then present the range of neutron techniques. Only after that the rigorous formalism for the scattering process will be given and the quantitative description of the various effects will be discussed. The intention is that, given that this is a course over two terms, already after the first term the students should be able to understand the basics of the relevant neutron techniques and to decide whether a given question can be answered by performing a specific neutron experiment, which is the main competence from the users' perspective.

Literature

- Emphasis on neutron properties and interactions:
 - J. Byrne: *Neutrons, Nuclei and Matter. An Exploration of the Physics of Slow Neutrons*, Institute of Physics Publishing, Bristol/Philadelphia (1994).
- Emphasis on neutron scattering theory:
 - G. L. Squires: *Introduction to the Theory of Thermal Neutron Scattering*, Cambridge University Press, Cambridge (1978), also Dover Publications, New York (1996).
 - S. W. Lovesey, *Theory of Neutron Scattering from Condensed Matter I, II*, Oxford University Press, Oxford (1984).

- Emphasis on neutron scattering experiments:
 - B. T. M. Willis, C. J. Carlile: *Experimental Neutron Scattering*, Oxford University Press, Oxford (2009).
 - A. Furrer, J. Mesot, T. Strässle: *Neutron Scattering in Condensed Matter Physics*, World Scientific, Singapore (2009).
 - A. Furrer: *Frontiers in Neutron Scattering*, World Scientific, London (1999).
 - G. Shirane, S. M. Shapiro, J. M. Tranquada: *Neutron Scattering with a Triple-Axis Spectrometer*, Cambridge University Press, Cambridge (2004).
- Swiss army knife of neutron knowledge:
 - A.-J. Dianoux, G. Lander (eds.): *Neutron Data Booklet*, Old City Publishing, Philadelphia (2003). Freely available at www.ill.eu/quick-links/publications.
- Internet resources:
 - J. K. Cockcroft, P. Barnes, et al.: *Powder Diffraction on the Web*. A very detailed tutorial on powder diffraction (touching also related aspects) available at <http://pd.chem.ucl.ac.uk/pd/welcome.htm>.

Chapter A

The neutron

A.1 On the neutron itself

In nature at ambient conditions, the neutron is exclusively located in atomic nuclei. How it was discovered and the properties it was found to have will be detailed here.

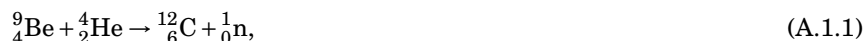
A.1.1 History

The approximately linear relation between the charges and masses of most nuclei suggested the nuclei of different elements to be made up of different amounts of the same building blocks. However, compared to the hydrogen nucleus, which was known to possess the unit of electric charge, heavier nuclei have mass/charge ratios that are higher by about a factor of two. This led Ernest Rutherford in 1920 to propose a neutral nuclear particle to be responsible for this added mass in the heavier nuclei. He imagined this to be not a new fundamental particle but rather a bound proton-electron pair, thereby explaining the electron being emitted from the nucleus during beta decay.

In 1930, Walther Bothe and Herbert Becker found that when beryllium was subjected to alpha radiation (emitted from polonium), a very penetrating radiation resulted. As it was not deflected by an electric field, they assumed it to be gamma radiation. In 1932, Irène Joliot-Curie and Frédéric Joliot found this radiation to be able to eject high-energy protons from paraffin, which they explained by a proton-Compton effect.

Upon learning of this phenomenon, James Chadwick quickly recognized that the Klein-Nishina formula, which, being derived from quantum electrodynamics, was able to quantitatively describe the electron-Compton effect, predicted much less scattered protons than observed, and those at much lower energy. Having himself previously tried unsuccessfully to detect Rutherford's neutron, he realized that it was a candidate for the observed penetrating radiation. Within just 10 days

of experimentation, he reproduced the Joliot-Curie observation and was able to observe also kick-out events from light elements other than hydrogen. Measuring the transferred energy and assuming elastic collisions, he could explain his results by a mass of the neutral particle of about $m_n = 1.15$ u, with an estimated error of 10%. In today's notation, he proposed the nuclear reaction



with ${}^1_0\text{n}$ the neutron.

Later, he repeated the experiment with the reaction



which had the advantage that for all nuclei high-precision mass-spectrography masses were known, giving a value of

$$m_n = 1.0067 \pm 0.0012 \text{ u}. \quad (\text{A.1.3})$$

This conclusion that the neutron mass is in first order equal to the proton mass, but actually slightly larger, is valid to this day. For his demonstration of the existence of the neutron Chadwick received the 1935 Nobel Prize.

The question of whether the neutron was a new fundamental particle or a closely bound proton-electron pair was not yet settled. Obviously, the latter option required a restriction of the validity of quantum mechanics, as normally a bound proton-electron pair would give an ordinary hydrogen atom. Along with other paradoxes of the proton-electron model, this had to be weighted against the added complexity of theories assuming a new elementary particle, which sprang up after the demonstration of the neutron's existence.

Chadwick proposed to settle the question by determining the neutron mass to even higher accuracy: if it was definitely heavier than the combined mass of proton and electron, it had to be an elementary particle, as a hypothetical binding energy would lead to a relativistic mass deficiency. In 1935, by photodisintegrating deuterium with 2.6 MeV quanta and determining the kinetic energies of the reaction products in



he obtained a value of m_n either 1.0084 or 1.0090 u, depending on the used values for proton and deuteron, compared to $m_p + m_e = 1.0078$ u. This demonstrated that the neutron was not a closely-bound proton-electron pair, and at the time it was considered as an elementary particle. At the same time this measurement showed that as a free particle the neutron is unstable against beta decay, as predicted by Enrico Fermi in 1934.

A.1.2 Properties of the neutron

The neutron is a baryon, which means that it is made up of three quarks. Today it is known that it is not an elementary particle, but composed of one up and two

down quarks, giving it a charge of exactly zero according to the current theoretical description. Experimentally, the electrical charge's absolute value is bounded by $10^{-21}e$. The neutron radius is on the order of femtometers. The neutron acts as a fermion with spin $\frac{1}{2}$.

As mentioned above, a free neutron is unstable against beta decay. It will decay with a mean lifetime of 881.5 ± 1.5 s into a proton, an electron, and an electron anti-neutrino (in rare cases also a gamma quantum can be emitted). This decay mode is also active in neutron-heavy radioactive isotopes, with lifetimes that depend on the energetics of parent and daughter nuclei and that can be both much longer or shorter than the free-neutron value, while the neutron is stable in stable or neutron-lean isotopes. On the other hand, neutrons can result from inverse beta decay, where one proton in a proton-heavy nucleus decays into a neutron, a positron, and an electron neutrino, or from electron capture, where instead of a positron being emitted an electron is captured.

Because of its internal structure of charged quarks, the neutron has a magnetic moment. This moment has a negative value, which means that the dipole moment is oriented anti-parallel to the neutron spin. Due to the (small) violation of CP symmetry in the weak interaction, the neutron is expected to have a small electric dipole moment. Experimentally, no such finite dipole moment has yet been found, and the Standard Model would predict a value about 5 orders of magnitude smaller than the present experimental limits. However, the zoo of theories beyond the Standard Model has differing predictions on the neutron electric dipole moment, so a further reduction of its bounds would rule out some of those, while the demonstration of a finite value would be a strong argument in favour of specific kinds of theories. Together with the question of the free neutron lifetime, which is a critical parameter in post-Big Bang nucleosynthesis, this is therefore an active venue of experimental research at different institutes.

A.1.3 The neutron in nuclear physics

The neutron is vital for the existence of atomic nuclei heavier than hydrogen. Specifically, nucleons interact via the nuclear force, which can be seen as a short-range leaking-out of the strong force acting between the quarks within the nucleons. Due to the internal structure of nucleons, there is no fundamental, exact description of this interaction. Phenomenologically, however, it can be described as a predominantly pair interaction, which is attractive at distances around 1 fm. In this regime, it is much stronger than the Coulomb repulsion, but it decays faster with distance than a power law. The interaction does not depend on the kind of the nucleon, be it between two neutrons, two protons, or a proton and a neutron. However, it depends on the relative spins of the nucleons, where the attraction is stronger if the spins are parallel. This leads to the fact that the quantum-mechanical system of two neutrons does not have a bound state, as due to the Pauli principle their spins are anti-parallel for the ground-state symmetrical spatial wave-function. For a di-proton, the same applies, with the added repulsion due to the Coulomb interaction. However, a deuteron can have a spin 1 configuration, leading to a bound state.

For heavier nuclei, the role of the neutrons is analogous, in that their being different particles than the protons allows for more parallel spin configurations over close distances and therefore higher attractions due to the nuclear force. The Coulomb repulsion among the protons is only of secondary importance, which explains that the properties of light mirror nuclei (i.e. those that are related by exchanging all neutrons for protons and vice versa) correspond to each other to a large degree. Specifically, this implies that for light nuclei the stable configurations have approximately equal numbers of protons and neutrons. However, for larger nuclei it becomes on average more favourable to add a neutron than a proton to a stable nucleus, as the former doesn't add to the electrostatic energy, which increases faster than linearly with Z , leading to higher neutron per proton-ratios, with the heaviest primordial nuclide ${}^{238}_{92}\text{U}$ having 146 neutrons to its 92 protons. This excess electrostatic energy makes heavy nuclei unstable with respect to splitting up. In such instances, the daughter nuclei would have a surplus of neutrons. Some of those are released immediately with energies in the MeV range (called prompt neutrons), while the rest is converted by beta decay to protons (the liberated energy of which can also lead to additional neutrons being emitted, called delayed neutrons).

Apart from large-scale facilities, which will be discussed later, there are a number of techniques that can provide neutron beams of low fluxes with comparably low effort. Historically, the first of those is to use the (α, n) -reaction as discovered by Bothe and Becker and discussed above. Nowadays, this is optimally done by sealing powder mixtures of compounds containing an α emitter such as Po and specific light elements such as Be (having a large (α, n) cross section) in a low- Z matrix. Further, a (γ, n) -reaction can be employed in analogous devices. Finally, there is spontaneous fission (with associated neutron emission) of transuranic elements, with ${}^{252}\text{Cf}$ the most commonly used isotope.

A.1.4 Quantitative properties of the neutron

The mass of the neutron is

$$m_n = 1.674927471(21) \times 10^{-27} \text{ kg} = 1.00866491588(49) \text{ u} \quad (\text{A.1.5})$$

$$= 939.5654133(58) \text{ MeV}/c^2. \quad (\text{A.1.6})$$

In terms of the proton mass, it is

$$m_n = 1.00137841898(51) m_p, \quad (\text{A.1.7})$$

that is, it is heavier by about 0.13 %.

The other fundamental quantity relevant for neutron scattering is the magnetic dipole moment, it is given by

$$\mu_n = -0.96623650(23) \times 10^{-26} \text{ J/T} = -1.91304273(45) \mu_N, \quad (\text{A.1.8})$$

where the nuclear magneton

$$\mu_N = \frac{e\hbar}{2m_p}. \quad (\text{A.1.9})$$

In analogy to the Bohr magneton, which corresponds to the classical value of magnetic moment that is induced by the current of an electron on a circular path corresponding to an angular moment of \hbar , it sets the order of magnitude of a nucleon's magnetic moment in a classical view of the quark dynamics.

As discussed above, the neutron is expected to have a small electric dipole moment, but experimentally no significant finite value has been determined yet. Experiments constrain it to below $2.9 \times 10^{-13} e \cdot \text{fm}$, which, given the fact that its radius is on the order of fm and the charge of its constituting quarks on the order of e , shows that the centers of mass of its charge positive and negative charge distributions have to be extremely close.

A.1.5 Rules of thumb

For quick calculations in scattering and condensed matter physics, a few rules of thumb are collected here. Here only a few digits of accuracy will be reported.

Boltzmann's constant is

$$k_B = 8.617 \times 10^{-5} \text{ eV/K}, \quad (\text{A.1.10})$$

therefore room temperature of $T_R = 300 \text{ K}$ corresponds to

$$k_B T_R \approx 25 \text{ meV}. \quad (\text{A.1.11})$$

For photons in vacuum, we have $E = h\nu$ and $c = \lambda\nu$, therefore

$$\lambda \approx \frac{1240 \text{ eV nm}}{E}. \quad (\text{A.1.12})$$

For neutrons, we have $p = m_n v$, $p = h/\lambda$ and $E = \frac{m_n v^2}{2}$, therefore

$$\lambda = \frac{h}{m_n v} \approx \frac{4000 \text{ \AA m/s}}{v} \approx \frac{9 \text{ \AA}}{\sqrt{E/\text{meV}}}. \quad (\text{A.1.13})$$

Neutrons with 25 meV, corresponding to room temperature, have therefore velocities $v \approx 2200 \text{ m/s}$ and wavelengths $\lambda \approx 1.8 \text{ \AA}$.

The Bohr magneton

$$\mu_B \approx 0.058 \text{ meV/T}, \quad (\text{A.1.14})$$

therefore fields on the order of 15 T (corresponding to the high end of what can be applied as external field in the laboratory) give a Zeeman splitting on the order of 1 meV due to the spin of free electrons, so that at about 10 K paramagnetic spins become appreciably polarized in such fields. Conversely, the nuclear magneton of

$$\mu_N \approx 3.2 \times 10^{-5} \text{ meV/T} \quad (\text{A.1.15})$$

shows that nuclear spins will only become polarized in the millikelvin regime.

A.2 The neutron's interaction with matter

This section deals with the basic aspects of the interaction between free neutrons and matter. It introduces the concepts that allow to discuss the different experimental techniques phenomenologically, while the quantum-mechanical description of the scattering process will be given later.

A.2.1 Kinds of interaction

A free neutron interacts with matter principally in two ways:¹ First, it interacts with the sample's nuclei via the nuclear force as discussed above. For a given nucleus, the potential felt by the neutron corresponds to the difference in energy of the original, unmodified nucleus compared to the compound nucleus. For neutrons of not too high energy, the neutron wavelength is much larger than nuclear dimensions. Therefore, for practical purposes the nuclear potential can be assumed to be confined to a point, which is called the Fermi pseudo-potential

$$V_F(\mathbf{r}) = \frac{2\pi\hbar^2}{m_n} b\delta(\mathbf{r}). \quad (\text{A.2.1})$$

Here $\delta(\mathbf{r})$ is Dirac's delta distribution, and b is the scattering length, the significance of which will be treated in more detail below. As was discussed above, the interaction due to the nuclear forces depends on the relative spins of nucleus and neutron, therefore for all nuclei with non-zero spin there are scattering lengths b_+ and b_- , corresponding to parallel and antiparallel spin configurations, respectively. Note that the purpose of the Fermi pseudo-potential is only to correctly describe the scattering due to a nucleus placed in a neutron beam. It does not aim to correctly describe the situation at the position of the nucleus, specifically a positive scattering length corresponding to a repulsive Fermi pseudo-potential does not imply that the neutron does not have a bound state with the nucleus, with b_+ of ^1H being such a counterexample.

Apart from the interaction with the nuclei via the nuclear force, a neutron also interacts with a sample's magnetic fields due to its magnetic dipole moment. Specifically, in a local field $\vec{B}(\mathbf{r})$ the neutron experiences a potential

$$V_{\text{mag}}(\mathbf{r}) = -\vec{\mu}_n \vec{B}(\mathbf{r}), \quad (\text{A.2.2})$$

which again depends on the neutron spin.² However, in contrast to the random orientations of the nuclear spins, in a magnetic sample the electronic system causes systematic local variations of the field, which can be observed in the scattering.

Different from most other probe particles, the neutron is neutral, therefore there is no electric interaction with the sample. Due to the comparably large mass and

¹Strictly speaking, there is also gravitational interaction, but due to its vanishing importance compared to the other interactions it is irrelevant for describing scattering processes. Its only effect will be to modify the trajectories of low-energy neutrons.

²Quantum-mechanically, the neutron magnetic dipole moment is an operator, the consequences of which will be treated later.

correspondingly small magnetic dipole moment, also the magnetic interaction is comparably weak (by three orders of magnitude compared to the effect on electrons), and while the nuclear force can be strong, most of space is devoid of nuclei. As a consequence, the penetration length of neutrons into matter is comparably large. Further, in contrast to the case of X-rays, the probability for a neutron to be absorbed normally is even smaller than to be scattered. This leads to the fact that in neutron scattering experiments care has to be taken to suppress multiple scattering. Often one chooses the sample dimensions so that only 10 % of the incident beam is scattered, which implies that only about 1 % of the incident beam is scattered two times, giving a multiple-scattering contribution to the signal on the order of 10 %. This is again in contrast to X-ray scattering, where typically absorption limits the optical path length through the sample to values where multiple scattering can be neglected.

A.2.2 Concepts of neutron scattering

The flux Φ of a particle beam is defined as the number of particles that go through an area normal to the beam direction per time and area. The absorption cross section σ_{abs} of a system put into a homogeneous flux is the number of particles that are absorbed from the beam per time and normalized to the incident flux Φ . It has the dimensions of an area, and classically it is nothing else than the area enclosed by the outline of an absorbing medium as seen along the beam.

Conversely, if the medium scatters the particles out of the beam instead of absorbing them, the corresponding quantity is the total scattering cross section σ_{tot} . The differential scattering cross section $\frac{d\sigma}{d\Omega}$ is the flux-normalized number of particles scattered per time into the solid angle $d\Omega$. For scattering systems with internal structure, it varies with the direction of $d\Omega$, and obviously its integral over all directions gives the total cross section

$$\int d\Omega \frac{d\sigma}{d\Omega} = \sigma_{\text{tot}}. \quad (\text{A.2.3})$$

Further, for non-static samples the particle can also experience an energy transfer, leading to so-called quasi-elastic or inelastic scattering (to be defined later). Such scattering processes are described by the double differential cross section $\frac{d^2\sigma}{d\Omega dE_f}$, where E_f is the final energy of the out-going particle. Again,

$$\int dE_f \frac{d^2\sigma}{d\Omega dE_f} = \frac{d\sigma}{d\Omega}. \quad (\text{A.2.4})$$

As will be treated in more detail later, on a basic level and for static samples the physics of the scattering of particles such as neutrons and of photons are very much alike: A nucleus with scattering length b at the origin within a incident flux of neutrons described by a wave function

$$\psi_i(\mathbf{r}) = e^{i\mathbf{k}_i \cdot \mathbf{r}} \quad (\text{A.2.5})$$

leads to a spherical outgoing wave function

$$\psi_f(\mathbf{r}) = -b \frac{e^{i|\mathbf{k}_f||\mathbf{r}|}}{|\mathbf{r}|} = -b \frac{e^{ik_f r}}{r}. \quad (\text{A.2.6})$$

The minus sign is just convention, it leads to repulsive potentials having positive scattering lengths. Scattering length and total cross section of a single nucleus are related by

$$\sigma_{\text{tot}} = 4\pi b^2. \quad (\text{A.2.7})$$

The absolute value of the scattering length is large if the neutron-nucleus system is near to a resonance, that is, if the neutron energy is close to the energy of an excited state of the compound nucleus. In this case, it has also a significant imaginary part, corresponding to absorption. As the typical energy differences of nuclear states are much larger than the energy range of thermal neutrons, only in rare coincidences such a resonance falls into the thermal range. Examples are ^{113}Cd and ^{157}Gd . However, in the typical case the scattering length in the thermal range can be considered to be independent of energy.

For tabulations of scattering lengths and cross sections, normally the nucleus is considered to be fixed during the scattering event. The corresponding values are the so-called bound scattering lengths and cross sections. If the nucleus was allowed to recoil, the appropriate way to solve the scattering problem would be to pass into the center-of-mass frame. With the appearance of the reduced mass

$$\mu = \frac{A}{A+1} \quad (\text{A.2.8})$$

in units of u , where A is the atomic mass number, the scattering lengths are reduced by the same factor $A/(A+1)$, and the cross sections by its square, which specifically for the lightest elements such as hydrogen has an appreciable effect. For atoms in a solid, such a recoil event would have to excite a phonon, which quantum-mechanically is unlikely at not too high temperatures.

For a system composed of a number of scatterers, the interference between the distinct scatterers leads to characteristic variations in the scattered intensity over the outgoing directions. Specifically, the sample's statistical degrees of freedom come in four kinds: the nuclear positions, the kind of elements these nuclei belong to, the isotope, and finally the nuclear spin orientation. While the first two classes are subject to chemical interactions on the scale of eV, the energy differences due to both different isotope assignments or nuclear spin orientations are typically much smaller.³ Therefore these last two classes of degrees of freedom are normally completely random. For reasons that will become clear below, in practical instances of neutron scattering one always measures ensemble averages instead of specific realizations, so the corresponding averaging can be done explicitly.

Consider a spin \mathbf{S}_1 with quantum number S_1 . Due to quantum mechanics, it has a multiplicity of $2S_1 + 1$, where the corresponding states for instance can be chosen as the eigenstates with respect to the projection of the spin along some coordinate, which gives eigenvalues $\{-S_1, -S_1 + 1, \dots, S_1\}$. Consider now a second spin \mathbf{S}_2 with multiplicity $2S_2 + 1$. Of course, the total multiplicity of the system is $(2S_1 + 1)(2S_2 + 1)$. Now also the total spin $\mathbf{S} = \mathbf{S}_1 + \mathbf{S}_2$ behaves like a quantum-mechanical spin. Specifically, according to the relative orientations of \mathbf{S}_1 and \mathbf{S}_2

³Only for the lightest elements different isotopic masses can lead to appreciably different chemical and physical properties via the quantum-mechanical zero-point energy, with heavy water an example.

its quantum number S can take values between $S_1 - S_2$ and $S_1 + S_2$ (without loss of generality assume $S_1 \geq S_2$), and each of those options has multiplicities $2S + 1$. As

$$\sum_{S=S_1-S_2}^{S_1+S_2} 2S + 1 = (2S_1 + 1)(2S_2 + 1) \quad (\text{A.2.9})$$

this is consistent.

Consider now a given nucleus of some isotope with total spin quantum number I and a neutron with spin $1/2$. For random nuclear spin orientation and/or neutron polarization the sum spin of the compound nucleus can have spin quantum numbers $I + 1/2$ or $I - 1/2$. As already mentioned above, the nuclear forces depend on the relative orientations, giving differing scattering lengths b_+ and b_- , respectively. The corresponding multiplicities are $2I + 2$ and $2I$, leading to weighting factors

$$w_+ = \frac{I + 1}{2I + 1} \quad \text{and} \quad w_- = \frac{I}{2I + 1}. \quad (\text{A.2.10})$$

Taking a step back, if the nucleus is only constrained to be of a given element, then it can be of any of a number of isotopes, with the weighting factors according to the isotopical make-up of the sample.

As will be derived later, the uncorrelated randomness of isotope and spin orientation assignments give rise to a perfectly flat (i.e., independent of outgoing direction) contribution to the scattering, while real-space correlations in nuclear positions and kinds of atoms lead to characteristic modulations in the scattering. Colloquially, these contributions are called 'incoherent' and 'coherent' scattering, respectively. The corresponding cross sections and phenomenological scattering are lengths

$$\sigma_{\text{coh}} = 4\pi \langle b \rangle^2 = 4\pi b_{\text{coh}}^2 \quad (\text{A.2.11})$$

with

$$b_{\text{coh}} = \langle b \rangle \quad (\text{A.2.12})$$

and

$$\sigma_{\text{inc}} = 4\pi (\langle b^2 \rangle - \langle b \rangle^2). \quad (\text{A.2.13})$$

Note that these element-specific statistical quantities actually are not inherent properties of the elements. They depend on the weighting factors of the different fundamental scattering lengths, and therefore vary with the isotopical make-up of the sample. Specifically, for measuring weak signals such as excitation spectra it can be advantageous to use isotopically pure samples so as to suppress the isotope-incoherent part and lower the background.

A.2.3 Absorption, activation and transmutation

Guiding neutrons onto a sample can also affect the sample. For thermal neutrons, the dominant effect is due to the absorption of neutrons. While in X-ray scattering

the ratio of absorbed to scattered photons is much higher, these photons only excite the electronic structure. The energy quickly dissipates, so that the net effect of the X-ray beam is a minuscule heating of the sample, and specifically for metallic systems typically no significant irradiation effect is discernible. On the other hand, neutrons are absorbed via their incorporation into some nucleus, corresponding to an irreversible change of the absorbing nucleus.

The severity of this change depends on the nucleus in question: If the absorption leads to a stable isotope, then apart from the release of the neutron binding energy, typically in the form of MeV-range γ photons, no further events will happen. However, if the resulting nucleus is unstable, it will decay radioactively at some later time, and potentially a whole decay chain follows. From the neutron experimenter's point of view, such a potential activation of the sample in the neutron beam necessitates care being taken with regard to radiation safety. As regards samples, as a rule after an experiment the activity of the sample is measured. Typically, the activity is due to a range of different isotopes with different half-lives, where the shortest half-lives give initially the highest activities. In order to minimize exposure it can therefore be beneficial to let the sample cool down⁴ for a few minutes, then dismount it quickly and keep it for a few days to months in a lead-walled safe until it is safe to handle. Further, this pertains also to all parts of the instrumentation exposed to neutrons: here the used materials are chosen also in order to minimize the induced radioactivity.

Consequently, the critical elements with respect to activation are those that have a high natural ratio of an isotope with large absorption cross section for which neutron absorption leads to an unstable isotope, and that decay with a high-energy γ emission. Out of these, the most problematic are those with half-lives on the order of years. In such cases the resulting activity is proportional to the integrated neutron flux they received, as only an insignificant part decayed during the irradiation, it would take too long to wait out the decay of activity, while on the other hand the activity per nucleus is still appreciable, in contrast to isotopes with half-lives on the order of millenia. An example is cobalt: its single stable isotope ^{59}Co has a comparatively large absorption cross section of 37 b for thermal neutrons, and upon neutron absorption it becomes ^{60}Co which beta-decays with a half-life of 5 years to ^{60}Ni , emitting γ quanta of approximately one MeV.

The final effect of induced activity is *transmutation*, the conversion of nuclei to other elements. In terms of the physics of the sample, this typically has no significant consequences, that is, for typical fluxes in neutron experiments the proportion of converted nuclei is too small to change the properties of the sample: assuming a typical incident flux of $10^8 \text{ cm}^{-2}\text{s}^{-1}$, even an absorption cross section of 100 b gives only 10^{-14} absorptions per atom and second, or a proportion of 10^{-9} transmuted nuclei after an experiment on the order of days. On the other hand, the large energies released within the sample for each neutron absorption of radioactive decay event can lead to enhanced diffusive dynamics or radiation damage affecting a large number of atoms per event, as will be discussed below.

In order to intentionally induce activation, one can place samples within the

⁴In this regard, a jargon in analogy to aspects of heat is used: Hot samples are those that are radioactive, and with time they cool down.

moderator of a reactor near to the core, where the thermal neutron flux is highest. This is done mainly for three purposes:

- in the context of *neutron activation analysis*, which will be discussed in the context of experimental techniques
- for producing radioactive isotopes to be used for medical applications (diagnosis and specific internal radiation therapy)
- for *neutron transmutation doping* of semiconductors

The last item would historically have fallen into the domain of alchemy, whose ultimate goal was to commute base metals into precious metals. Nowadays it is indeed possible to transmute mercury into gold, but, ironically, the converse process can be effected much easier by placing gold into a neutron beam, yielding ^{198}Hg after β^- decay. However, this is just a curiosity, as no natural element has a value that would make such an operation economically viable.

In contrast, in neutron transmutation doping it is not the bare number of transmuted nuclei, but their spatial distribution: Due to the wide penetration of neutrons into matter, in this specific case Si, the phosphorus atoms that result from the reaction



have a very uniform distribution. Using pure single-crystalline ingots gives single-crystalline n-type doped Si with a superior doping homogeneity than what can be obtained by Czochralski growth or float-zoning with the doping P in the melt. Materials with such high homogeneity are desirable for power semiconductor devices, such as for DC to AC inverters necessary for coupling solar plants to the electrical grid. Its parasitic production in research reactors is economically profitable, with output in the range of tens of tons per year.

Apart from the cases where a resonance falls into the thermal range, the absorption cross section of a given nucleus for thermal neutrons can be written as

$$\sigma_{\text{abs}}(v) = \sigma_0 \frac{v_0}{v}, \quad (\text{A.2.15})$$

with v the neutron velocity. This is the so-called $1/v$ -law. It corresponds to the frequency of absorptions being

$$A = N_t \int dv n(v) v \sigma(v) = N_t \sigma_0 v_0 n, \quad (\text{A.2.16})$$

where N_t is the total number of nuclei in the target and $n = \int dv n(v)$ is the integrated neutron density. In other words, the $1/v$ -law is equivalent to the absorption rate per neutron depending only on the density of absorbing nuclei and not on the relative velocities. This in turn is due to the nuclear potential extending over much smaller lengths than thermal neutron de Broglie wavelengths. Analogously, the $1/v$ -law can be deduced from the transit time of a neutron by a given nucleus scaling just with this relation. When values of the thermal absorption cross section σ_0 are given, they are typically defined with respect to a reference velocity of $v_0 = 2200 \text{ m/s}$.

A.2.4 Knock-on effects

Apart from issues of activation and transmutation, which directly affect only a very small part of the atoms in a given sample, the interaction of neutrons with matter can also lead to more drastic effects, when significant quantities of energy and momentum are imparted to the sample. This pertains both to direct effects due to high-energy neutrons as well as to indirect effects due to high-energy γ , β , β^+ or α particles emitted either promptly after a neutron absorption or radioactively afterwards. In all these cases, a qualitative understanding can be gained already by a classical discussion in terms of elastic collisions.

The fundamental rule of thumb governing the physics of radiation damage in metals is that the displacement energy, which is the energy threshold that has to be imparted to an atom to make it permanently leave its lattice site even without neighbouring vacancies, is on the order of 25 eV. Of course, in reality this will vary from system to system as well as with the direction. Due to the kinematics of elastic collisions, for this energy to be transferred onto a typical transition metal atom, an incident neutron needs at least a kinetic energy of 300 eV, an α particle needs 100 eV, and an electron needs on the order of 400 keV, where a relativistic treatment becomes necessary. For heavier atoms, the energies have to be increased correspondingly. Also γ quanta can transfer their energies to the lattice, either directly via the electromagnetic interaction with nuclei (which becomes increasingly important for heavier atoms) or indirectly via exciting an electron. As the electron energies are in the relativistic regime, the necessary γ energy is on the same order of magnitude.

The primary knock-on atom is the one that obtained its energy directly from the high-energy irradiation. On its way through the crystal it will continuously lose energy due to inelastic processes with the electronic system, but it can also scatter with the other atoms, thereby transferring energy. If this energy is still above the displacement threshold, secondary displacements will result.

Since the typical energies of radioactive transitions are on the order of MeV, the above values show that the β and β^+ -transitions, which are the normal decay route of activated nuclei and are often accompanied by γ emission, can transfer a few times the displacement threshold energy per collision, and therefore can lead to the displacement of a large number of atoms over small distances, generating interstitials and vacancies, i.e. Frenkel defects. On the other hand, an unmoderated fission neutron also in the MeV range can transmit a far larger energy to a single primary atom. Such high-energy primaries can travel quite far, specifically when they are scattered into directions parallel to atomic columns, which is called *channeling*.

Towards the end of their path a primary will scatter with practically every atom along the way and therefore dump a very large energy into a comparatively small volume. This gives rise to the concept of *displacement or thermal spikes*, where on the order of 10^4 atoms are momentarily heated to temperatures on the order of 10^4 K. Due to the small spatial scales, the time scale of the cooling down lies at a few phonon cycles, which corresponds to quenching rates that cannot be reached otherwise. As a consequence, the system typically does not find back to the state

of equilibrium. Instead, a high local concentration of vacancies and interstitials remains, perhaps also small-scale dislocation loops, or the sample becomes even amorphous. This radiation-induced accumulation of defects is called the Wigner effect. Even when no permanent lattice defects are introduced, irradiation can lead to athermal, non-equilibrium disordering or radiation-enhanced diffusion.

Around the 1950s, the field of radiation damage physics constituted a main part of solid state physics. Its relevance came from both the applied aspects with respect to nuclear reactors, as well as the fact that the recovery of radiation damage gives direct experimental evidence on quantities such as the migration enthalpy of vacancies and interstitials, which otherwise are in general inaccessible. Specifically interstitials have so small migration enthalpies, that Frenkel defects typically would anneal out during a room-temperature irradiation. However, by increasing the temperature slowly after irradiation at cryogenic temperatures, distinct stages can often be discerned in the defect density, which are assigned to the temperatures where specific defects become mobile. This annealing of defects is termed *recovery*.

Recovery is an exothermic process, and at the same time it is thermally activated. This can have drastic consequences: In graphite, defects become mobile at around 250°C, releasing the Wigner energy. If a graphite-moderated nuclear reactor is operated below this temperature, periodic annealings of the moderator have to be performed. In such an annealing in 1957 at the Windscale Plant in England, which was of the first generation of reactors designed to produce plutonium for nuclear weapons, fuel elements ignited due to runaway release of the Wigner energy, which constituted the first major release of radioactivity due to a reactor accident.

Chapter B

Instrumentation and techniques

B.1 Neutron instrumentation

This section will present the concepts of how free neutrons can be generated, brought into well-defined conditions, guided towards a sample, and afterwards analyzed, covering all the instrumental aspects of neutron experiments.

B.1.1 Neutron sources

As was discussed already, the free neutron is unstable against β decay, therefore in nature neutrons are found only bound in atomic nuclei. The proportion of neutrons to protons increases with increasing mass number, and further, the binding energy per nucleon decreases for heavy nuclei. This shows that events where a heavy nucleus is divided into smaller fragments are exothermic and can therefore be made to happen comparatively easily, and that the resulting nuclei will have a higher than preferred neutron ratio and therefore a tendency to emit those neutrons. Using this fact, free neutrons are generated today in large-scale experimental facilities by one of two principles.

B.1.1.1 Nuclear chain reactions in reactors

In a simple picture, by imparting energy to a heavy nucleus its shape can be excited into oscillations. As the heavy nucleus is only a metastable state, there is a threshold energy above which the amplitude of the oscillation is so large that there is no restoring force, instead the nucleus splits into two daughter nuclei that are accelerated away from each other due to the Coulomb repulsion. Such an event is called *nuclear fission*. For instance, it can be induced by γ irradiation, from where it is deduced that approximately 5 MeV are the energy threshold for

the relevant nuclei.

With exception of the most extreme neutron-heavy nuclei, a free neutron has a positive binding energy with a nucleus. In the relevant range, this is also on the order of 5 MeV. Therefore, as the energy freed when a neutron is absorbed goes in the first place into excitations of the compound nucleus, such a neutron absorption can potentially lead to fission. If the binding energy is larger than the fission threshold, thermal neutrons suffice. Nuclei with this property are called *fissile*. If the binding energy should fall short of the fission threshold, the deficiency has to be made up by the kinetic energy of the absorbed neutron. Nuclei that can be fissioned by fast neutrons are called *fissionable*. The kinetic energy threshold is always on the order of 1 MeV.¹

The most prominent nuclear fuels are the uranium isotopes ${}^{235}_{92}\text{U}$ and ${}^{238}_{92}\text{U}$ as well as ${}^{239}_{94}\text{Pu}$. Of these, ${}^{235}_{92}\text{U}$ and ${}^{239}_{94}\text{Pu}$ are fissile with thermal fission cross sections of 583 b and 748 b, respectively, while ${}^{238}_{92}\text{U}$ is only fissile with a threshold energy of 1 MeV. Due to the $1/v$ -law, in the fast regime the high absorption cross sections have decayed, giving fission cross sections on the order of 1 b due to resonances. Also here the ${}^{238}_{92}\text{U}$ cross section is lowest. The reason lies in the fact that the additional bound neutron can occupy a lower level with spin compensation for the odd-neutron nuclei ${}^{235}_{92}\text{U}$ and ${}^{239}_{94}\text{Pu}$ than for the even-neutron nucleus ${}^{238}_{92}\text{U}$. This pairing effect is on the order of 1 MeV and distinguishes fissile from fissionable.

Apart from the daughter nuclei, which are in the overwhelming majority of cases two of number with a preferred asymmetry of masses, also neutrons can be released in the initial scission. Further, the resulting daughter nuclei are in highly excited states, where further neutrons can evaporated off. This happens on rapid timescales, and the released neutrons are called prompt neutrons. Subsequently, the still neutron-heavy daughter nuclei will β -decay, where due to the excitation of the nuclei further neutrons are emitted, the so-called delayed neutrons. In all, the average number of neutrons emitted from a ${}^{236}_{92}\text{U}$ compound nucleus is 2.5, 0.7% of those are delayed neutrons.

This multiplication of free neutrons can give rise to a nuclear chain reaction. When on average more than one of those emitted neutrons induces another fission event, the assembly is said to be supercritical. As the timescale of prompt neutrons is on the order of 10^{-13} s, an explosive multiplication would result from a prompt-supercritical assembly. *Nuclear reactors* are facilities where chain reactions proceed in a controlled way. This is possible thanks to the delayed neutrons: their timescales of seconds to minutes allow to keep the reactor in a prompt-subcritical state by actively adjusted control rods consisting of strongly neutron-absorbing materials, where the delayed neutrons make up for a time-averaged neutron multiplication of exactly one. Put another way, a given delayed neutron will generate on average $1/(1 - 0.997) \approx 333$ prompt neutrons immediately, and on average one delayed neutron seconds to minutes later. For keeping the reactor at a given power, in the prompt-subcritical state only the multiplication of the delayed neutrons has to be controlled, which is mechanically possible. In other types of

¹Note that due to quantum-mechanical tunneling, there is no strict fission threshold. Exciting a fissionable nucleus will in general always increase the spontaneous fission rate, but the dependence on energy is quite steep, so that the threshold can be meaningfully defined as the energy where the fission rate becomes detectable.

reactors, an inherent reduction of the reactivity with increased core temperature is used for regulation, or criticality is reached periodically by a rotating neutron reflector next to the fuel element, leading to a pulsing.

During the operation of a reactor, the reaction products can affect the multiplication rate, typically decreasing it. Such nuclei are called *neutron poisons*, with $^{135}_{54}\text{Xe}$ the most prominent example. This isotope has an extremely large thermal neutron absorption cross section of 3.5×10^6 b, as it is just one neutron away from the magic neutron number 82. For the most part, it results from $^{135}_{53}\text{I}$ by β decay with half-life of 6.7h. If it does not absorb a neutron, with a half-life of 9.2h it would decay further to the long-lived isotope $^{135}_{55}\text{Cs}$. Under steady reactor operations, these decay rates lead to an equilibrium $^{135}_{54}\text{Xe}$ concentration (depending on the neutron flux in the reactor), but once the reactor is shut down, its concentration increases as it is produced faster than it decays. For reactors without large reactivity margins, this buildup would inhibit a startup for a few days, until it has decayed again due to the depletion of $^{135}_{53}\text{I}$.

As detailed above, neutrons have a high probability of leading to a fission event either when they are very slow (such that the absorption cross section is large, relevant for fissile nuclei), or when they are fast (above the fission threshold for non-fissile fissionable nuclei). Reactors that depend on either of those channels are called thermal or slow reactors, on the one hand, and fast reactors, on the other hand. A fast reactor needs a compact arrangement, so that as many as possible fast neutrons hit the fissionable nuclei, before they have leaked out or lost their energy. On the other hand, a thermal reactor relies on a moderator, which slows the fission neutrons by elastic collisions. The moderation concept will be discussed below. Nuclear power reactors as well as research reactors are nearly always thermal reactors.

In thermal reactors, it is primarily ^{235}U that keeps the chain reaction going, and with progressive burn-up also ^{239}Pu . ^{238}U , by far the most abundant uranium isotope, is a priori detrimental to the chain reaction, as it absorbs neutrons. By a judicious laying-out of the reactor configuration and choice of moderator, the comparatively large dimensions of power reactors give rise to a good neutron economy (i.e. where as little as possible neutrons leak out), so that ^{235}U enrichments of a few percent, or in some cases even natural uranium, suffice for achieving criticality. In contrast, for research reactors large neutron fluxes are desirable, which implies high power densities. These are only achievable by significant enrichments. High-flux research reactors (that is, those with the main purpose to deliver high neutron fluxes to scattering instruments) therefore have been laid out to use high-enriched uranium (HEU), with enrichments up to about 90%. In the last years, this has started to become a political problem: HEU is defined to have ^{235}U concentrations above 20%. As also weapons-grade uranium falls into this category, specifically the US government pushes for the conversion of these research reactors to low-enriched uranium (LEU). For keeping the neutron flux at present levels, a nuclear fuel with a higher chemical uranium density would therefore be needed, development of which is done for instance at the FRM II in the framework of the HEU-MEU program.

B.1.1.2 Spallation sources

Spallation denotes the chipping-off of particles from a larger body due to an impact onto it. Specifically with regard to nuclear physics, it is the emission of a large number of nucleons after a nucleus is hit by a high-energy particle.

To induce this process, protons are accelerated in particle accelerators to energies of about 1 GeV. As the corresponding wavelengths of 1 fm are below the characteristic size of nucleons, upon hitting a nucleus such a proton does not form a compound nucleus that is coherently excited, but instead can transfer its energy to single nucleons. These nucleons can then collide with further nucleons. With the initial energy on the order of 1 GeV, many of them can get energies above the nucleon binding energy of typically 8 MeV, enabling them to leave the nucleus. This is termed the intra-nuclear cascade. As the struck nucleus is still in an excited state, in a further process nucleons are evaporated. Finally, the fast nucleons from the intra-nuclear cascade can also hit other nuclei, giving rise to the inter-nuclear cascade. The charged protons will be stopped within the target, but the neutrons can be extracted and used. The heavier the nucleus, the more neutrons are released, with about 40 neutrons per 1 GeV spallation event in uranium. In most cases, a single heavy nucleus is the product apart from the emitted neutrons and protons (and to a smaller degree deuterons and α particles), but with smaller probability the high-energy incident particle can also induce fission.

Both reactors and spallation sources can either be pulsed or continuous. In the conventional formulation of neutron techniques, typically the average neutron flux determines the count rate and therefore the performance of the instrument. However, as will be discussed below, with time-of-flight techniques essentially all the neutrons within a short pulse can be used, and therefore the peak flux is the deciding figure of merit. For both reactors and spallation sources, the thermal power dissipation limits the achievable fluxes, as high neutron fluxes directly correspond to a high density of fission/spallation rates and therefore a high power density. Per fission event, about one neutron is released along with about 200 MeV. For spallation, the ratio is somewhat better. Further, thermal power dissipation obviously limits the average power. This shows the potential of pulsed sources, which indeed can supply much higher peak neutron fluxes than continuous sources, with, e.g., an average flux at the ILL of 1.5×10^{15} n/cm²s compared to the SNS' average flux of 4×10^{13} n/cm²s, but a peak flux of 3×10^{16} n/cm²s.

B.1.2 Neutron moderation

Immediately after their emission from nuclei, neutrons have energies on the scale of nucleon binding energies, that is, in the MeV range. Both for keeping up the chain reaction in thermal reactors as well as for most experimental applications that use neutrons, these energies are much too high. The concept of letting such neutrons dissipate their energy by elastic collisions with nuclei is called *moderation*. Due to the kinematics of elastic collisions, the average proportion of the neutron energy that is transferred per collision is inversely proportional to the nucleus mass. Therefore, the preferred moderator materials are composed of light

nuclei. Further, the absorption cross section should not be too high (excluding Li and B), the moderator should be in a condensed phase (excluding He), it should be in the thermodynamic ground state (excluding molecular matter, which would suffer severe radiation damage due to the fast neutrons), and it should not be hazardous (excluding Be). As a consequence, only three materials are used as moderators, viz. light water H₂O, heavy water D₂O, and graphite. These different materials have different neutron path lengths, so depending on the circumstances, either of the three can be the optimal choice.

B.1.2.1 Statistical distributions

Due to statistical mechanics, after a few tens of collisions the neutrons have become thermalized, that is, the occupation of a given state is given by a Boltzmann distribution

$$p(E) \propto e^{-E/k_B T}, \quad (\text{B.1.1})$$

where E is the kinetic energy of the neutron and T is the temperature of the moderator. In classical mechanics, the state variables are position and momentum (or equivalently velocity vector), and the density of states is constant over \mathbb{R}^6 . Specifically, the probability density of neutrons as a function of velocity vector is

$$P_{\text{mod}}(\vec{v}) \propto e^{-m_N |\vec{v}|^2 / 2k_B T}. \quad (\text{B.1.2})$$

States with a given absolute value of the velocity lie on the surface of a sphere in \mathbb{R}^3 , therefore the corresponding density of states goes with v^2 , so that the probability density as a function of velocity is

$$P_{\text{mod}}(v) \propto v^2 e^{-m_N v^2 / 2k_B T}. \quad (\text{B.1.3})$$

This is the Maxwell-Boltzmann distribution, and it describes the probability density of thermalized neutrons within the moderator.

For applications, thermalized neutrons are extracted from a moderator by beam tubes. Typically, in a sloppy way of speaking, the velocity distribution of the resulting neutron beam is also called Maxwell distribution. However, care has to be taken here, as the probability distribution scales with an additional power of v

$$P_{\text{beam}}(v) \propto v^3 e^{-m_N v^2 / 2k_B T}. \quad (\text{B.1.4})$$

This can be understood along the following lines: First, in the moderator, no direction is special, therefore the distribution is isotropic. As a consequence, also the distribution of neutrons at a given point \vec{r} that are travelling towards some solid angle $d\Omega$ is proportional to $P_{\text{mod}}(v)$.² However, the larger v , the larger the contribution to the flux due to these neutrons at \vec{r} , giving (B.1.4).

The mean velocity resulting from this distribution is

$$\bar{v} = \frac{3}{4} \sqrt{\frac{\pi 2k_B T}{m_N}} \approx 171 \sqrt{T/\text{K}} \text{m/s}, \quad (\text{B.1.5})$$

²More fundamentally, this follows also from the Gaussian distribution $P_{\text{mod}}(\vec{v})$. Assuming without loss of generality that $d\Omega$ points along the x coordinate, the probability for a given \vec{v} to point towards $d\Omega$ goes with $v_x^2/v_y v_z$, as the three velocity components are independent.

and its mode (the most probable velocity) is

$$v^* = \sqrt{\frac{3k_{\text{B}}T}{m_{\text{N}}}} \approx 157\sqrt{T/\text{K}}\text{m/s.} \quad (\text{B.1.6})$$

With (A.1.13) these expressions can be converted to wavelengths.

At research reactors such as the FRM II, the moderator necessary for keeping up the chain reaction is at room temperature. Some beam tubes directly obtain their neutrons from this moderator, and the corresponding spectrum is called the thermal spectrum. Further, within the moderator tank there is both a cold source, consisting of an actively cooled chamber of liquid D_2 at 25 K, as well as a hot source, consisting of a passively heated graphite block at 2200 K. Thermal neutrons from the moderator tank migrate into these secondary sources, thermalize again, and can then be extracted by other beam tubes, providing neutrons of longer or shorter wavelengths.

Specifically for pulsed spallation sources, where neutrons are extracted from the moderator quite early in order to keep the pulses short, but to a lesser degree also elsewhere, there is a spectral contribution of neutrons that are not yet thermalized. Fission neutrons can be suppressed by pointing the beam tubes not directly towards the core, but tangential to it, but such *epithermal* neutrons, which are scattered into the beam tubes after an insufficient number of scattering events, can in principle not be avoided.

B.1.2.2 Figures of merit

For a neutron scattering experiment (or, more generally, for any scattering experiment) the relevant figure of merit is the brilliance of the source. It is defined as the neutron flux per time, per area, per solid angle and per energy window. For instance, to derive an order of magnitude estimate of the FRM II thermal moderator's brilliance observe that 200 MeV thermal energy per emitted neutron and 20 MW thermal power gives a neutron generation rate of $6 \times 10^{17} \text{ s}^{-1}$. With a diffusion constant of thermal neutrons in D_2O

$$D = \frac{\langle d \rangle \langle v \rangle}{6} \approx 15 \text{ m}^2/\text{s}, \quad (\text{B.1.7})$$

where $\langle d \rangle \approx 4.5 \text{ cm}$ is the mean free path length, a neutron density of $6 \times 10^{15} \text{ m}^{-3}$ at 50 cm from the source, assuming an isotropic geometry, results. This gives a brilliance on the order of

$$\Psi \approx 1 \times 10^{14} \frac{1}{\text{cm}^2 \text{sterads} \text{Å}} \quad (\text{B.1.8})$$

in the maximum of the thermal spectrum. In contrast, synchrotron X-ray sources have about 20 orders of magnitude higher brilliances.

The importance of the brilliance lies in the fact that it is conserved under optical manipulations due to Liouville's theorem, as will be treated in more detail below. To illustrate this by a simple example, assume a scenario where neutrons are

extracted via a beam tube of 3 m length and entrance and exit windows of 1 cm^2 . This corresponds to a solid angle of $(3.3 \text{ mrad})^2$, giving an integral neutron flux of about 10^9 neutrons per second and \AA through the exit window, or about 10^7 neutrons per second monochromatized to 1 % bandwidth.

B.1.3 Components of neutron instruments

Having produced free neutrons and brought them to some convenient energy range by moderation, their phase space volume typically has to be shaped further, and they have to be brought via the sample to the detector. The pertinent devices will be discussed here.

B.1.3.1 Neutron mirrors and guides

As will be discussed in more detail later, in many aspects a beam of neutrons behaves very much like a beam of light. Specifically, a neutron beam (and also single neutrons, behaving like rays of light) can display phenomena belonging to the realm of neutron optics, where the path of a ray is determined by refraction and reflection, following formally the same laws as in (photon) optics.

For neutrons, the wavelength-dependent index of refraction is given by

$$n = \sqrt{1 - \frac{\lambda^2 \rho b}{\pi}}, \quad (\text{B.1.9})$$

where ρ is the number density³ of nuclei with (mean coherent) scattering length b . That is, for a given material the index of refraction is determined by the scattering length density ρb with dimension of an inverse squared length. For example, in natural crystalline Ni the scattering length density has the value $\rho b = 4b/a^3 \approx 9.4 \times 10^{14} \text{ m}^{-2}$, where $a = 3.52 \text{\AA}$ is the lattice constant. For thermal neutrons of $\lambda = 1.8 \text{\AA}$, this gives $n - 1 \approx -5 \times 10^{-6}$. This a representative case, showing that deviations of n from 1 are very small and, for the typical case of positive scattering lengths, are negative. This smallness of the deviations from 1 implies for instance that neutron lenses would be very inefficient for focussing.

A material with $n < 1$ is neutron-optically less dense than vacuum. As a consequence, if a neutron hits a surface with a glancing angle ϕ below the critical glancing angle $\phi_c = \pi - \theta_c$, it will be reflected totally. In the limit of small $n - 1$, the defining relation $n = \sin \theta_c$ gives

$$\phi_c = \lambda \sqrt{\frac{\rho b}{\pi}}. \quad (\text{B.1.10})$$

Considering again natural Ni at $\lambda = 1.8 \text{\AA}$ gives a critical glancing angle of 3.1 mrad or 0.18° .

³Here ρ is not the mass density! If the symbol n was not taken by the index of refraction, the number density would better be denoted n .

The most important application of this theory with respect to neutron instrumentation are the *neutron guides*. They typically have rectangular cross sections and consist of glass plates onto which (in the simplest case) Ni is evaporated. In contrast to conventional beam tubes, that are essentially just evacuated flight paths for the neutrons, in a neutron guide the neutrons below the critical wavelength are guided along via total reflection. They have a number of beneficial aspects:

First, they can be utilized for the quite prosaic goal of having more floor space per instrument. Where with a beam tube of fixed cross section the flux at the sample position would fall quadratically with the distance from the source (admittedly, due to Liouville's theorem, with a corresponding sharpening of collimation, which however is useless below a certain value), with neutron guides questions of flux/collimation are decoupled from the distance from the source. For the same reason, they are the natural choice for those sections of the beam path in a time-of-flight instrument that serve to select or analyze energies by the time of flight.

Further, they can serve as an effective filter both against γ contamination and high-energy neutrons. Those are not reflected at the neutron guide walls and therefore automatically decay with the square of the guide length. However, curved neutron guides are even more effective for this purpose. These are constructed such that there is no direct line of sight between entrance and exit of the neutron guide, so that neutrons have to be reflected at least once to pass the guide. This suppresses the high-energy contribution to the minute amount that corresponds to scattering at the guide walls.

Finally, focussing neutron guides fulfill the role of lenses, that is, deform the neutron phase space by trading collimation for focus size. This is done by reducing the guide cross section towards the exit window.

Building neutron guides with a good performance is not easy: First, it requires a very precise alignment of the sections of the guides (typically 1 m), which of course has to be stable over duration of operation and therefore poses requirements on the stability of the building floor. Further, a very good surface flatness is required for high reflectivities up to the critical angle: if the surface is wavy, then there are deviations between the glancing angle with respect to the idealized surface and with respect to the actual surface, which gives a corresponding smearing of the ideally sharp transition in reflectivity at the critical angle.

In the early years after their first installation at the ILL in the 1970s, the domain of neutron guides was only cold neutrons, as the higher critical angles simplify fulfilling the necessary conditions. This has changed with the introduction of neutron supermirrors in the 1990s: due to the developments in sputtering techniques (effected by their relevance for computer hard disks), it has become possible to deposit high numbers of layers in a very controlled and uniform way. By depositing a superlattice, neutrons with the corresponding transversal wavevector component k_{\perp} can be made to be Bragg-scattered. A supermirror consists now of layers with gradually increasing d -spacing. In this way, not only neutrons with a given k'_{\perp} , but with all k_{\perp} below some maximum value are Bragg-diffracted, as in a given depth they find the corresponding d .

Typically, a sequence of Ni and Ti layers is used, corresponding to the widest span of scattering length densities. The performance of a supermirror is quantified by m , which is the proportional increase in critical angle for a given wavelength compared to a natural Ni guide. Values of m up to 8 have been demonstrated with up to 16000 layers. However, in this case the reflectivity at the critical angle has already decreased to 40%.

Note that a significant difference between neutron and photon optics lies in the fact that neutrons are described by a scalar wave function. Therefore the Brewster angle has no analogon. However, when a ferromagnetic material is magnetized, due to the interaction of the neutron magnetic moment with the electrons the spin states of the neutrons experience different indices of refraction, leading to a range of glancing angles where neutrons of one spin state are totally reflected while the others are not, giving a polarizing mirror. This way of polarizing a neutron beam becomes competitive when employing the supermirror concept.

B.1.3.2 Crystal monochromators and analyzers

As with X-rays, the most obvious way to select neutrons with a given wavelength out of a polychromatic neutron beam is by utilizing Bragg's law, that is, to scatter the beam at a single crystal so that only those neutrons are scattered that correspond to a wavevector transfer coinciding with a reciprocal lattice vector. However, while this gives the correct qualitative idea, actually the kinematical theory of scattering is inadequate to quantitatively describe the effect of scattering at a perfect single crystal, and the dynamical theory has to be used (see the pertinent discussion below).

Consider a perfect single crystal in Bragg (or reflection) geometry, that is, where the incident beam leaves the crystal through the same surface as it entered. In the dynamical theory, the intensity of the incident beam is reduced along the way into the crystal, as it is transferred into the scattered beam. Therefore, there is only a finite penetration depth (this effect is called *extinction*), and as a consequence the Bragg condition will not need to be ideally fulfilled. In the dynamical theory neglecting absorption, in this ideal case the total incident intensity is reflected for a finite range of wavelengths. On the other hand, the less frequent Laue (or transmission) geometry corresponds to the case where the crystal has a finite thickness and the scattered beam exits the crystal on the other side. Here dynamical theory would lead to a distribution of intensity into the transmitted and scattered beam with equal weights.

Different from the X-ray case, even with the finite widths of reflexes in dynamical theory perfect single crystals would make very inefficient neutron monochromators, as their angular widths of acceptance are much smaller than the typical beam divergences. Therefore, imperfect crystals with mosaicities η around 1 mrad are typically used. These can be seen as polycrystals with very strong texture, that is, where the crystallites have Gaussian distributions of orientation with standard deviation η . With finite η , neutrons from a larger volume in phase space will eventually hit upon a crystallite that scatters them, giving worse resolution (which, as mentioned above, is no problem) and higher scattered intensities.

The resulting width in energy is

$$\frac{\Delta E}{E} = \Delta\theta \cot\theta, \quad (\text{B.1.11})$$

with

$$\Delta\theta = \sqrt{\frac{(\alpha_i^2 + \alpha_o^2)\eta^2 + \alpha_i^2\alpha_o^2}{\alpha_i^2 + \alpha_o^2 + 4\eta^2}}, \quad (\text{B.1.12})$$

where θ is the angle with respect to the scattering planes and α_i and α_o the incoming and outgoing Gaussian acceptances or divergences. This shows that η can be increased up to the smaller value out of the incoming and outgoing acceptances without hurting the resolution. It also shows that the energy resolution is optimal when $\theta = \pi/2$, that is, in backscattering. This is used with backscattering spectrometers.

To increase intensities further, one can bend the reflecting lattice planes (or equivalently compose the monochromator of properly oriented small plane single crystals), which works like a focussing mirror. Again due to Liouville's theorem, one has to pay for the increased intensity by increased divergences. However, normally the conditions on wavevector resolution are more stringent in the scattering plane, which typically is horizontal, than in the perpendicular plane. Therefore vertical focussing is often used, but also double focussing (i.e. vertical and horizontal) setups are used.

An important point to note is that if a given wavevector transfer corresponds to a reciprocal lattice vector, then so does every integer multiple of it. This means that neutrons of wavelengths λ/n for integer n will fulfill the scattering condition for a monochromator that is set to a nominal wavelength of λ , giving higher-order contaminations. Therefore, one typically uses filters in addition to monochromators (see below). It can also be an option to use the (lll) reflection of a crystal with the diamond lattice with odd l . As the structure factor of the (lll) reflection for even l vanishes, the first contamination here is $\lambda/3$, with correspondingly lower intensities.

The preferred monochromator material has a small incoherent scattering cross section and a small absorption cross section. Further, it should either have inherently a high Debye temperature (which follows from strong binding and small atomic masses) or it should be actively cooled, so that the thermal diffuse scattering contribution is low (see the discussion of phonons). Often, the main problem in obtaining good neutron monochromator crystals is not so much to get large single crystals, but rather to get good imperfect crystals with large and controlled (that is, isotropic Gaussian) mosaic spreads. Note that pyrolytic graphite, a material that is often used as a neutron monochromator, is actually not a crystal at all, as it consists of graphite planes that are regularly stacked above each other, but that have no in-plane orientational relation. Therefore, all reflections apart from the $(00l)$ families are not Bragg peaks, but rather rings in reciprocal space. This has also very desirable consequences for its use as wavelength filter.

Monochromators can additionally function as polarizers. For ferromagnetic materials, there is a scattering contribution due to the electronic polarizations in

addition to the nuclear contribution, the sign of which depends on the neutron polarization. For a specific choice of materials and wavelength (note that the magnetic form factor, in contrast to the nuclear form factor, decays with wavevector transfer), those two contributions can be made to cancel exactly for one spin channel, so that only the other channel is scattered. The most important material here is the Heusler alloy Cu_2MnAl .

Finally, where monochromators select neutrons of some given wavelength out of a polychromatic beam before it hits the sample, in quasi-elastic or inelastic neutron scattering also the outgoing neutrons have to be passed through such a device for resolving energy differences, as neutron detectors in the thermal regime have no inherent energy resolution.⁴ These are called analyzers, and all aspects discussed here with respect to monochromators apply there as well.

B.1.3.3 Mechanical velocity selectors and choppers

Where in the section above the wave nature of neutrons has been utilized to select neutrons of a certain energy, the same is also possible with the particle nature. Devices operating in this mode are called mechanical velocity selectors. They are closely related to choppers, which have the primary purpose to select neutrons that pass a certain point at a certain time, so those will also be treated here.

The first mechanical velocity selector for neutrons consisted of two disks rotating on a common axis, where each disk was made up of alternating stripes of aluminium and cadmium sectors with shifted phase. For a given rotation speed, only neutrons with given velocities find an aluminium strip at the second disk after passing an aluminium stripe at the first disk. In essence, this is the same idea as used in Fizeau's determination of the velocity of light.

The problem with such a device is that due to the stroboscopic effect also neutrons with l times the fundamental wavelength for l odd can pass the velocity selector by skipping a few aluminium stripes. Today, such velocity selectors therefore have the form of a drum with helical absorbing blades on it, thereby eliminating higher-wavelength contaminations. Obviously, the transmitted spectrum has a relative width of s/l , with s the distance between blades and l the length. The transmitted velocity of such a helical velocity selector is continuously tunable by the rotational speed, which typically is a few hundred Hz.

A device consisting of a single disk of a Fizeau-type velocity selector is called a chopper due to its action of chopping a continuous beam of neutrons into pulses. It is used for providing the timing structure for time-of-flight instruments on continuous sources, for better defining the pulsing of pulsed sources, or for reducing frame overlap. Typically such choppers have only a single transparent slice, and for good definition of the window of transmission they are combined with a fixed slit immediately next to them or even a second counter-rotating chopper disk.

Another principle is constituted by the Fermi chopper: here the axis of rotation is not along the beam, but perpendicular to it, and in the original realization the

⁴Of course, this does not apply to time-of-flight or spin-echo instruments, where the energy is resolved via the velocity encoded in time.

transmitting element was a bore through the rotating block of absorbing material perpendicular to the axis of rotation. In addition to the pulsing, in this realization it provides also a cutoff towards low velocities, as the time window that a straight flight path is open is shorter than the time slow neutrons would need to pass. Today, Fermi choppers typically use Soller-type collimators (see below). For curved collimators, the chopper functions also as velocity selector, as in this case there is only a given window of velocities that can travel through the rotating curved collimator on a straight path. Further, a Fermi chopper can directly be used for temporal focussing, so that neutrons of different velocities arriving from different directions arrive at the detector at the same time, assuming elastic scattering at the sample.

Choppers typically have to be operated at the limit of mechanical stability in order to give desirable timing structures. In general, this is most easily fulfilled for slow neutrons. Due to the compact design, Fermi choppers show the best performance in this regard.

A related device that is able to give very sharp pulses also at short wavelengths is a rotating crystal chopper, which reflects a neutron beam that rotates like the light beam of a lighthouse. At a given take-off angle, the resulting pulse has a length of equal to the divergence (determined by incident collimation and mosaicity) divided by the rotating frequency.

B.1.3.4 Collimators

At various stages of a neutron scattering instrument, for a good performance it is necessary to control the angular divergence of the neutrons. In principle, on the source side this can directly be effected by the dimensions of the beam tube, with the exit window defining the size of the spot on the sample, and the beam tube length and entrance window dimensions defining the divergences in horizontal and vertical dimensions. Apart from the fact that an analogous approach on the detector side would need to dictate the size of the detectors (which often are not freely scalable), it would also be impractical due to the necessary beam tube lengths and the fact that the divergences cannot be varied after the construction of the instrument. Therefore, one rather uses dedicated collimators, which cut out the desired volume of phase space (in this case, specific distributions of directions in the horizontal and vertical dimensions).

A Soller collimator (also called Soller slits) consists of a stack of parallel blades coated with an absorbing material. Only neutrons with flight paths that do not touch any of those blades can pass, which in the ideal case of infinitely thin totally absorbing blades leads to full transmission for neutrons that are parallel to the blades, decreasing linearly to zero for angular deviations

$$|\Delta\phi| = \alpha = \frac{w}{L}, \quad (\text{B.1.13})$$

with L the length of the blades along the beam path and w their separation. If for a given collimator the value for the divergence is quoted, it typically pertains to α as defined here, which is also the full width at half maximum of the triangular transmission.

Typically, at a given instrument a number of different collimators can be used, allowing to configure the divergence and thereby trading intensity for resolution. Also, it decouples the divergences in horizontal and vertical dimension. As mentioned already above, typically one wants small divergences only in the scattering plane, that is, in the horizontal dimension, so in most cases Soller collimators are oriented vertically.

In effect, a Soller collimator works as a number of parallel beam tubes with emitted beams that overlap at the sample. Obviously, one can consider also the analogous concept with neutron guides, which can be realised by evaporating nickel onto the absorbing blades. Naturally, as in the case of a neutron guide this gives rectangular transmission functions. Further, such a device consisting of curved blades can be used as a *beam bender*, being much more compact than a curved neutron guide, as the smaller blade separations guarantee much shorter paths between successive total reflections on the outside blades and therefore allow to use correspondingly smaller radii of curvature.

B.1.3.5 Energy filters

The main purpose of energy filters is to suppress unwanted minor components in a neutron beam whose energy spectrum has already been shaped in some way. For instance, while a crystal monochromator selects neutrons within a certain quite sharp window of wavelength around the nominal value, due to its working principle neutrons with an integral multiple of momentum are scattered in the same direction. Such contaminations could increase the background in neutron scattering experiments, or worse, lead to spurious peaks.

In principle, the filtering effect can be due to scattering processes or absorption processes. A neutron guide is effectively already a low-pass filter due to the variation of the critical angle of reflection with neutron energy. In the same way, high-pass filtering can be achieved by passing the beam through a mirror at low glancing angle and utilizing the transmitted neutrons.

A very effective kind of low-pass filter with a sharp cut-off is given by a simple piece of polycrystalline material with high coherent scattering cross section. Due to Bragg's law, neutrons can be scattered elastically with respect to those wavevector transfers that coincide with a reciprocal lattice vector of the crystal. For a polycrystal, these reciprocal lattice vectors lie on concentric spheres with some defined radii around the origin of reciprocal space. On the other hand, in elastic scattering the possible wavevector transfers for a given wavelength fall on a sphere in reciprocal space, the so-called Ewald sphere, which has the origin on its pole. As a consequence, for large wavelengths the Ewald sphere is too small to reach any sphere of reciprocal lattice vectors, and no elastic scattering will result. However, for shorter wavelengths the Ewald sphere starts to overlap with the spheres of reciprocal lattice vectors, meaning that there will be some crystallite in the polycrystal with respect to which the scattering conditions are fulfilled. In effect, this gives a transmission function with a sharp cutoff at some critical wavelength below which only a very reduced amount of neutrons is transmitted, which is given by $\lambda_c = 2d_{\max}$, with d_{\max} the maximum spacing of lattice planes

(for instance $a/\sqrt{2}$ in a bcc crystal and $a/\sqrt{3}$ in an fcc crystal). Due to the lattice spacings of available crystals, λ_c is typically in the cold neutron region, with the smallest values of 3.96 Å in Be and 4.38 Å in BeO.

For optimal transmission above the threshold, such polycrystalline filters often have to be cooled well below their Debye temperature to suppress inelastic scattering, which is not tied to the Bragg condition. On the other hand, for filtering in the epithermal regime one can rather use single crystals out of the Bragg condition and rely on inelastic scattering, with sapphire (Al_2O_3) as the most prominent representative, having high transmissions above 1.0 Å and transmissions below 3% below 0.4 Å.

In the thermal region, single crystals of pyrolytic graphite are the most prominent beam filters. Oriented with the c -axis normal to the beam, they transmit neutrons of $\lambda = 2.36$ Å quite efficiently while strongly suppressing $\lambda/2$ and $\lambda/3$ contributions.

At higher energies, resonant absorption becomes attractive as filtering method. For instance, ^{239}Pu has a resonance around 300 meV, which can be used to suppress the $\lambda/2$ (i.e. $4E$) contribution of a monochromator set to 75 meV, which corresponding to $\lambda = 1.04$ Å.

Note that such filters can also make efficient energy analyzers. For instance, the density of states of vibrations of an incoherent scatterer (that is, in most cases hydrogen) can be determined by scanning the incident energy by a monochromator and detecting the outgoing radiation after a polycrystalline graphite filter (backed up by Be for better suppression of higher energies). Only energies below 2 meV can pass such a filter, which corresponds to a satisfactory energy resolution, and much higher detector acceptances than in the case of a single-crystal analyzer can be used.

B.1.3.6 Polarizers

Just as a monochromator yields a monochromatic beam by discarding all other neutrons, a beam can be polarized by selecting only neutrons of one of the two possible spin eigenstates (remember that the neutron is a spin 1/2-particle). The two microscopic effects that can be utilized for this end are the spin-dependent coherent scattering cross section due to the unpaired electrons in ferromagnetic materials or spin-dependent absorption cross sections.

As regards the first option, all principles have already been treated above in the non-spin-dependent cases. Specifically, ferromagnetic monochromators can be tuned to have a vanishing structure factor for one spin channel, reflecting purely neutrons of the other spin state, conversely the efficiency of the Bragg-cutoff of a ferromagnetic polycrystalline filter depends on the relative spin orientation, transmitting preferentially one spin state, and finally the neutron index of refraction of a ferromagnetic material depends on the spin state, giving different angles of total reflection. The last effect is best exploited by Fe-Si-supermirrors, most effective a cold wavelengths. However, this becomes even more practicable when using a ferromagnetic beam bender (corresponding to a curved Soller collimator), decreasing the dimensions from a few meters for a supermirror (due to the small

angles of total reflection) to a few tens of centimeters.

Polarizing absorption filters rely on resonances in the low-energy region, with ^{149}Sm as an example. Such filters rely on the orientation of the nuclear spins, which due to the energy scale of nuclear moments in a field reaches significant values only at the highest achievable fields in the range of tens of mK. Another option is to use ^3He gas, which can be polarized by optical pumping with a laser at low pressures. For good polarizing efficiency at practical dimensions, the gas is then compressed above atmospheric pressure. In this state, the polarization of the ^3He nuclei decays on the order of days. At a ^3He polarization of only 55%, a beam polarization of 80% at transmissions of 20% can be reached.

B.1.3.7 Spin guiding and manipulation

In a magnetic field, a magnetic dipole moment $\vec{\mu}$ experiences a torque

$$\vec{\tau} = \vec{\mu} \times \vec{B} = \gamma \vec{J} \times \vec{B}, \quad (\text{B.1.14})$$

with \vec{J} the vector of angular momentum and γ the gyromagnetic ratio. As

$$\frac{d\vec{J}}{dt} = \vec{\tau}, \quad (\text{B.1.15})$$

under a constant field this leads to *Larmor precession* of the magnetic moment around the axis of the field, with the Larmor angular frequency

$$\omega_L = \gamma |\vec{B}|. \quad (\text{B.1.16})$$

The neutron gyromagnetic ratio is $\gamma_N = 1.832 \times 10^8 \text{ rad s}^{-1} \text{ T}^{-1}$, therefore for instance at fields as small as $B = 0.1 \text{ mT}$ the neutron magnetic moment would precess with a frequency of about 2.9 kHz. The earth's magnetic field has this order of magnitude, and various electrical appliances around a neutron beam can increase the background field even higher. As a consequence, without taking precautions the well-defined polarization state of a neutron beam after a polarizer would quickly be lost.

The solution lies in having a guide field along the path of the neutrons. As long as this field is significantly larger than the magnetic background noise, the neutrons will precess around this field with conserved component along the guide field. Further, the polarization of the neutrons will follow a turning of the guide field if the rate of turning is much slower than the Larmor period, which is called *adiabatic guiding*. Assuming a guiding field strength of $B = 1 \text{ mT}$ and thermal neutron velocities of 2200 m/s, during the Larmor period of $t = 0.034 \text{ ms}$ the neutrons cover distances of 7.5 cm. In this situation, turning the field over distances on the order of 1 m would therefore happen adiabatically.

For scattering techniques utilizing polarized neutrons, it can be necessary to turn the polarization within a small distance, typically by angles of $\pi/2$ or π . Such devices are called $\pi/2$ - or π -coils, the latter also spin flipper.

There are a number of principles how such devices can be built: The first is to use a radiofrequency resonance coil as in nuclear magnetic resonance, which shall not

be covered in more detail here. Second, a current sheet spin-rotator consists of a thin sheet of metal with a current parallel to the guide field along it (for now assumed to be vertical). This leads to a configuration of a field slowly turning away from the guide field in the sheet plane by an angle of θ . As a neutron approaches the sheet, it follows this turning adiabatically. Passing through the sheet, it finds itself in a field in direction of $-\theta$ with respect to the guide field, and therefore acquires a further angle of θ as it adiabatically follows the field back to the vertical orientation. For a perfectly thin current sheet, in contrast to the radiofrequency resonance coil, this gives turning angles that are independent of the neutron velocity, as long as it is small enough for the neutrons to be able to follow the field adiabatically on both sides of the spin current sheet. However, the necessary large stray fields of this device render it disadvantageous.

In neutron scattering instrumentation, a popular type of spin rotator is the so-called Mezei coil, having the significant advantage over the radiofrequency coil in being a static device. It is a coil of rectangular cross section, oriented perpendicular to the neutron flight path. Inside the coil, the field is at an angle θ to the guide field, while outside there is no interference with the guide field. When for a specific neutron velocity the passage time through the coil is equal to half the Larmor frequency, the neutrons exit the coil with an acquired angle of 2θ with respect to the guide field.

B.1.3.8 Shielding

Not only for reasons of radiation safety, but also for reducing the background count rate in the detectors, it is necessary to suppress all possible flight paths of neutrons apart from the intended one from the source via the sample to the detector. In contrast to the case of X-rays, where one just has to generously distribute lead, shielding a neutron beam involves distinct physical processes, each of which needs for optimal efficiency different kinds of materials.

First, as neutron absorption cross sections vary as $1/v$, specifically the fast neutron contribution has to first lose its energy by elastic collisions.⁵ The singularly most effective element here is hydrogen, both due to the large incoherent scattering cross section and the small mass, enabling large energy transfers in a single collision.

Neutrons thus slowed down can be effectively absorbed. Elements with very high capture cross sections are Cd and a number of the rare earths, with Gd the most prominent example. These elements have isotopes with resonances in the thermal region, e.g. for ^{113}Cd at 178 meV, while it is practically transparent above 500 meV. In addition, those resonant absorption processes generate high-energy prompt gamma radiation. Therefore, one often rather uses the light elements Li and B, which also have rather large non-resonant capture cross sections (^{10}B has $\sigma_{\text{abs}} = 3835\text{b}$ at the standard thermal energy of 25.3 meV), and where the prompt gamma radiation is much weaker.

⁵Of course, microscopically this is the same process as in moderation, but different from the case of neutron moderation, the energies will not reach the thermal distribution here, as the neutrons will be absorbed before.

Finally, the gamma radiation due to the absorption of neutrons in the shielding or in the sample has to be absorbed in turn. In the MeV-range, the attenuation coefficient is roughly proportional to the mass density, where a few cm thickness of lead are necessary for a reduction by an order of magnitude.

In reactor neutron sources, the shielding around the moderator tank consists typically of about 1 m of heavy concrete, with added iron and boron. Around the detectors as well as separating the instruments from the control hatches on the ground floor thinner shielding is used, with boronated plastics often a main component. In this way, in modern facilities the gamma background is decreased to levels comparable to the natural background.

B.1.4 Neutron detectors

The final task in neutron experimentation is to detect them. Here, two of the neutron's properties that make them so valuable as scattering probes render the task of their detection much harder compared to the X-ray case. Specifically, on the one hand the charge neutrality that leads to small absorptions in general samples would also lead to small detection efficiencies. Therefore, neutron detectors invariably have to contain elements (or even isotopes) with anomalously large absorption cross sections in the relevant energy ranges. On the other hand, their kinetic energy is on the order of magnitude of phonon energies,⁶ which shows that it is in principle impossible to directly detect their kinetic energies. Thus, it is the MeV-range energies after capture reactions that are detected, which also implies that there are no neutron detectors with inherent energy resolution apart from the effect of resonances in the capture cross sections.

Apart from the large cross sections, one would like the capturing nuclei to follow the $1/v$ law to a sufficient degree, as well as to emit charged particles (with correspondingly small free path lengths in the detector). The most prominent isotopes with respect to these criteria are ^3He , ^6Li and ^{10}B , with the first emitting a proton and the other two an α particle. He and B (the latter in the form of the toxic gas BF_3) are typically used in gas detectors, while Li is used in solid-state detectors that employ the scintillation effect.

A popular type of detector is the gas tube detector. It consists of a tube of a conducting material and a few cm diameter, with a wire along the tube axis that is isolated against it. When now a neutron is absorbed in the detector gas, the emitted high-energy particles will ionize the gas. Keeping the wire at a positive voltage against the tube, the resulting electrons will be accelerated towards the wire and the resulting charges can be detected, with the number of the generated electrons being proportional to the energy deposited in the gas. For not too high voltages (a few keV), the accelerated electrons lead to further ionizations and thereby increase the proportionality factor, giving better energy resolution. In this proportional region, the detector can therefore selectively count events with energies characteristic for the nuclear reactions and discriminate against background gamma events. Dead times are on the order of one microsecond.

⁶That is, apart from fission neutrons, which however cannot be used as probes in most techniques.

For many neutron scattering techniques, it is desirable to have a detector covering a large solid angle, where also the positions of the neutron absorption events can be detected. A trivial possibility is to arrange a number of counters next to each other. For gas tubes as described above, this gives a detector with one-dimensional position resolution. However, by making the anode wire resistive, also information of the position along the detector axis is can be gained via the division of the charges on either end of the detector tube. Typically, the corresponding resolution is worse than the spacing between adjacent detector tubes, giving anisotropic two-dimensional resolution. Such multi-detectors are therefore suited for requirements as in powder diffraction.

An example for an isotropic gas detectors is the multi-wire proportional counter, where a fine mesh of anode wires is mounted between cathode plates. These cathode plates are segmented into conducting strips, where the two plates have perpendicular orientation of the strips. As a consequence, the two coordinates of the detection event can be determined by detecting which strips received the most charge. Such detectors are suited for instruments with isotropic resolution requirements such as small-angle scattering.

In recent times, there is a tendency to move away from ^3He . This is because its main source is from the decay of ^3H used in nuclear weapons. With the reduction in nuclear stockpiles since the end of the cold war, the supply is correspondingly decreasing, and prices have risen drastically. However, also the other option of BF_3 is problematic, as it forms hydrofluoric acid when it encounters water.

Solid-state detectors employ the scintillation effect, which is that specific ionic crystals emit flashes of light around the optical regime when energy is deposited into them. This process normally relies on a third element as dopant, so that the crystal is transparent to the radiation created at the defects. For neutrons, ^6Li -doped ZnS is typically used as scintillator. The time resolution of such detectors is not governed by the motion of ions, but rather by the electrons in the photomultipliers used to convert the light into currents. As a consequence, they can be much faster than gas detectors, and are therefore suited for pulsed sources. A disadvantage is the worse energy resolution, making them sensitive to a gamma background.

Apart from the possibility of arranging independent scintillator crystals/photomultipliers to make up a position-sensitive detector, an Anger camera consists of a large flat scintillator, to which a regular array of photomultipliers is coupled. Just as with the multi-wire counter, also here the position can be determined by computing the center of mass of the signals of the respective photomultipliers.

The image plate principle, which is a routine technique for X-ray detection, can also be used for neutrons by coating or dotting the material with ^6Li . An image plate consists of a phosphorescing material, integrating the absorbed radiation. After the exposure, a laser beam is rastered over the plate, emitting the stored energy as optical light via photostimulation. As in principle with all integrating detectors, there is no way to discriminate against gamma radiation. Image plates are advantageous for applications where good resolution over large solid angles is needed, but no time or energy resolution, such as for protein crystallography.

Apart from the main detectors that detect the neutrons exiting the sample, for techniques where for instance the outgoing energy is scanned over time it is necessary to keep track of the instantaneous flux. This is done by beam monitors. Such devices have to have a very low efficiency in order not to attenuate the incident beam.⁷ For this purpose, fission chambers can be used, where the flux is determined by the ionization currents of, for instance, low-pressure UF₆.

B.2 Neutron-based experimental techniques

As has transpired above already a few times, the neutron has a number of properties that make it a very useful probe for properties of condensed matter. First, its wavelength can be chosen to be on the order of interatomic separations. While this fact is not specific to neutrons, it is a very happy coincidence that such wavelengths correspond to neutrons with energies as can be extracted from a moderator around ambient temperature. From this it follows that the change in neutron energy due to the creation or annihilation of a typical thermal excitation of the sample is on the same order of magnitude as the energy of the neutron, and therefore can be conveniently resolved. Further, the absorption of neutrons in matter is often weak, leading to large penetration lengths. Finally, the value of the neutron's magnetic moment makes magnetic aspects of the system as easily observable as structural aspects. The main experimental techniques how these properties can be exploited to probe condensed matter will be presented in their principles here.

The focus in the presentation will lie on scattering methods, which is also where the major part of the neutron community is active. In these methods, the aim is to determine the probabilities for incoming neutrons to be scattered into distinct outgoing states, which are quantified by differential scattering cross sections. These methods can be divided into diffractometry, where only the change in neutron wavevector (called wavevector transfer \mathbf{Q}) is of interest, and spectroscopy, where also (or only) the change in energy is of interest. Conversely, scattering methods do not resolve absolute positions.⁸ On the other hand, for instance in radiography it is the absolute position that is the primary independent variable.

Generally, there are two principally different ways to perform neutron scattering experiments. First, there is the conventional approach with a continuous beam, which is analogous to all methods of X-ray scattering. However, as neutrons are massive probe particles, there is a correspondence between their velocity and energy. As a consequence, when one has a pulsed beam (either intrinsically at a pulsed source or by chopping a beam from a continuous neutron source), one can forego one step of enforcing narrow energy windows in the incident or outgoing neutrons and instead use the full spectrum at once and determine energies via the time of arrival at the detector. This is called the time-of-flight approach. The specifics of these methods will be discussed at the example of powder diffraction, but they hold analogously also for the spectroscopic methods treated later.

⁷The incident flux is typically orders of magnitude larger than the scattered signals, so counting statistics are no issue here.

⁸Of course, an inhomogeneous sample can be scanned through the beam, giving spatially varying differential cross sections.

B.2.1 Powder diffractometry

Diffractometry is the study of the probabilities for incident neutrons to experience changes in wavevector when interacting with a sample. In powder diffractometry, the sample is a fine powder of crystalline material, but with some caveats also polycrystalline samples can be used. As all orientations of grains are equally probable, only the absolute value of the wavevector transfer, a one-dimensional quantity, is the independent variable. The defining features of a powder diffractogram are the intensities, positions and shapes of the Bragg peaks, which correspond to elastic scattering. Inelastic scattering, for instance due to thermal oscillations of the atoms (phonons), give smoothly varying intensities over all of reciprocal space, which in this regard is subsumed into the background of the signal. As a consequence, the neutrons that contribute to the signal, that is to the Bragg peaks, can safely be assumed to have had equal energies on the incident and outgoing side.

For a given elastically scattered neutron, the absolute value of the wavevector transfer is determined by the scattering angle

$$|\mathbf{Q}| = 2|\mathbf{k}| \sin(2\theta/2), \quad (\text{B.2.1})$$

where \mathbf{k} is the wavevector of the neutron (and which is determined by its direction of propagation and its energy or equivalently wavelength).

At continuous beams, the energy is defined typically by a crystal monochromator. In practice, this is always done on the incident rather than the outgoing side, as this first reduces the neutron flux on the sample (and consequentially activation and background), and second allows to use a multidetector for optimal neutron economy.⁹ Specifically, often a bank of vertically arranged gas tubes is employed. The resolution is defined by Soller collimators before and after the monochromator, as well as by a collimator in front of each gas tube. This greatly reduces the background and gives resolutions that are independent of the diameter of the sample.

For having high count rates, high sample volumes are desirable, with dimensions typically a few cm in height and 1 cm in diameter. Resolution can be traded for intensity in some degree via the collimations and the used wavelength. Typical resolutions are on the order of 10 arc minutes. For practical reasons, the angular stepping of the respective gas tubes is on the order of a few degrees, so in order not to miss any features of the signal, one drives the multidetector in steps on the order of the resolution. It is advisable to use some overlap here: As the distinct gas tubes will have different counting efficiencies as well as unavoidable misalignments of their collimators, such a multidetector has to be calibrated. The adequacy of the calibration can be ascertained by checking whether the overlapping curves coincide. As a sophistication, also the (low-resolution) vertical position of the events can be determined by position-sensitive gas tubes. This allows to correct in first order for the peak asymmetries due to the incompatibility of curved Debye-Scherrer cones and straight gas tubes.

⁹In contrast, in X-ray diffractometers normally only a single detector is scanned around the sample, as statistical precision is no issue here.

For pulsed beams, one can use a much larger spectral window of the incident beam. Conceptually, as for a given pulse the neutrons were emitted at the same known time, all neutrons that hit the detector at some specific later time have the same known velocity, given by the path from source to detector divided by the time of flight, and thereby energy and wavelength (as all scattering is assumed to be elastic). Thereby, the instantaneous readout corresponds to the diffractogram for some specific wavelength. At a later time within the same pulse, the diffractogram for a longer wavelength is obtained. In practice, all these data are reduced in software to a single diffractogram with \mathbf{Q} as the independent variable. As a consequence, also the expressions for the Lorentz factor (to be defined later) and peak shape are more complicated than for diffractometry with a monochromated beam.

A concept that is critical to the successful operation of a time-of-flight instrument is *frame overlap*: This means that with a finite pulse repetition rate, there is some critical velocity so that slower neutrons would arrive at the detector later than the fastest neutrons from the following pulse. Of course, this would give a contamination of the data and therefore has to be prohibited. By doing the math, one arrives at the result that for given length of flight path L and pulse repetition frequency ν , there is a maximum window of incident wavelengths without frame overlap

$$\Delta\lambda = \frac{h}{m_n L \nu} \approx \frac{4000 \text{ \AA m/s}}{L \nu}, \quad (\text{B.2.2})$$

which can be enforced with velocity-defining choppers. In diffractometry one typically wants much better resolution than in spectroscopy, which implies long flight paths. In order to avoid frame overlap, one therefore has to work at quite narrow wavelength bands or use choppers to remove whole pulses from the incident beam, thereby decreasing ν . Depending on the range of scattering angles covered by the detector, it can be advantageous to perform experiments at different wavelength bands for different ranges of \mathbf{Q} to be probed with high resolution and statistical accuracy.

B.2.2 Single-crystal diffractometry

If a single crystal of a given system is available, its elastic scattering signal conveys more information than the corresponding powder signal. Specifically, the assignment of peaks to reciprocal lattice points is trivial, and anisotropic peak shapes are directly accessible.

The classical instrument for such high-precision measurements is the *four-circle diffractometer*. Here the crystal is mounted on a Eulerian cradle, which allows to turn the crystal into any orientation. In the typical configuration the crystal is mounted on the goniometer head, with the degree of freedom corresponding to a rotation with respect to this goniometer head conventionally called ϕ , the goniometer head itself can drive around the χ circle, so that the crystal always stays in the center of the χ circle, and finally the plane of this circle can be rotated around the vertical axis, corresponding to ω . The fourth circle is described by the position of the point detector in the horizontal plane with scattering angle 2θ . With

a monochromatic incident beam and narrow collimation, such diffractometers give the best Q resolution achievable, albeit at the cost of long measurement times.

A disadvantage of the four-circle diffractometer is its incompatibility with any non-ambient sample environments, such as cryostats, furnaces, pressure cells or magnets. Here the *normal-beam geometry* constitutes an alternative, where the only degree of freedom of the sample is a rotation around the vertical axis ϕ , which can either be performed by mounting the sample on a rotatable stick that reaches into the sample environment cell, or rotating the sample environment with the sample. The third degree of freedom necessary for reaching all of reciprocal space at fixed wavelength is constituted by rotating the detector arm out of the horizontal plane.

In such point-detector instruments, only the regions of interest, that is, often only the vicinities of the Bragg peaks (the positions of which are known once the crystal is oriented), are scanned. A more complete survey of reciprocal space at the cost of worse resolution is obtainable by using an area detector. In the extreme opposite case, also the requirement of monochromatization is dropped, leading to the *Laue method*. Here an incident white beam is used in order to fulfill the scattering conditions for all reflexes at the same time. In this way, samples can quickly be checked for single-crystallinity as well as be oriented. However, if a given reciprocal lattice vector fulfills the scattering conditions with some wavelength, then any multiple of it will also fulfill it with a correspondingly reduced wavelength. These intensities coincide on the detector, therefore prohibiting a quantitative determination of peak intensities.

The so-called *quasi-Laue method* constitutes a middle ground. Here a narrow incident wavelength band is used, which for not too dense reciprocal crystal lattices ensures the absence of overlaps and thereby allows the determination of peak intensities at high efficiencies. However, such a method suffers from quite high background levels due to the diffuse scattering in the regions between the Bragg peaks.

With pulsed beams and the time-of-flight method, it is of course possible to cover whole regions of three-dimensional reciprocal space with one crystal setting without overlap in the Laue setting, i.e. with a white beam.

A further field of single-crystal diffractometry is *protein crystallography*. The goal with this experimental method is to solve the structure of the proteins making up the repeating cell of the crystal rather than the repetition itself. As a consequence, it is the envelope of the Bragg peaks that has to be sampled over large areas of reciprocal space, which is invariably done with area detectors.

Finally, the study of elastic diffuse scattering, e.g. due to short-range order, deserves mentioning. While this is in principle a problem of diffractometry, such diffuse intensities are much lower than Bragg peaks and on the same order as thermal diffuse scattering, which is what one calls inelastic scattering due to, e.g., phonons when one does not have energy resolution. Thus, while compared to Bragg peaks this thermal diffuse scattering contributes only to the background, here one actually needs to perform energy analysis in order to extract the purely elastic part. This is therefore done with spectroscopy set-ups.

B.2.3 Small-angle scattering

Probing correlations at small \mathbf{Q} and thereby large real-space scales is, according to Eq. (B.2.1), the domain of *small-angle scattering* (SANS for small-angle neutron scattering). Specifically, by using cold neutrons and sample-detector distances up to a few tens of meters, \mathbf{Q} from 1\AA^{-1} to below 10^{-3}\AA^{-1} can be achieved. At continuous-beam instruments, tight incident collimation is necessary for achieving acceptable resolutions, which leads to the lengths of such instruments being on the order of 100 m. On the other hand, the energy resolution is set to quite coarse values of around 10% by helical velocity selectors in order to have high fluxes at the sample. In contrast, with pulsed beam and the time-of-flight technique, the resolution is effectively only dictated by the collimation. Scattered neutrons are detected at area detectors with ideally isotropic resolutions. Different ranges of probed \mathbf{Q} are accessible by driving the detector along the direction of the beam. This is done within an evacuated flight tube in order to avoid absorption in air. Where the direct beam would hit the detector, an absorbing beam stop is positioned, as the high intensities of the direct beam would harm the detector.

In conventional SANS as opposed to grazing-incidence SANS (see below), transmission geometry is used. For systems with correlations in the small-angle regime, the associated differential cross-section can become quite large. Thus, for avoiding significant contributions due to multiple scattering, often sample thicknesses in the mm range have to be used. This is in contrast to most other cases of neutron scattering, where small-angle scattering events that can be resolved here vanish in the forward direction. Often, soft matter samples with isotropic scattering signals are investigated, allowing to reduce the detector read-outs to one-dimensional diffractograms.¹⁰

B.2.4 Reflectometry

The properties of surfaces and thin films can be studied by reflectometry. Specifically, the intensity of the specular reflection as a function of \mathbf{Q} encodes the variation of the scattering length density with depth, where the specular reflection corresponds to a symmetric path of the neutrons with respect to the surface normal. Neutron reflectometers are normally set up so that the scattering plane is vertical, which facilitates studies of liquid films. At continuous sources with monochromatic beams, it is necessary to rock the sample to detect the reflection curve, while for pulsed white beams the time-of-flight method allows to determine it with fixed detector position and sample orientation. Here it is possible to incline the incident beam with respect to the horizontal direction, allowing to study liquid surfaces, which are horizontal due to gravity. Another main field of study is the magnetism of thin films, done by polarized reflectometry.

If the samples are not homogeneous within the surface plane, off-specular intensity occurs. This is then called grazing-incidence small-angle neutron scattering (GISANS), where both the shapes as well as the correlations of particles on a sub-

¹⁰Note that somewhat inconsistently to the diffractometry/spectrometry distinction, here often the data are also called “small-angle spectra.”

strate, or more general inhomogeneous films are investigated. As in conventional small-angle scattering, the intensity is detected by an area detector.

B.2.5 Triple-axis spectrometry

The purpose of a triple-axis spectrometer (TAS) is to study the intensity at a given point in (\mathbf{Q}, ω) space. Classically, it has been typically used to determine phonon or magnon dispersion relations, but in more recent times weak excitations beyond those fundamental ones have been increasingly studied. As it can measure only one point at a time, its great flexibility and resolution is paid for by long measurement times. In contrast, when larger regions of reciprocal space are of interest (or when one wants to be sure not to miss anything outside of the high-symmetry directions typically measured with TAS), time-of-flight spectrometers are a better choice. Along the same reasoning, it is nearly always single crystals which are measured at these instruments. Triple-axis spectrometers use either thermal (for high count rates) or cold (for high resolution) neutrons. Specifically for studying magnons with high ω at low \mathbf{Q} also instruments at hot sources can be the best choice.

A triple-axis spectrometer has crystal monochromators and analyzers both before and after the sample. Therefore, it can detect energy transfers between the neutrons and the sample. Further, the scattering angle can be varied, and the sample can be rotated around the vertical axis. The three axes correspond to the vertical axes through, first, the monochromator, around which monochromator and the rest of the instrument is turned, second through the sample, around which the sample itself and the analyzer and detector are turned, and third, through the analyzer, around which the detector is turned. Of course, at the monochromator and analyzer always $\theta/2\theta$ -configurations are used, so that these three axes correspond to four degrees of freedom. Further, along each of the four straight sections of the flight path from source to detector there is a collimator. The detector will typically be a vertical gas tube.

In effect, a TAS allows to freely set the incident wavevector relative to the crystal lattice by the monochromator angle (length) and the sample rotation (orientation), as well as the outgoing wavevector by the analyzer angle and the rotation of the analyzer position with respect to the crystal lattice. Thereby, wavevector transfer and energy transfer are decoupled. Indeed, it can be seen that in the two-dimensional scattering plane incident and outgoing wavevectors correspond to four degrees of freedom, while wavevector transfer and energy transfer only to three. Therefore, there is one degree of freedom left. For reasons of more direct correspondence between counting rates and fundamental properties, often this is used to keep the length of the outgoing wavevector, that is, the energy at the detector, fixed.

For studying dispersion relations, typically scans through the excitation in (\mathbf{Q}, ω) space are done. Here there are two main possibilities: The so-called constant- \mathbf{Q} scans are more typical, where a given wavevector transfer is set and the energy is scanned. The result of such a scan is then the energy of the excitation at the corresponding \mathbf{Q} . The other main possibility is the constant- E scan, where for a

constant energy transfer \mathbf{Q} is varied. Which of those two is more advantageous is determined by the slope of the dispersion at the point of interest: If the dispersion is steep, a constant- E scan will show a sharp minimum, while a constant- \mathbf{Q} scan will show an ill-defined peak. At flat regions of the dispersion, the situation will be reversed.

Setting the spectrometer to a given point in (\mathbf{Q}, ω) space entails solving the constituting equations for the four axes corresponding to the degrees of freedom. Nowadays, this is done by a computer program. Also, it is advisable to do a simulation of the necessary axes positions before each scan, in order to check whether these are in principle possible (the values of the incident and outgoing energies limit the wavevector transfer \mathbf{Q} and vice versa) and practically possible due to available floor space. Mechanically, the driving is effected by air pads on a so-called “tanzboden”, that is, a granite floor polished to very high smoothness. If pressurized air is released into the air pads, the massive arms of the spectrometer can be moved by motors easily, and switching off the air once the positions are reached makes them immobile.

The resolution function of a TAS quantifies the sampling density over (\mathbf{Q}, ω) space for a given nominal spectrometer setup. This means that if, for example, monochromator and analyzer are set to accept a nominal energy difference ΔE , also neutrons that experienced slightly different energy transfers at the sample would be counted with some probability. Now this resolution function over four-dimensional space is quite complicated. In the typical approximation it is assumed to be given by a multivariate Gaussian distribution, colloquially called the *resolution ellipsoid*. Specifically, in general there will be some correlation between the components of \mathbf{Q} and ΔE . For optimally resolving the dispersions, it is desirable to perform the experiments so that the long axis of the resolution axis is parallel to the dispersion, which is called the focussing condition. This can imply a choice between the energy-gain and energy-loss branches of the dispersion.

B.2.6 Time-of-flight spectrometry

In contrast to diffraction, where the assumed elastic nature of scattering leads to the time of flight defining the energy of neutrons detected from a pulsed source unambiguously, with inelastic scattering the energy transfer at the sample makes it necessary to define the neutron energy either at the incoming or the outgoing side. The corresponding time-of-flight spectrometers are said to be operating in direct or inverted geometry, respectively.

Specifically, a time-of-flight spectrometer always starts with a pulsed white beam, either intrinsically at a pulsed source or defined by a chopper at a continuous source. In direct-geometry instruments, this white beam is then monochromatized either by a monochromator or by a second chopper at some distance. In the latter case typically also further choppers are used in order to suppress higher-wavelength contaminations. At continuous sources, the monochromatization and pulsing can be performed at the same time by using a rotating crystal chopper. The pulsed white beam is then passed onto the sample, and the energy transfers are detected by the time of flight to the detector over a distance of up to a few

meters.

In inverted geometry, the white beam pulse is passed onto the sample over a flight path that encodes the incoming neutron energy into the time when it hits the sample. On the outgoing side the neutrons are then monochromatized to a fixed energy, either by a crystal via Bragg scattering or via an energy filter, and counted. Here early neutrons are those that arrived early at the sample, therefore were fast on the incoming side and experienced a large energy loss to fit into the energy window enforced on the outgoing side. This is in contrast to the direct-geometry instruments, where early neutrons are those that experienced an energy gain at the sample to make them fast on the outgoing side. A disadvantage of inverted-geometry instruments compared to direct geometry is the higher flux on the sample and therefore larger background and activation.

Specifically for the direct-geometry instruments, there are neither analyzers nor collimators on the outgoing side between the sample and the detectors. Therefore one can cover as much of the solid angle with detectors as funds allow, giving high integral count rates. With a flight path of a few meters, already a simple array of gas tubes has a good resolution of direction. With such an instrument, the scattering signal resolved with respect to time of flight for a given sample orientation gives a curved three-dimensional cut through four-dimensional (\mathbf{Q}, ω) space. Turning the sample allows to cover all four dimensions. Therefore, such instruments are most suited when information over large regions of (\mathbf{Q}, ω) space is desired. Such data make impressive illustrations, but in their richness can be hard to get an overview of. Further, the resolution varies non-trivially over four-dimensional space.

B.2.7 Backscattering spectrometry

Diffusive motion leads to a broadening of the elastic line, the so-called quasi-elastic scattering. In order to detect these effects, small energy transfers (below a few meV) have to be resolved with a resolution on the order of a few μeV . This is the domain of backscattering spectrometers. Their name comes from the fact that due to Eq. (B.1.11) a crystal monochromator or analyzer gives the best resolution under the condition of backscattering, that is, $\theta = \pi/2$.

With backscattering spectrometers, the neutrons are reflected back from the analyzers and have to pass very closely next to the sample or even through it on their way to the detectors. Therefore, there is no geometric possibility to separate the analyzed neutrons from those that are scattered from the sample directly into the detectors. As a consequence, also on continuous sources a chopper is used to discriminate those two cases by the time of flight.

For reasons of efficiency, a number of analyzer-detector pairs are arranged around the sample, giving the quasi-elastic signal for different \mathbf{Q} . These analyzers are operated at constant energy, therefore the energy transfer has to be scanned on the incident side. This can be done either by driving the backscattering monochromator periodically back and forth and using the Doppler effect, by heating the monochromator and thereby changing the lattice constant, or at

pulsed sources by using the time-of-flight method with very long flight paths.

Due to the necessity of defining the energies with very high resolution, only a very small part of the moderated neutron flux can be used. Therefore count rates at such instruments are very low and the durations of experiments are long.

B.2.8 Spin-echo spectrometry

The spin-echo effect is a quite different way how energy transfers of neutrons can be detected. To begin with, assume a neutron beam along the x direction having some spectral width, into which a polarizer and analyzer, both set to longitudinal polarization, are inserted. Let there be a homogeneous longitudinal field. If now two $\pi/2$ spin rotators, the first from longitudinal x to transversal z direction and the second back to x , separated by a macroscopic distance, are inserted into the beam, the intensity will be decreased (essentially to half its value), as the neutrons will have performed many cycles of Larmor precession within the y - z -plane between the two spin rotators, so that their effective phase $\exp(i\phi)$, which depends sensitively on the velocity of the respective neutron, will be undefined. However, when a π spin flipper with respect to the y component of the spin is additionally inserted *exactly* between the two $\pi/2$ rotators, the full intensity should ideally be recovered. This is because if a neutron of some velocity v should acquire an angle $\phi(v)$ (up to multiples of 2π corresponding to full rotations), the action of the π flipper is just to subtract this angle. This is true for any neutron velocity v (provided the spin flipper and the rotator function independent of v). This focussing, where the depolarized neutrons meet at the second rotator again with equal polarizations, is called the *spin-echo effect*.

In a spin-echo spectrometer, the two precession paths are realized as coils, with a low field region in between.¹¹ The sample is placed there, next to the π flipper, and the outgoing arm is rotated with respect to the incoming arm to some scattering angle 2θ . If a given neutron is scattered elastically, it will fulfill the spin-echo condition and be counted. On the other hand, if it experiences some small energy transfer in the quasi-elastic at the sample, the flight time through the second coil will be affected, leading to a depolarization and decreased counting probability. Note that, different from the presentation above, experimentally it need not be guaranteed that the two flight paths have the same length, it suffices if the product of field and length is equal.

The total accumulated phase along a path of length l and field B according to Eq. (B.1.16) is

$$\phi = \gamma_N \frac{Bl}{v}, \quad (\text{B.2.3})$$

and for two arms with a π flipper in between it is

$$\Delta\phi = \gamma_N Bl \left(\frac{1}{v_1} - \frac{1}{v_2} \right) \approx \gamma_N Bl \frac{\Delta v}{v^2} \quad (\text{B.2.4})$$

¹¹The more obvious solution, where opposite field polarizations instead of a π flipper give rise to the spin-echo effect, is not practicable, as the necessary field-free region between the coils would lead to a degeneracy of neutron spin states there.

if $\Delta v = v_2 - v_1$ and $|\Delta v| \ll v$. On the other hand, the energy transfer is given by

$$\hbar\omega = \frac{m_N}{2}(v_2^2 - v_1^2) \approx m_N v \Delta v, \quad (\text{B.2.5})$$

therefore

$$\Delta\phi = \frac{\gamma_N B l \hbar\omega}{m_N v^3}. \quad (\text{B.2.6})$$

Defining the spin-echo time as

$$t = \frac{\Delta\phi}{\omega} \quad (\text{B.2.7})$$

shows that setting the instrument to a certain value of $B l$ at some mean neutron velocity v corresponds to measuring the intensity for a spin-echo time

$$t = \frac{\gamma_N \hbar B l}{m_N v^3}. \quad (\text{B.2.8})$$

With increasing t , depolarization becomes more severe, and therefore intensity decays. The scale of this decay in t can therefore be interpreted as the timescale of the fluctuations giving rise to the quasi-elastic broadening.

Due to the spin-echo effect, the resolution of such a spectrometer is (in first order) independent of the used wavelength spectrum. As a consequence, it can be used to probe timescales (or energy transfers) that cannot practically be reached by backscattering spectrometers. With typical values of $B l$ below one Tm and using cold neutrons, spin-echo times on the order of a few tens of ns can be reached at relative wavelength spreads on the order of 10%. Of course, such coarse monochromatization also limits the \mathbf{Q} resolution.

Above values correspond to the neutrons performing a few tens of thousands of cycles in incoming and outgoing precession coils. Therefore, for the spin-echo effect to work, the fields have to be stable and homogeneous to better than 10^{-5} . This constitutes the main challenge in building and operating a spin-echo spectrometer.

B.2.9 Incoherent spectrometry

Different from the cases treated above, where the energy transfer is always considered for a given wavevector transfer \mathbf{Q} , specifically for the case of incoherent scattering the signal does not depend on \mathbf{Q} . In this case it is obviously desirable to cover as large a solid angle as possible. The so-called beryllium filter spectrometers give a simple solution to this problem. In principle, these spectrometers are analogous to triple-axis spectrometers where the energy analysis is performed by a beam filter, prototypically a polycrystalline beryllium or beryllium oxide block. As discussed in B.1.3.5, these filters have a fixed window of transmission below their cutoff wavelength, which is independent of the direction the neutrons pass through. Thus, the detector can be very close to the sample and cover a large part of the solid angle.

Scanning the incident energy gives the inelastic spectrum on the energy-loss side. For instance, it can be used for studying the vibrational spectra of hydrogen in molecules, which, due to the cross sections of ^1H , is nearly purely incoherent.

B.2.10 Neutron radiography

In contrast to the scattering methods, which give information resolved in reciprocal space, radiography studies the spatial structure of samples in real space. In the most simple case, it consists in measuring the transmitted intensity as the beam is scanned over the sample. Using a spatially resolved detector with a collimated wide beam is more efficient. Another option is to use a divergent beam with the pinhole camera principle, giving an enlarged image at the detector and therefore an increase in spatial resolution. Values on the order of $100\ \mu\text{m}$ are typical.

The advantages of neutron radiography over X-ray radiography include the higher penetration of neutron as well as the ability to resolve also light elements. As in the X-ray case, by acquiring a series of transmission images as the sample is rotated through the beam, the three-dimensional absorption density can be reconstructed from the transmission images, which correspond to projections of the three-dimensional density, by tomographic techniques.

There are other possibilities besides the absorption contrast: For instance, a Talbot-Lau interferometer consists of two absorption gratings on either side of a phase grating. The phase grating leads to periodic diffraction maxima under small angles. Depending on the configuration of the two absorption gratings with respect to each other, these maxima either pass through the gaps, giving high intensity, or are blocked by the second absorption grating, giving low intensity. When a sample that produces small-angle scattering is inserted into this interferometer, the additional scattering smears the interference effects. Thus, images of inhomogeneities that give scattering on the corresponding order of magnitude can be obtained. This technique is analogous to dark-field imaging in transmission electron microscopy.

B.2.11 Activation analysis

Neutrons can also be used to determine the composition of samples. There are two options: On the one hand, in neutron activation analysis the sample is irradiated by neutrons, for instance by placing it into the reactor pool, and afterwards the emitted γ radiation spectrum is measured. As each radioactive decay has specific transition energies, the peaks in the energy spectrum can be assigned to those transitions and correspondingly to the isotopes the initially corresponded to. With this technique, only isotopes that have not too small absorption cross sections as well as that become radioactive with practicable lifetimes can be detected.

The latter restriction is lifted by prompt gamma activation analysis: Here the prompt γ spectrum is acquired, that is, the emitted photon energies as the sample is in the beam. Here it is not (only) the radioactive transition energies that are sampled, but the energies corresponding to the capture of neutrons by the nuclei.

The unique property of these methods is their ability to detect trace elements or the isotopic make-up of samples non-destructively. For instance, this can be used to match archeological artifacts to ore deposits. In contrast, if it is the chemical composition that is required, and if at least small parts of the sample can be sacrificed, other methods can give results with better precision and accuracy.

Chapter C

Theoretical descriptions of scattering

C.1 Theories of weak elastic scattering

According to the de Broglie hypothesis, also massive particles behave in some aspects, specifically those that are relevant for the interaction with matter at low energies, as if they had a wave nature. Thus, moderated neutrons display non-trivial scattering phenomena. While the actual microscopic theories differ, the most fundamental principles are common to all kinds of scattering, be it of massive particles or electromagnetic waves. As a motivation for the detailed theory of neutron scattering to be derived below, these principles will be presented here, specifically the scattering of scalar waves from static potentials.

C.1.1 Huygens-Young-Fresnel theory

Towards the end of the 17th century, the nature of light was a prominent question. On the one hand, specifically Isaac Newton, motivated by his studies of the separation of white light into colours, propagated a particle view. On the other hand, it was known that rays of light are refracted at boundaries between different media according to Snell's law, which was understood as a special case of Fermat's principle, stating that any observed path of rays correspond to local extrema of the time taken.

To put Fermat's principle on a more fundamental basis, and specifically to explain the phenomenon of birefringence, Christiaan Huygens (1690) proposed that the propagation of light has a wave-like and thus transversally extended nature, in marked contrast to the geometric paths inherent to corpuscular theories. In his hypothesis, a point source of light initially emits a circular wave. Each point on the crest of this wave then emits secondary circular wavelets, and the new wave surface is constituted by the envelope of these wavelets. Iterating this process

with infinitesimal step sizes yields the observed geometric behaviour of rays of lights.

The main deficiencies of this theory lie first in the additional requirement that the wavelets contribute only where they touch the envelope and not radiate in other directions, and second that only the forward envelope is allowed. This was solved by Augustin Fresnel (1818), who abandoned the idea of propagating pulses corresponding to the secondary wavelets in the original theory in favour of temporally continuously varying wave trains, with the resulting wave given by interference, another new effect which had been demonstrated by Thomas Young (1802). This theory predicts also non-rectilinear propagation phenomena near edges, which subsequently were experimentally verified.

The validity of this theory for both electromagnetic radiation and massive particles such as neutrons in the quantum-mechanical regime follows from the assumed spherical wavelets (and also plane waves) being solutions both to the Maxwell equations as well as the Schrödinger equation in vacuum.

C.1.2 A fixed point scatterer in an incident plane wave

As motivated above, given appropriate initial and boundary conditions radiation (from now on understood to include both electromagnetic waves as well as massive particles at the relevant energies) will propagate in vacuum as plane waves

$$\psi(\mathbf{r}, t) = e^{i(\mathbf{k}_i \mathbf{r} - \omega t)}, \quad (\text{C.1.1})$$

with $\omega/|\mathbf{k}_i| = \omega/k = v$ being the phase velocity.

Consider now the spatial homogeneity of the vacuum being broken by a static disturbance that is confined to a region around the origin ($|\mathbf{r}| < R$). For $|\mathbf{r}| > R$, the relevant wave equation of course still has to be fulfilled, but the solution will be modified with respect to the incident plane wave, with the difference being termed the scattered wave ψ_s . Due to the linearity of the wave equation, also ψ_s alone has to be a solution.

The disturbance is assumed to be static, so any explicit time dependence $e^{-i\omega t}$ can be factored out of the expression, which shows that also the spatial periodicity of the scattered wave has to be given locally by k . If now $R_s k \ll 1$, the scattering process is not sensitive to any internal structure of the disturbing potential. Thus, with the coupling between ψ_i and ψ_s being only through the potential that can be treated as a point-like disturbance at the origin, the scattered wave ψ_s has to be spherically symmetric around the origin, with a temporal amplitude given by the effect of ψ_i at $\mathbf{r} = 0$. Thus

$$\psi_s(\mathbf{r}, t) = -b \frac{e^{ik|\mathbf{r}|}}{|\mathbf{r}|} \psi_i(0, t) = -b \frac{e^{ikr}}{r} e^{-i\omega t} \quad (\text{C.1.2})$$

is a spherical outgoing wave, with the proportionality constant b called the scattering length. This spherically symmetric scattering is also called *s*-wave scattering, and is always adequate for the scattering of thermal neutrons from nuclei.

Now both for electromagnetic radiation and massive particles the scattered intensity is the absolute square of the scattering amplitude (in the latter case it corresponds to the spatial probability density of the particles). Thus, it is given by

$$I(\mathbf{r}) = b^2 \frac{1}{r^2}. \quad (\text{C.1.3})$$

This decay of intensity with squared distance from the scattering center is consistent with conservation of energy or particle number, respectively, as the area of the enclosing sphere grows accordingly. Obviously, the total scattering cross section is given by

$$\sigma_{\text{tot}} = 4\pi b^2. \quad (\text{C.1.4})$$

C.1.3 Extended scatterers and the Born approximation

The more interesting case is when the condition $Rk \ll 1$ is not fulfilled, so that the actual spatial structure of the disturbance, which in the above case was hidden in the scalar parameter b , has to be explicitly considered. In a first instance, consider an arrangement of point-like scatterers at positions \mathbf{r}_i with respective scattering lengths b_i . Conceptually, the task of solving the relevant wave equation can be approached by assuming an incoming plane wave that hits the distinct scatterers, which in turn send out circular waves. Then, these waves emanating from scatterer i will reach scatterer j , leading to secondary scattered waves, and so on. If the scattering is weak, this procedure can be expected to converge. The formal method corresponding to this sketched approach is called the *Born series*. Typically, this series is truncated after the first term, that is, it is assumed that each scatterer feels only the unperturbed incident wave. This is also called the *Born approximation*.

In the particle view of scattering, the regime of validity of the Born approximation can be easily understood. Specifically, it corresponds to the probability of any scattered particle to be scattered a second time instead of leaving the scattering volume, or equivalently of any incident particle being scattered at all instead of passing through the scattering volume unperturbed, being very small. As in the neutron case the scattering cross sections of the distinct scatterers are given by $4\pi b_i^2$ according to Eq. (A.2.7), this is the case if the summed scattering cross section of the ensemble of scatterers $4\pi \sum_i b_i^2$ is much smaller than the cross section of the volume over which they are distributed.

If the Born approximation is valid, there is a simple expression for the scattering from a static sample in the far field. Specifically, by summing up the contributions from all scatterers, the scattering field results as

$$\psi_{\text{s}}(\mathbf{r}, t) = - \sum_j b_j \frac{e^{ik|\mathbf{r}-\mathbf{r}_j|}}{|\mathbf{r}-\mathbf{r}_j|} \psi_i(\mathbf{r}_j, t) = -e^{-i\omega t} \sum_j b_j \frac{e^{i(k|\mathbf{r}-\mathbf{r}_j| + \mathbf{k}_i \cdot \mathbf{r}_j)}}{|\mathbf{r}-\mathbf{r}_j|}. \quad (\text{C.1.5})$$

Defining now the outgoing wavevector as

$$\mathbf{k}_{\text{f}} = k \frac{\mathbf{r}}{|\mathbf{r}|}, \quad (\text{C.1.6})$$

for $|\mathbf{r}| \gg R$ we have

$$k|\mathbf{r} - \mathbf{r}_i| \approx \mathbf{k}_f(\mathbf{r} - \mathbf{r}_i) \quad (\text{C.1.7})$$

and thus

$$\psi_s(\mathbf{r}, t) = -\frac{e^{i(\mathbf{k}_f \mathbf{r} - \omega t)}}{|\mathbf{r}|} \sum_j b_j e^{i\mathbf{Q} \mathbf{r}_j}, \quad (\text{C.1.8})$$

where the wavevector transfer is defined as

$$\mathbf{Q} = \mathbf{k}_i - \mathbf{k}_f. \quad (\text{C.1.9})$$

This relation between incident and outgoing wavevectors on the one hand and wavevector transfer on the other hand is called the scattering triangle. Due to the law of cosines we have

$$|\mathbf{Q}|^2 = |\mathbf{k}_f|^2 + |\mathbf{k}_i|^2 - 2|\mathbf{k}_i||\mathbf{k}_f| \cos(2\theta), \quad (\text{C.1.10})$$

where the angle between \mathbf{k}_i and \mathbf{k}_f is called the scattering angle 2θ . For the case of elastic scattering as relevant here this reduces to

$$|\mathbf{Q}| = 2k \sin(2\theta/2). \quad (\text{C.1.11})$$

Of course, for a general scattering length density distribution $\rho(\mathbf{r})$ the above expression can be generalized to

$$\psi_s(\mathbf{r}, t) = -\frac{e^{i(\mathbf{k}_f \mathbf{r} - \omega t)}}{|\mathbf{r}|} \int d\mathbf{r}' \rho(\mathbf{r}') e^{i\mathbf{Q} \mathbf{r}'}, \quad (\text{C.1.12})$$

This shows that in the limit of weak interaction and a static sample, the scattered field is essentially proportional to the Fourier transform of the scattering length density in the sample. This theory is also called the theory of kinematical scattering or diffraction, to be contrasted with the dynamical theory of diffraction to be treated below, where multiple scattering effects are explicitly included.

C.1.4 Kinematical diffraction from perfect crystals

We now consider kinematical diffraction from static crystals. A crystal is defined as a periodic arrangement of scatterers, and for simplicity we will assume here point-like scatterers as is appropriate for the scattering of neutrons from non-magnetic samples. The periodic arrangement is realized as a tiling of identical unit cells, which are placed at positions

$$\mathbf{r}_n = n_1 \mathbf{a}_1 + n_2 \mathbf{a}_2 + n_3 \mathbf{a}_3, \quad (\text{C.1.13})$$

where n is the coordinate vector with respect to the basis spanned by the lattice vectors \mathbf{a}_j . In the simple cases with just one atom per unit cell, this atom can be assumed to be situated at these lattice position, while in the more complicated cases there are Λ sites per unit cell at positions \mathbf{r}^λ relative to the lattice positions, populated by atoms with respective scattering lengths b_λ .

Inserting this spatial arrangement into Eq. (C.1.8) and dropping the prefactor corresponding to the expanding scattered wave gives

$$\psi_s \propto \sum_n \sum_\lambda b_\lambda e^{i\mathbf{Q}\mathbf{r}_n} e^{i\mathbf{Q}\mathbf{r}^\lambda} = \sum_n e^{i\mathbf{Q}\mathbf{r}_n} \sum_\lambda b_\lambda e^{i\mathbf{Q}\mathbf{r}^\lambda}. \quad (\text{C.1.14})$$

For non-zero scattering, obviously both sums have to be different from zero. The lattice sum $\sum_n e^{i\mathbf{Q}\mathbf{r}_n}$ runs over a finite, but very large number of cells N . If now \mathbf{Q} is chosen such that $\mathbf{Q}\mathbf{r}_n$ is some integer multiple of 2π for all n , this first sum is equal to N . In the converse case, there will be destructive interferences to a large degree, as the values of $e^{i\mathbf{Q}\mathbf{r}_n}$ will be distributed with practically uniform density over the complex unit circle. Thus, the first factor leads to the elastic scattering from a perfect crystal being concentrated in sharp peaks with a width on the order of the inverse of the crystal dimensions. These peaks are called *Bragg peaks*.

The condition that there exists an integer m such that $\mathbf{Q}\mathbf{r}_n = 2\pi m$ for all n can be taken as the definition of the *reciprocal lattice*. Specifically, defining

$$\mathbf{g}_1 = 2\pi \frac{\mathbf{a}_2 \times \mathbf{a}_3}{\mathbf{a}_1 \cdot (\mathbf{a}_2 \times \mathbf{a}_3)} \quad (\text{C.1.15})$$

with \mathbf{g}_2 and \mathbf{g}_3 defined by cyclic permutation of indices, the vectors

$$\mathbf{G}_n = n_1 \mathbf{g}_1 + n_2 \mathbf{g}_2 + n_3 \mathbf{g}_3 \quad (\text{C.1.16})$$

again with integer coordinate vectors n are exactly those vectors that fulfill $\mathbf{G}_n \cdot \mathbf{r}_n = 2\pi m$ for all n and n' . They are called reciprocal lattice vectors and are the only positions in reciprocal space where a perfect crystal scatters elastically. The corresponding condition $\mathbf{Q} = \mathbf{G}_n$ for some n is called the *Laue condition*.

The other factor in Eq. (C.1.14) is called the *structure factor*

$$S = \sum_\lambda b_\lambda e^{i\mathbf{Q}\mathbf{r}^\lambda}. \quad (\text{C.1.17})$$

Apart from other factors to be treated below, it determines the scattering intensity of the Bragg peaks. For primitive lattices with just one atom per unit cell, it is just the scattering length¹ and thus constant with \mathbf{Q} , while for non-primitive structures it shows a characteristic variation over the different Bragg peaks given by the positions of the sites within the unit cells and their respective average scattering lengths. Differences in the chemical make-up of inequivalent sites are known as *long-range order*.

When the requirement of the crystal being made up of point scatterers is relaxed, the scattering lengths b_λ depend on \mathbf{Q} . For X-ray scattering, the corresponding expression is called the *atomic form factor* and essentially is the Fourier transform of the electronic distributions within the atoms, which directly follows from Eq. (C.1.12). On the other hand, nuclei are much smaller than the relevant neutron wavelengths, so for nuclear neutron scattering the scattering lengths show no dependence on \mathbf{Q} . However, magnetic moments of the atoms couple to the neutrons'

¹Actually, the phase of the structure factor depends on the choice of origin. Experimentally, only its absolute value is accessible, therefore it can always be chosen real and non-negative.

magnetic moments, so in this case also in neutron scattering atomic form factors and thus \mathbf{Q} -dependent scattering lengths appear, which now follow from the spatial distributions of the unpaired electrons. Further, the effect of atomic oscillations on the elastic scattering can also be understood as a broadening of the spatial distributions, with a concomitant decay of the scattering length with \mathbf{Q} . This so-called Debye-Waller factor will be treated in more detail below. Finally, the scattering lengths can also depend on the frequency of the radiation, showing resonant behaviour, specifically with respect to electronic transitions in the case of X-rays and nuclear transitions in the case of neutrons. These give the so-called *dispersion corrections*, which however are negligible for most nuclei in the case of thermal neutron scattering.

C.1.5 Scattering with uncorrelated scattering length randomness

To bring out an aspect of the effect of randomness in the scattering lengths, we write b_j in Eq. (C.1.8) as

$$b_j = \langle b_j \rangle + \Delta b_j, \quad (\text{C.1.18})$$

with Δb_j understood as uncorrelated random variables with zero mean, that is,

$$\langle \Delta b_j \rangle = 0 \quad \forall j \quad (\text{C.1.19})$$

and

$$\langle \Delta b_j \Delta b_k \rangle = \langle \Delta b_j \rangle \langle \Delta b_k \rangle = 0 \quad \forall j \neq k. \quad (\text{C.1.20})$$

The expected value for the intensity is then

$$\begin{aligned} I(\mathbf{Q}) &= |\psi_s(\mathbf{Q})|^2 \\ &\propto \sum_{j,k} \langle b_j b_k \rangle e^{i\mathbf{Q}(\mathbf{r}_j - \mathbf{r}_k)} \\ &= \sum_{j \neq k} \langle b_j b_k \rangle e^{i\mathbf{Q}(\mathbf{r}_j - \mathbf{r}_k)} + \sum_{j=k} \langle b_j b_k \rangle e^{i\mathbf{Q}(\mathbf{r}_j - \mathbf{r}_k)} \\ &= \sum_{j \neq k} \langle b_j \rangle \langle b_k \rangle e^{i\mathbf{Q}(\mathbf{r}_j - \mathbf{r}_k)} + \sum_j \left(\langle b_j b_j \rangle + \langle b_j \rangle \langle b_j \rangle - \langle b_j \rangle \langle b_j \rangle \right) \\ &= \sum_{j,k} \langle b_j \rangle \langle b_k \rangle e^{i\mathbf{Q}(\mathbf{r}_j - \mathbf{r}_k)} + \sum_j \left(\langle b_j^2 \rangle - \langle b_j \rangle^2 \right) \\ &= \sum_{j,k} \langle b_j \rangle \langle b_k \rangle e^{i\mathbf{Q}(\mathbf{r}_j - \mathbf{r}_k)} + \sum_j \langle \Delta b_j^2 \rangle. \end{aligned} \quad (\text{C.1.21})$$

This shows that uncorrelated randomness in the scattering lengths gives only a flat (i.e., independent of \mathbf{Q}) background to the scattered signal, while any variation with \mathbf{Q} is only due to the mean values of the scattering lengths.

For X-rays, this derivation is not relevant: X-rays scatter from the atomic electrons, therefore any variation in the atomic scattering lengths directly entails different chemical behaviour. As the corresponding energies are on the same

order as temperature, there is no true randomness. On the other hand, in the case of neutrons this leads to the phenomenon of so-called incoherent scattering as mentioned in A.2.2. However, as is obvious from the derivation given here, it would be wrong to assume that the incoherent contribution is due to some scattering process that is not affected by interference. The point is rather that this contribution would be sensitive to correlations that do not correspond to appreciable energy differences, specifically differences only in isotopes or nuclear spin orientation, therefore all these interference effects are washed out in the statistical averaging.

To be specific, with the definitions of the coherent scattering length and the incoherent scattering cross sections as given in A.2.2 the scattered intensity (C.1.21) reads

$$I(\mathbf{Q}) \propto \sum_{j,k} b_{\text{coh}}^j b_{\text{coh}}^k e^{i\mathbf{Q}(\mathbf{r}_j - \mathbf{r}_k)} + \frac{1}{4\pi} \sum_j \sigma_{\text{incoh}}^j. \quad (\text{C.1.22})$$

C.1.6 Scattering and pair correlations

Diffuse scattering is the term applied to everything in the scattering signal distinct from the Bragg peaks. Apart from inelastic scattering (to be discussed below), incoherent neutron scattering as treated above is an example, which however in the elastic case does not convey any information on the sample and is thus often an undesirable contamination of the signal. This is in contrast to diffuse scattering due to chemical disorder, where the characteristic variation over reciprocal space encodes correlations between the elements that occupy nearby lattice sites and possible small deviations from the ideal positions.

Specifically, according to Eq. (C.1.12) the scattering amplitude is the Fourier transformation of the scattering length density

$$\psi_s(\mathbf{Q}) \propto \int d\mathbf{r}' \rho(\mathbf{r}') e^{i\mathbf{Q}\mathbf{r}'}. \quad (\text{C.1.23})$$

The scattered intensity is the absolute square of the amplitude, thus

$$I(\mathbf{Q}) \propto \iint d\mathbf{r}_1 d\mathbf{r}_2 \rho(\mathbf{r}_1) \rho(\mathbf{r}_2) e^{i\mathbf{Q}(\mathbf{r}_1 - \mathbf{r}_2)} = \iint d\mathbf{r} d\Delta\mathbf{r} \rho(\mathbf{r}) \rho(\mathbf{r} - \Delta\mathbf{r}) e^{i\mathbf{Q}\Delta\mathbf{r}} \quad (\text{C.1.24})$$

assuming for simplicity real scattering length densities and substituting $\mathbf{r}_1 = \mathbf{r}$ and $\mathbf{r}_2 = \mathbf{r} - \Delta\mathbf{r}$. This shows that the elastic scattered intensity is equal to the Fourier transform of a (static) pair-distribution function

$$g(\Delta\mathbf{r}) = \int d\mathbf{r} \rho(\mathbf{r}) \rho(\mathbf{r} - \Delta\mathbf{r}). \quad (\text{C.1.25})$$

This expression allows to rederive the earlier results: for a perfect lattice (assume for simplicity a Bravais lattice) populated by scatterers with equal scattering lengths, $\rho(\mathbf{r})$ is just a sum of regularly arranged δ distributions

$$\rho(\mathbf{r}) = b \sum_n \delta(\mathbf{r} - \mathbf{r}_n). \quad (\text{C.1.26})$$

Of course, then also $g(\Delta\mathbf{r})$ has such a form

$$g(\Delta\mathbf{r}) = Nb^2 \sum_n \delta(\mathbf{r} - \mathbf{r}_n), \quad (\text{C.1.27})$$

and the scattered intensity being the Fourier transformation of $g(\Delta\mathbf{r})$ is again a sum of δ distributions, but now being arranged on the sites of the reciprocal lattice, corresponding to the sharp Bragg peaks.

For the case of uncorrelated random deviations in the scattering lengths from the mean value $\langle b \rangle$, the static pair-distribution function is modified by an additional contribution at the origin, while due to the absent correlations the off-origin deviations average out

$$g(\Delta\mathbf{r}) = N \left(\langle b \rangle^2 \sum_n \delta(\mathbf{r} - \mathbf{r}_n) + (\langle b^2 \rangle - \langle b \rangle^2) \delta(\mathbf{r}) \right). \quad (\text{C.1.28})$$

Of course, the Fourier transformation of a δ distribution at the origin gives a contribution that is constant over all of reciprocal space, corresponding to incoherent scattering.

However, if the deviations of the scattering lengths are correlated over short distances, such as in the case of an alloy due to chemical interactions, the prefactors of the respective δ distributions in $g(\Delta\mathbf{r})$ are not constant any more. Thus, the diffuse scattered intensity is modulated, where the amplitudes of the distinct modulations directly give the prefactors of the peaks in $g(\Delta\mathbf{r})$ and thus of the correlations in the occupations. Qualitatively, here a clustering tendency between equal elements leads to increased values in $g(\Delta\mathbf{r})$ for small $\Delta\mathbf{r}$, and thus to increased intensity at small \mathbf{Q} . Note that this is consistent with the small-angle scattering that would result when a stronger clustering tendency leads to an actual phase separation. Conversely, a preference for pairs of unequal atoms will give increased intensity between the Bragg spots, which in the extreme case of long-range order will evolve to superstructure peaks.

Another possibility is the case of a binary ideal solid solution (where the occupations of the lattice sites by the two kinds of atoms are random and uncorrelated), but where chemical interactions lead to static deviations from the ideal lattice sites. In this case, $g(\Delta\mathbf{r})$ ceases to consist of a regular lattice of δ distributions. In a first approximation for small displacements the additional contributions can be assumed as dipoles at the lattice sites, which can still be treated with analytical expressions, giving intensities that increase with \mathbf{Q} .

For a liquid or amorphous system, the pair correlation function $g(\Delta\mathbf{r})$ is the principal experimentally observable quantity with respect to the short-range atomic arrangement. Note that in this case it only depends the absolute value of $\Delta\mathbf{r}$.

C.2 Beyond kinematical scattering

In the field of elastic scattering, there are two relevant aspects where kinematical scattering theory is inadequate, that is, where the amplitude of the scattered

wave becomes significant compared to the incident wave. Specifically, these are the phenomena of refraction and reflection of plane waves, which assume homogeneous media separated by laterally homogeneous interfaces and are the direct analoga of the respective phenomena in optics, and dynamical diffraction from perfect single crystals, where the discrete spatial structure is fundamental.

C.2.1 Propagation through matter

For deriving how an incident plane wave is modified when it enters a medium, we first treat the kinematical scattering from a thin homogeneous slab of material.

Assume an incident plane wave ψ with wavevector $\mathbf{k} = (0, 0, k)$ falling onto a slab of material oriented perpendicular to the z direction with thickness Δ , situated at $z \in [-\Delta/2, \Delta/2]$. Assume that $\Delta k \ll 1$, then an infinitesimal piece of the material situated at (x, y) will emit spherical waves with an amplitude $-b\rho\Delta dx dy$, where ρ is the number density of scatterers, each having scattering length b . In polar coordinates this reads $-b\rho\Delta r dr d\phi$, thus the contribution of all these elements to the scattered field at position $x_0 = (0, 0, z)$ is

$$\psi_s(x_0) = \int_0^{2\pi} d\phi \int_0^\infty dr r (-b\rho\Delta) \frac{e^{ikR}}{R} = -2\pi b\rho\Delta \int_0^\infty dr \frac{r}{R} e^{ikR}, \quad (\text{C.2.1})$$

with $R = \sqrt{r^2 + k^2}$. Using

$$\frac{dR}{dr} = \frac{r}{R}, \quad (\text{C.2.2})$$

substitution gives

$$\psi_s(x_0) = -2\pi b\rho\Delta \int_z^\infty dR e^{ikR}. \quad (\text{C.2.3})$$

Of course, the anti-derivative does not converge for an upper limit of $R = \infty$. However, for a finite slab of material with a density that goes smoothly to zero at the outside, the corresponding contribution averages out, giving

$$\psi_s(x_0) = -\frac{2\pi i b \rho \Delta}{k}. \quad (\text{C.2.4})$$

Clearly, an analogous result also holds for all other points (x, y, Δ) . Thus, also the scattered field would propagate as a plane wave in the vacuum with wavevector \mathbf{k} . Combining incident and scattered wave to an outgoing wave, we see that

$$\psi_o = \psi + \psi_s = \psi \left(1 - \frac{2\pi i b \rho \Delta}{k}\right) = \psi e^{-i(2\pi b \rho \Delta/k)} \quad (\text{C.2.5})$$

after the passage of a slab of thickness Δ , where the last equality is in the limit of small Δ . Stacking now such slabs on top of each other, we see that the wave inside the medium is given by

$$\psi'(x, y, z) = \psi(x, y, z) e^{-i2\pi b \rho z/k} = e^{ikz} e^{-i2\pi b \rho z/k} = e^{ik'z} \quad (\text{C.2.6})$$

with $k' = k - 2\pi b\rho/k = k(1 - 2\pi b\rho/k^2)$.

Defining the index of refraction

$$n = 1 - \frac{2\pi b\rho}{k^2} = 1 - \frac{b\rho\lambda^2}{2\pi}, \quad (\text{C.2.7})$$

we get

$$k' = nk. \quad (\text{C.2.8})$$

Note that in this derivation, the scattered field was assumed to propagate unperturbed from the point of scattering to x_0 . Thus, the derived expression for n is only valid in the limit $|n - 1| \ll 1$, that is, for weak interactions. An exact expression for the case of neutron scattering can be derived by considering the energetics of the process: As will be shown below, the nuclear scattering length can be connected to the potential felt by the neutrons via the Fermi pseudo-potential

$$V_{\text{F}}(\mathbf{r}) = \frac{2\pi\hbar^2}{m_{\text{n}}} b\delta(\mathbf{r}). \quad (\text{C.2.9})$$

For forward scattering, as is relevant here, the spatial structure is irrelevant, so these pseudo-potentials at the positions of the nuclei can be replaced by a homogeneous average potential inside the medium

$$V(\mathbf{r}) = \frac{2\pi\hbar^2}{m_{\text{n}}} b\rho. \quad (\text{C.2.10})$$

With the kinetic energy of the neutron

$$E = \frac{\hbar^2 k^2}{2m_{\text{n}}}, \quad (\text{C.2.11})$$

conservation of energy leads to

$$k^2 = k'^2 + 4\pi b\rho. \quad (\text{C.2.12})$$

Thus, requiring (C.2.8) gives

$$n = \sqrt{1 - \frac{4\pi b\rho}{k^2}}, \quad (\text{C.2.13})$$

to which (C.2.7) is equal up to first order in $|n - 1|$.

According to our first derivation, the reason for the change in wavevector when entering a medium is due to the scattered field having a phase of $\pm\pi/2$ with respect to the incident wave, which either accelerates or retards the revolution of the phase with position, but leaves the absolute value of the amplitude unchanged. Conversely, a change in the absolute value due to absorption is consequently described by the imaginary part of the scattering length. Specifically, for a phase shift of π with respect to the incident wave this contribution has to be equal to $-i\beta$ with $\beta > 0$, giving

$$n = 1 - \frac{2\pi b\rho}{k^2} + i\frac{2\pi\beta\rho}{k^2}. \quad (\text{C.2.14})$$

Thus, the intensity of the transmitted beam decays with depth according to

$$|\psi'(z)|^2 = |e^{ik'z}|^2 = e^{-\mu z} \quad (\text{C.2.15})$$

with the attenuation coefficient

$$\mu = \frac{4\pi\beta\rho}{k}. \quad (\text{C.2.16})$$

As we have on the other hand

$$\mu = \rho\sigma_{\text{abs}} \quad (\text{C.2.17})$$

we see

$$\sigma_{\text{abs}} = \frac{4\pi\beta}{k}, \quad (\text{C.2.18})$$

which proves the $1/v$ law of neutron absorption (A.2.15), using $v = \hbar k/m_n$ for freely propagating neutrons.²

The phase velocity of a plane wave is given by $c = \omega/k$. In the absence of dynamics, ω is constant (and indeed the periodic dependence on time has been factored out in above derivation), therefore we see that the phase velocity changes as

$$c' = c/n \quad (\text{C.2.19})$$

and thus is larger inside a medium with repulsive potential ($n < 1$) than outside. This result seems counter-intuitive and shows that the phase velocity is different from the velocity that is responsible for transport of matter (the group velocity), the latter of which being relevant for the most part here.

C.2.2 Refraction

When a ray passes non-perpendicularly from one medium to the next, it changes its direction of propagation. This phenomenon is termed *refraction*. Here we assume without loss of generality an interface oriented perpendicular to the z -direction and a wavevector of the incident radiation of $\mathbf{k} = (k_x, 0, k_z)$.

The interface between the two media breaks translation invariance in z -direction but not perpendicular to it. Thus, the in-plane periodicity of the incident wave is retained also in the medium

$$k'_x = k_x \quad \text{and} \quad k'_y = k_y = 0. \quad (\text{C.2.20})$$

Together with (C.2.12), this implies

$$k_z^2 = k_z'^2 + 4\pi b\rho. \quad (\text{C.2.21})$$

For $k_z < k_z^c = 2\sqrt{\pi b\rho}$, k'_z becomes purely imaginary. Thus, the wavefunction decays exponentially into the medium with a penetration depth on the order of a

²As stated earlier, this is of course only valid away from resonances, that is, for b independent of k , which is assumed everywhere in this chapter.

few hundred Ångström and no true refracted ray forms. Instead, due to intensity conservation the incident wave has to be totally reflected. Of course, the analogon of (C.2.20) holds also here, leading to so-called *specular reflection*, that is, an exiting ray that lies in the plane of incident ray and the surface normal and has an equal angle to the surface normal as the incident ray.

However, also in the case of $k_z^2 > 4\pi b\rho$ there exists a specularly reflected wave in addition to the refracted wave. Specifically, continuity (in zeroth and first derivative) at the interface requires

$$\alpha + \alpha'' = \alpha' \quad \text{and} \quad \alpha k_z - \alpha'' k_z = \alpha' k'_z, \quad (\text{C.2.22})$$

where α , α' and α'' are the amplitudes of, respectively, the incident, refracted, and reflected waves.

Solving this for α'' and α' gives the amplitude reflectivities and transmittivities

$$r = \frac{\alpha''}{\alpha} = \frac{k_z - k'_z}{k_z + k'_z} \quad (\text{C.2.23})$$

and

$$t = \frac{\alpha'}{\alpha} = \frac{2k_z}{k_z + k'_z}. \quad (\text{C.2.24})$$

The probability for reflection is the ratio of the squared amplitudes of incident and reflected waves

$$R = |r|^2 = \left| \frac{k_z - \sqrt{k_z^2 - (k_z^c)^2}}{k_z + \sqrt{k_z^2 - (k_z^c)^2}} \right|^2 = \left| \frac{1 - \sqrt{1 - (k_z^c/k_z)^2}}{1 + \sqrt{1 - (k_z^c/k_z)^2}} \right|^2, \quad (\text{C.2.25})$$

which for $k_z \gg k_z^c$ can be expanded to

$$R \approx \frac{(\pi b\rho)^2}{k_z^4}. \quad (\text{C.2.26})$$

Of course, the intensity transmittivity (which for particle waves is the probability for the particle to enter the medium) has to fulfill

$$T = 1 - R, \quad (\text{C.2.27})$$

implying that

$$T = t^2 \frac{k'_z}{k_z}. \quad (\text{C.2.28})$$

Using again (C.2.12) and (C.2.13) gives

$$k_z'^2 + k_x^2 = n^2(k_z^2 + k_x^2). \quad (\text{C.2.29})$$

Taking the square root and multiplying by $k_x/\sqrt{(k_z^2 + k_x^2)(k_z'^2 + k_x^2)}$ leads to Snell's law

$$\sin\theta = n \sin\theta' \quad (\text{C.2.30})$$

with θ and θ' being the angles of incidence and refraction, respectively.

C.2.3 Reflectivity of a slab

In the derivation given above, the effect of a single interface between two media was considered. For the geometry of a slab, which consists of a medium bounded by two parallel planes, specifically the interference between the waves reflected at the two interfaces gives rise to a characteristic variation of reflectivity and transmittivity.

Let r_{out} and r_{in} be the amplitude reflectivities at the interface for a wave that arrives from the outside or the inside of the slab, respectively, and analogously t_{out} and t_{in} the corresponding amplitude transmittivities, given by (C.2.23) and (C.2.24). We assume the slab to be bounded by vacuum on either side, thus these quantities are the same for both interfaces. Let Δ be the thickness of the slab.

The amplitude reflectivities and transmittivities are conditions that relate the amplitudes of the three waves (incident, reflected and transmitted) at an interface so that the wave equation is fulfilled. As the wave equation is linear, any general situation with four waves (two on either side of the interface) can be written as the suitable superposition of the three-wave solutions. Thus, the amplitude reflectivities and transmittivities of a slab can be calculated as follows:

- Consider an incident wave of amplitude equal to unity at the upper interface. With a reflected wave of amplitude r_{out} and a wave with amplitude t_{out} that is transmitted into the medium, the wave equation is fulfilled at the upper interface.
- However, the wave inside the slab is now the incident wave on the lower interface. At this position, it has an amplitude of pt_{out} where $p = e^{ik'_z\Delta}$ is the acquired phase. Setting an amplitude for the outgoing wave into the vacuum of $pt_{\text{out}}t_{\text{in}}$ and an amplitude of $pt_{\text{out}}r_{\text{in}}$ for the wave reflected back into the medium satisfies now the wave equation at the lower interface.
- With the back-reflected wave, now again the continuity conditions at the upper interface have to be recovered, giving an additional contribution of $p^2t_{\text{out}}r_{\text{in}}t_{\text{in}}$ to the upper outgoing wave and $p^2t_{\text{out}}r_{\text{in}}^2$ downwards-propagating wave inside the slab.
- Now again the lower interface has to be considered. . .

This construction leads to an infinite series, which is absolutely convergent as $|pr_{\text{in}}| < 1$.

The corresponding amplitude reflectivities and transmittivities of the slab are

$$r_{\text{slab}} = r_{\text{out}} + r_{\text{in}}t_{\text{out}}t_{\text{in}}p^2 \frac{1}{1 - r_{\text{in}}^2p^2} = \frac{r_{\text{out}}(1 - p^2)}{1 - r_{\text{out}}^2p^2} \quad (\text{C.2.31})$$

and

$$t_{\text{slab}} = e^{-ik_z\Delta} \frac{pt_{\text{out}}t_{\text{in}}}{1 - r_{\text{out}}^2p^2}, \quad (\text{C.2.32})$$

where for the simplification of r_{slab} the identities

$$r_{\text{in}} = -r_{\text{out}} \quad (\text{C.2.33})$$

and

$$r_{\text{out}}^2 + t_{\text{in}}t_{\text{out}} = 1 \quad (\text{C.2.34})$$

due to (C.2.23) and (C.2.24) were used, and the factor $e^{-ik_z\Delta}$ in the expression for t_{slab} is due to the acquired phase of the reference incident wave.

Specifically for not too small k_z , that is, away from the regime of total reflection, r_{out} is small and $k'_z \approx k_z$. Thus, according to (C.2.31) r_{slab} shows periodic oscillations as a function of k_z , which are called *Kiessig fringes*. They are due to the interference of waves reflected from the two interfaces, where multiple reflections can be neglected. Note that the intensity is zero when the optical path length difference is a multiple of the wavelength in the medium, as $r_{\text{out}} = -r_{\text{in}}$. For $k_z \gtrsim k_z^c$, the wavelength inside the medium begins to be significantly deviate from the wavelength outside, thus the zeros of the reflectivity start to deviate from the kinematical expression, where they are perfectly periodic in k_z .

C.2.4 Reflectivity of a multilayer structure

Given the expressions for amplitude reflectivity and transmittivity of a homogeneous slab, the corresponding expressions for multilayer structures can be calculated quite easily.

Consider first a bilayer structure with layer thicknesses Δ_i and slab reflectivities and transmittivities r'_i and t'_i , respectively, with $i = 0$ for the bottom layer. For simplicity of notation we define $t''_i = t'_i e^{ik_z\Delta}$. Apart from direct reflection from the top layer, the wave can also be transmitted through it, bounce any number of times between the two layers and finally be transmitted back through the top layer to contribute to the total reflectivity of the bilayer. Thus, the amplitude reflectivity is given by

$$r_1 = r'_1 + t''_1 r'_0 t'_1 + t''_1 r'_0 r'_1 r'_0 t'_1 + \dots = r'_1 + \frac{t''_1 r'_0}{1 - r'_1 r'_0} = \frac{r'_1 + r'_0 (t''_1 - r'^2_1)}{1 - r'_1 r'_0}. \quad (\text{C.2.35})$$

Note that the lower layer only enters via its amplitude reflectivity as opposed to its thickness or other parameters of the internal structure. Thus, the above expression can also be used iteratively to calculate r_n , the reflectivity of an $n + 1$ layer system, given the reflectivity of the n layer system r_{n-1} and the reflectivity, transmittivity and thickness of the added top layer.

Reflectivity studies are the main experimental method to investigate properties of multilayers, thus these calculations are very relevant. While transmittivities are studied less frequently, they can be computed by an analogous approach. Here one would start at the top layer and compute both r_n and t_n given r_{n-1} and t_{n-1} and the properties of layer n .

Up to here, only perfectly flat and sharp interfaces were considered, which of course is not representative of actual interfaces. The first sophistication of the

model is to treat graded interfaces, with a gradual transition of the refractive index. This can be treated as the limiting case of a multilayer with a large number of thin layers of continuously varying properties. As a consequence, due to destructive interference between the large number of interfaces, the interface reflectivity decreases for large k_z . Of course, towards k_z^c the reflectivity is not affected, as in this regime the total reflectivity is due to the impossibility to sustain a travelling wave in the medium, regardless of the interface.

In a next step, interface roughness can be considered. This means that the local interface height $z(x, y)$ varies laterally with x and y and is modelled as a random variable. In the absence of lateral correlations, that is for $\langle z(x_1, y_1)z(x_2, y_2) \rangle = \langle z(x_1, y_1) \rangle \langle z(x_2, y_2) \rangle = \langle z \rangle^2$ for $z(x_1, y_1) \neq z(x_2, y_2)$, the same expression results as in the case of the graded interface, with the decrease in reflectivity essentially given by the Fourier transform of the distribution of local heights, as this is in effect the same model. For correlated interface heights, one can distinguish the cases where the fluctuations remain bounded or are unbounded. In the first case, the reflectivity shows a perfectly specular component (due to the profile of the average refractive index) on top of a diffuse contribution due to the fluctuations. In the converse case, there is no strictly specular component, instead the reflected beam is broadened as in small-angle scattering. This can be understood by conceptually replacing the actual interface with a coarsened version thereof, having locally fluctuating interface normals. The reflected beam can then be considered to be specularly reflected on these fluctuating interface normals, giving a finite width.

C.2.5 Dynamical diffraction from single crystals

Up to now, the medium was treated in a continuum description, where the actual discrete atomic nature of matter was averaged out to give a homogeneous scattering length density. For this approximation to be valid two conditions have to be met: First, the wavevector transfers have to be small so that interference effects between the atoms can be neglected, and, further, the effect of a single atom on the resulting wave has to be small. For both X-rays and neutrons with wavelengths in the Ångström regime, the latter condition is in general satisfied,³ and for small angles of incidence with respect to high-symmetry lattice planes, also the first condition is realized.

On the other hand, for wavevector transfers in the vicinity of a low-index Bragg condition at a perfect crystal, interference effects have to be considered. The kinematical treatment has shown that reflections will appear exactly where the condition is satisfied, with a width that is given by the inverse of the dimensions of the crystal and an area that is proportional to the volume of the crystal. From this it is obvious that the kinematical approximation has to fail for large crystals, as the reflected intensity has to be bounded by the incident intensity. Of course, the solution to this problem is to enforce intensity conservation at the transmissions and reflections at the respective interfaces, which are guaranteed in the full dynamical description. Qualitatively, for a crystal oriented in symmetric Bragg

³Even ¹⁵⁷Gd, the isotope with the largest neutron resonance in the thermal regime, has a cross section of only about $2 \times 10^{-3} \text{Å}^2$, thus a lattice plane attenuates a thermal beam only by a factor of about 10^{-3} .

geometry (where the surface is parallel to the reflecting planes and the reflected beam leaves on the side of the incident beam instead of transiting the sample) at each plane a given part of the intensity is transferred from the incident to the reflected beam. Of course, this also happens in the reverse direction, but for a semi-infinite non-absorbing crystal all the intensity will eventually reach the surface after a number of back-and-forth reflections, giving a reflectivity of unity.

Further, also in the non-absorbing case there is only a finite penetration length. This diminishing of the wave in the crystal is called *extinction*. Specifically, *primary* extinction refers to the situation in a perfect crystal just related. As this limits the number of interfering lattice planes and thus the sharpness of the Bragg reflections, Bragg reflections inherently have finite linewidths also in the case of perfect crystals.

On the other hand, actual crystals host crystal defects, and can be described as a mosaic of small crystallites, assumed to be perfect apart from their finite size, with the spread of orientations called *mosaicity*. In an *ideally imperfect crystal*, the crystallites are much smaller than the primary extinction length. However, in an analogous argumentation due to intensity conservation also here the wave inside the crystal becomes attenuated, which is then called *secondary* extinction. For employing single crystals as neutron monochromators and analysators, the angular widths of the reflections due to primary extinction are unnecessarily small compared to the used beam divergences, giving away intensity. Therefore, here ideally imperfect crystals are better suited, as their wider reflections reflect a larger part of the beam.

The dynamical scattering from crystals in symmetric Bragg geometry can be computed along the lines of the case of multilayers. Specifically, let d be the spacing between atomic layers. In the case of non-magnetic neutron scattering, describing the scattering length density as a function of z leads to a sequence of infinitesimal slabs corresponding to the atomic nuclei separated by slabs of vacuum. Of course, the amplitude reflectivities and transmittivities of the vacuum slabs are zero and one, respectively, while the corresponding limits of (C.2.31) and (C.2.32) give

$$r_{\text{slab}} = \gamma \quad \text{and} \quad t_{\text{slab}} = 1 + \gamma \quad \text{with} \quad \gamma = \frac{-2i\pi b n}{k_z}, \quad (\text{C.2.36})$$

where n is now the density of scatterers per area in one layer. Note that for perpendicular incidence this again recovers (C.2.4), and in fact can be obtained directly by generalizing the derivation of (C.2.4) to non-perpendicular incidence.

Now the crystal is built up of a repeating array of identical slabs that have the atomic plane at half height. The transmittivity of the repeating slab is just

$$t' = t_{\text{slab}} = 1 + \gamma, \quad (\text{C.2.37})$$

while the reflectivity acquires an additional phase factor to account for the path from the logical slab boundary at half height between the atomic layers to the layer and back

$$r' = e^{ik_z d} r_{\text{slab}} = \gamma e^{ik_z d}. \quad (\text{C.2.38})$$

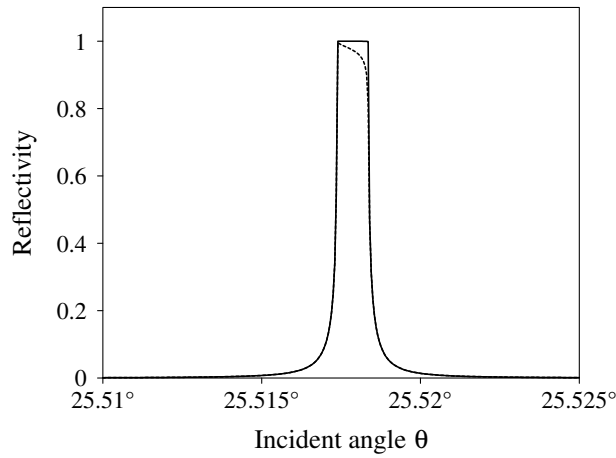


Figure C.1: Solid: Reflectivity curve of (111) reflection of a semi-infinite elemental copper single crystal in symmetric Bragg geometry for thermal neutrons of 2200 m/s. Dashed: Analogous curve when the absorption cross section is artificially increased by a factor of 100.

These expressions can now directly be used in the framework of Sect. C.2.4 to compute the reflectivity and transmittivity of a finite crystal.

The amplitude reflectivity r of a semi-infinite crystal can also be derived in a simpler way: Naturally, when a further layer is added to the top of such a crystal, the reflectivity has to stay the same. With (C.2.35), this implies

$$r = \frac{r' + r(t'^2 e^{2ik_z d} - r'^2)}{1 - r'r}, \quad (\text{C.2.39})$$

which in turn gives

$$r^2 + r \underbrace{\left((e^{ik_z d} - e^{-ik_z d})/\gamma + 2e^{ik_z d} \right)}_p + 1 = 0. \quad (\text{C.2.40})$$

This equation has the solutions

$$r_{1,2} = -\frac{p}{2} \pm \sqrt{\frac{p^2}{4} - 1}. \quad (\text{C.2.41})$$

As $r_1 r_2 = 1$, in the generic case of a non-vanishing imaginary part of p exactly one solution fulfills $|r_i| < 1$ and thus corresponds to the physically possible solution. Indeed, this solution is given by

$$r = \frac{p}{2} \left(-1 + \sqrt{1 - 4/p^2} \right). \quad (\text{C.2.42})$$

The corresponding intensity reflectivity for the (111) reflection of elemental copper is given in Fig. C.1, a so-called *Darwin curve*.

As was argued above, for weak absorption the reflectivity curve shows total reflectivity over a finite width. Specifically, for $e^{ik_z d} = -1$, which corresponds to

the Bragg condition, $p = -2$ and thus $r = 1$ (which incidentally is also valid in the case of finite absorption). For the typical case of positive scattering lengths, this is realized at the low-angle limit of the region of total reflectivity. On the other hand, in the no-absorption case $p = 2$ is realized for $e^{-ik_z d} = -1 - 2\gamma$, giving the high-angle boundary of total reflectivity with $r = -1$. For small γ and lowest-order Bragg reflection, i.e. $k_z d \approx \pi$, this implies $\Delta k_z = 4bn$ with notation as in (C.2.36), which is the so-called *Darwin width*.

The qualitative shape of the reflection curve can also be explained by concepts that are fundamental to solid-state physics: A quantum-mechanical neutron inside a single crystal experiences a periodic potential. Thus, the free-volume parabolic dispersion relations are modified, specifically for a weak potential the effects are significant only at the Brillouin zone boundary, where a band gap opens. Consider now only the perpendicular dimension z . Due to the band gap there are perpendicular neutron energies that have no periodic solution of the Schrödinger equation inside the crystal. Such neutrons can therefore only be reflected. Near the Brillouin zone boundary for weak potentials, the Bloch states are composed of essentially two plane waves, with the states above and below the gap differing in the phases of those two waves relative to each other. Specifically, the Bloch waves are either symmetric or anti-symmetric with respect to the atomic positions, giving either large or vanishing probabilities at the atomic positions. For positive scattering lengths and thus repulsive pseudo-potentials, the anti-symmetric wave has lower energy. That is, this is the state that is entered by a neutron with an incidence angle θ_0 just at the lower boundary of the region of total reflectivity.

For incidence angle θ_0 , the neutron has vanishing probability density at the atomic positions. Thus, there will be no refractive effects, so that $k'_z = k_z$ and therefore θ_0 is given by the Bragg condition without refractive corrections. An additional interesting consequence is that neutrons are also not absorbed even for non-vanishing nuclear absorption cross sections. On the other hand, an incidence angle at the high-angle boundary (assuming positive b) would give symmetric Bloch waves, subject to refractive effects (which thus explain qualitatively the shifting of the region of total reflectivity with respect to the Bragg condition) and absorption. This explains the decrease of the reflectivity towards higher angles in the case of significant absorption as illustrated in Fig. C.1, which is called the *Borrmann effect*.

The only approximation in the above derivation was the kinematical treatment of the effect of single atomic planes on the wave fields, which as a rule is valid. For single crystals at non-zero temperatures with displacements of the atoms from the ideal sites, the atomic planes become diffuse. Also for magnetic crystals, where neutrons are scattered at the spatially inhomogeneous magnetization, as well as in the X-ray case with scattering at the electronic clouds, the situation is analogous. In these cases, due to the partial destructive interference the extinction length increases, and the asymmetry in the reflection curves under absorption decreases, as for all Bloch states there is some probability for absorption.

A final comment concerns the situation in Laue (transmission) geometry or finite crystal thicknesses in Bragg geometry. Here the reflectivities and transmittivities vary sensitively with the crystal thicknesses. Specifically for Laue geometry, the intensity as it passes through the crystal shifts oscillatingly between the

diffracted and transmitted beam. This is called the *Pendellösung* effect. When large perfect single crystals with low absorption are available, a measurement of the corresponding period can give a very accurate value of the refractive effects in the medium and thus of the scattering lengths.

C.3 Quantum-mechanical treatment of scattering

For correctly describing scattering processes from samples that fail to be perfectly rigid and static configurations, a quantum-mechanical treatment is necessary. Specifically, this necessitates a consistent treatment of the compound system probe plus sample, going beyond merely considering the probe particle as waves as has been done up to now. The fundamentals of the pertaining theory will be derived here.

C.3.1 Basic expression for the differential cross section

The starting point is given by the expression for the first-order transition rate from state σ_i to state σ_f of a generic system

$$W_{\sigma_i \rightarrow \sigma_f} = \frac{2\pi}{\hbar} |\langle \sigma_f | V | \sigma_i \rangle|^2 \delta(E_{\sigma_i} - E_{\sigma_f}), \quad (\text{C.3.1})$$

where V is the interaction potential and the δ distribution term enforces energy conservation. This expression is often called Fermi's golden rule, and it follows from a treatment of the problem in time-dependent perturbation theory in lowest order. Specifically, the states σ_i and σ_f are assumed to be eigenstates of some unperturbed Hamiltonian and V is a weak perturbation thereof. For the problem at hand, we will assume σ_i and σ_f to be elements of the Cartesian product space of the eigenstates of free neutrons and those of the sample written explicitly as $|\mathbf{k}_i \lambda_i\rangle$ and $|\mathbf{k}_f \lambda_f\rangle$, and V to be their interaction potential. At first, we will consider only positional degrees of freedom of the neutrons explicitly, and treat effects due to spin as a later addition. With the derivation resting on lowest-order perturbation theory, its regime of validity is equal to the one of kinematical elastic scattering, and in effect the results will turn out to be equivalent when the sample can be treated as classical.

The (double) differential scattering cross section $\frac{d^2\sigma}{d\Omega dE_f}$ is the number of neutrons scattered per unit time into an infinitesimal solid angle $d\Omega$ lying in a given direction with a final energy within an infinitesimal window of width dE_f , divided by the incident flux Φ . To fix the prefactors, we assume to system (sample and neutrons) to be confined in some large box with size L , that is, all neutron states have to conform to the assumed boundary conditions, giving a density of allowed neutron states of $L/(2\pi)^3$. As we have

$$E_f = \frac{\hbar^2 k_f^2}{2m_n} \quad (\text{C.3.2})$$

and thus

$$\frac{dE_f}{dk_f} = \frac{\hbar^2 k_f}{m_n}, \quad (\text{C.3.3})$$

the number of final states within the windows of directions and energies to be considered is

$$\frac{L}{(2\pi)^3} d\Omega k_f^2 dk_f = \frac{L}{(2\pi)^3} d\Omega k_f^2 \frac{dk_f}{dE_f} dE_f = \frac{L}{(2\pi)^3} \frac{m_n k_f}{\hbar^2} d\Omega dE_f, \quad (\text{C.3.4})$$

into any of which the incident neutrons are scattered with a rate according to (C.3.1). On the other hand, a normalized incident wavefunction

$$\psi = \frac{1}{\sqrt{L}} e^{i\mathbf{k}_i \cdot \mathbf{r}} \quad (\text{C.3.5})$$

corresponds to a single neutron within the box, with a velocity of

$$v = \frac{\hbar k}{m_n}, \quad (\text{C.3.6})$$

and thus a flux (transiting particles per area and time) of

$$\Phi = \frac{v}{L} = \frac{\hbar k_i}{m_n L}. \quad (\text{C.3.7})$$

Putting all together, we get a number of scattered particles per flux of

$$d^2\sigma \Big|_{\lambda_i \rightarrow \lambda_f} = W_{\mathbf{k}_i, \lambda_i \rightarrow \mathbf{k}_f, \lambda_f} \frac{L}{(2\pi)^3} \frac{m_n k_f}{\hbar^2} d\Omega dE_f \frac{m_n L}{\hbar k_i} \quad (\text{C.3.8})$$

and thus

$$\frac{d^2\sigma}{d\Omega dE_f} \Big|_{\lambda_i \rightarrow \lambda_f} = W_{\mathbf{k}_i, \lambda_i \rightarrow \mathbf{k}_f, \lambda_f} \frac{m_n^2 L^2}{(2\pi\hbar)^3} \frac{k_f}{k_i}, \quad (\text{C.3.9})$$

which denotes the partial double differential cross sections for neutrons under the condition that the initial and final sample states are λ_i and λ_f , respectively.

As L becomes large in this expression, $W_{\mathbf{k}_i, \lambda_i \rightarrow \mathbf{k}_f, \lambda_f}$ decreases due to the normalization of the wavefunctions, while the second factor increasing correspondingly, giving a result that is independent of L . To state this more clearly in an expression that is independent of the box volume L , from here on we identify the state of the neutron \mathbf{k} with the unnormalized wavefunctions $\psi = e^{i\mathbf{k}\mathbf{r}}$. This gives the preliminary expression

$$\frac{d^2\sigma}{d\Omega dE_f} \Big|_{\lambda_i \rightarrow \lambda_f} = \frac{k_f}{k_i} \left(\frac{m_n}{2\pi\hbar^2} \right)^2 |\langle \mathbf{k}_f \lambda_f | V | \mathbf{k}_i \lambda_i \rangle|^2 \delta(E_{k_i} + E_{\lambda_i} - E_{k_f} - E_{\lambda_f}). \quad (\text{C.3.10})$$

With a potential made up of Fermi pseudo-potentials

$$V(\mathbf{r}, \mathbf{R}_1, \dots, \mathbf{R}_N) = \frac{2\pi\hbar^2}{m_n} \sum_j b_j \delta(\mathbf{r} - \mathbf{R}_j) \quad (\text{C.3.11})$$

where \mathbf{R}_j are the positions (or rather their associated operators) of the atoms in the sample and b_j the respective scattering lengths, which we constrain here to be real in order to make the Hamiltonian operators self-adjoint, the matrix element evaluates as

$$\begin{aligned} \langle \mathbf{k}_f \lambda_f | V | \mathbf{k}_i \lambda_i \rangle &= \frac{2\pi\hbar^2}{m} \langle \lambda_f | \int d\mathbf{r} e^{-i\mathbf{k}_f \mathbf{r}} \sum_j b_j \delta(\mathbf{r} - \mathbf{R}_j) e^{i\mathbf{k}_i \mathbf{r}} | \lambda_i \rangle \\ &= \frac{2\pi\hbar^2}{m} \sum_j b_j \langle \lambda_f | e^{i\mathbf{Q}\mathbf{R}_j} | \lambda_i \rangle. \end{aligned} \quad (\text{C.3.12})$$

The partial double differential scattering cross section conditional to sample transitions from λ_i to λ_f now reads

$$\left. \frac{d^2\sigma}{d\Omega dE_f} \right|_{\lambda_i \rightarrow \lambda_f} = \frac{k_f}{k_i} \left| \sum_j b_j \langle \lambda_f | e^{i\mathbf{Q}\mathbf{R}_j} | \lambda_i \rangle \right|^2 \delta(E_{k_i} + E_{\lambda_i} - E_{k_f} - E_{\lambda_f}). \quad (\text{C.3.13})$$

We proceed now by transforming the action of the δ distribution in energy, which is conceptually simple to understand but practically unwieldy, to a time propagation. Specifically, the Fourier transform of a δ distribution is just a constant

$$\int dx e^{i\xi x} \delta(x) = 1, \quad (\text{C.3.14})$$

thus the inverse transform of a constant is again a δ distribution

$$\frac{1}{2\pi} \int d\xi e^{-i\xi x} 1 = \delta(x). \quad (\text{C.3.15})$$

Substituting

$$x = E_{k_i} + E_{\lambda_i} - E_{k_f} - E_{\lambda_f} \quad (\text{C.3.16})$$

and

$$\xi = \frac{t}{\hbar} \quad (\text{C.3.17})$$

gives

$$\begin{aligned} \delta(E_{k_i} + E_{\lambda_i} - E_{k_f} - E_{\lambda_f}) &= \frac{1}{2\pi} \int d(t/\hbar) e^{i(E_{k_f} + E_{\lambda_f} - E_{k_i} - E_{\lambda_i})t/\hbar} \\ &= \frac{1}{2\pi\hbar} \int dt e^{i(E_{\lambda_f} - E_{\lambda_i})t/\hbar} e^{-i\omega t}, \end{aligned} \quad (\text{C.3.18})$$

where the neutron energy transfer is written as its frequency equivalent

$$E_{k_i} - E_{k_f} = \hbar\omega, \quad (\text{C.3.19})$$

which is positive for energy loss of the neutron. Plugging this into the expression for the partial double differential cross section gives

$$\begin{aligned} \left. \frac{d^2\sigma}{d\Omega dE_f} \right|_{\lambda_i \rightarrow \lambda_f} &= \frac{k_f}{k_i} \frac{1}{2\pi\hbar} \sum_{j,j'} b_j b_{j'} \langle \lambda_i | e^{-i\mathbf{Q}\mathbf{R}_{j'}} | \lambda_f \rangle \langle \lambda_f | e^{i\mathbf{Q}\mathbf{R}_j} | \lambda_i \rangle \\ &\quad \int dt e^{i(E_{\lambda_f} - E_{\lambda_i})t/\hbar} e^{-i\omega t}, \end{aligned} \quad (\text{C.3.20})$$

where it seems that apart from additional complexity nothing has been gained. However, as we have

$$H|\lambda\rangle = E_\lambda|\lambda\rangle \quad (\text{C.3.21})$$

for initial and final sample states, where H is the unperturbed Hamiltonian of the sample, we equally have

$$e^{-iHt/\hbar}|\lambda\rangle = e^{-iE_\lambda t/\hbar}|\lambda\rangle. \quad (\text{C.3.22})$$

Thus, the partial double differential cross section can be written as

$$\begin{aligned} \left. \frac{d^2\sigma}{d\Omega dE_f} \right|_{\lambda_i \rightarrow \lambda_f} &= \frac{k_f}{k_i} \frac{1}{2\pi\hbar} \sum_{j,j'} b_j b_{j'} \int dt \langle \lambda_i | e^{-i\mathbf{QR}_{j'}} | \lambda_f \rangle \langle \lambda_f | e^{iHt/\hbar} e^{i\mathbf{QR}_j} e^{-iHt/\hbar} | \lambda_i \rangle e^{-i\omega t} \\ &= \frac{k_f}{k_i} \frac{1}{2\pi\hbar} \sum_{j,j'} b_j b_{j'} \int dt \langle \lambda_i | e^{-i\mathbf{QR}_{j'}(0)} | \lambda_f \rangle \langle \lambda_f | e^{i\mathbf{QR}_j(t)} | \lambda_i \rangle e^{-i\omega t}. \end{aligned} \quad (\text{C.3.23})$$

The time-dependent Heisenberg operators

$$\mathbf{R}_j(t) = e^{iHt/\hbar} \mathbf{R}_j e^{-iHt/\hbar} \quad (\text{C.3.24})$$

used here are just a notational device to transfer the passing of time, which in the Schrödinger picture affects the wavefunctions describing the sample state with time-independent operators, to the operators.

The expression for the partial double differential cross section obtained above now lends itself nicely to derive the experimentally accessible double differential cross section, where any final sample state is possible and the initial states are given by their thermal population. This results in the compact expression

$$\frac{d^2\sigma}{d\Omega dE_f} = \frac{k_f}{k_i} \frac{1}{2\pi\hbar} \sum_{j,j'} b_j b_{j'} \int dt \langle e^{-i\mathbf{QR}_{j'}(0)} e^{i\mathbf{QR}_j(t)} \rangle e^{-i\omega t}. \quad (\text{C.3.25})$$

Here the notation

$$\langle A \rangle = \sum_\lambda p_\lambda \langle \lambda | A | \lambda \rangle \quad (\text{C.3.26})$$

denotes the thermal average of an operator A , where p_λ are the thermal populations of the respective states

$$p_\lambda = \frac{e^{-E_\lambda/k_B T}}{Z} \quad (\text{C.3.27})$$

with the partition function

$$Z = \sum_\lambda e^{-E_\lambda/k_B T}. \quad (\text{C.3.28})$$

In deriving (C.3.25) it was further used that the final sample states λ_f are a complete orthonormal basis of the sample's Hilbert space, thus summing $|\lambda_f\rangle\langle\lambda_f|$ over all λ_f is equal to the identity operator. Note that the operator in (C.3.25)

in general cannot be further contracted, as the operators $\mathbf{R}_{j'}(0)$ and $\mathbf{R}_j(t)$ do not commute for $t \neq 0$ because the Hamilton operator defining $\mathbf{R}_j(t)$ in (C.3.24) also includes $\mathbf{p}_{j'}$ which does not commute with $\mathbf{R}_{j'}$. The resulting consequences will be discussed in more detail below.

Apart from verifying the mathematical correctness of the techniques used in the derivation given here, it is instructive to consider also their physical implications. As stated above, the experimentally measured double differential cross section is the sum over all possible combinations of initial and final sample states, which in the original formulation (C.3.13) are connected by the requirement of energy conservation. In this formulation, the scattering process conceptually happens instantaneous. The mathematical trick of Fourier-transforming the requirement of energy conservation to the temporal domain and thus to define time-dependent operators allowed to sum over all final states. In this view, the neutron interacts with a dynamically evolving system over an extended time period, with energy conservation being encoded in the evolution of the system. The associated time-dependent operators give then rise to a further physical interpretation of the scattering signal, as will be discussed in Sect. C.4 below.

C.3.2 The neutron spin during scattering

The treatment above considered only the positional degrees of freedom of a neutron, thus neglecting its other degree of freedom, i.e. its spin. As neutrons are spin- $\frac{1}{2}$ particles, there are exactly two eigenstates with respect to the chosen quantization direction, which in the following will be denoted as $|u\rangle$ and $|v\rangle$. In some situations, analyzing whether the neutron spin changes in scattering (termed *spin-flip processes*) or not (*non-spin-flip processes*) can give much more direct access to specific properties of the sample. The pertinent issues will be treated here.

The precondition for being sensitive to spin flipping in the sample is to start out with a polarized beam. Specifically, when the beam has been polarized along some direction (which by convention is taken to be the z direction), the beam's *polarization vector* points along this direction and has a length that varies linearly from 1 (when all neutrons are in the same spin state) to 0 (when both states are equally probable). This length is also called *polarization*.

The necessary modification to the treatment in the previous section is that the states in (C.3.10) are now distinguished also by their spin states, and that the interaction potential with a given atom is replaced by

$$V_j(\mathbf{r}) = \frac{2\pi\hbar^2}{m} \delta(\mathbf{r} - \mathbf{R}_j) \underbrace{(\hat{b}_j + c_j \mathbf{I}_j \sigma)}_{=V_j}. \quad (\text{C.3.29})$$

Here \mathbf{I}_j are the spins of the respective nuclei (or rather their operators) and c_j the respective coupling strengths. Note that this formulation applies only to non-magnetic samples. The effects due to atomic magnetism will be treated in detail below, here it suffices to say that they are similar to the effect of nuclear spins with the added complication that the atomic spins can be ordered and that

the coupling strengths are effectively \mathbf{Q} -dependent via the magnetic form factor.

The action of the components of the spin operator onto $|u\rangle$ and $|v\rangle$, which are the eigenstates with respect to its z -component, are

$$\begin{aligned}\sigma_x|u\rangle &= |v\rangle & \sigma_y|u\rangle &= i|v\rangle & \sigma_z|u\rangle &= |u\rangle \\ \sigma_x|v\rangle &= |u\rangle & \sigma_y|v\rangle &= -i|u\rangle & \sigma_z|v\rangle &= -|v\rangle\end{aligned}\quad (\text{C.3.30})$$

The matrix elements in (C.3.25) are now

$$\langle \lambda_f \sigma_f | V_j e^{i\mathbf{QR}_j} | \lambda_i \sigma_i \rangle = \langle \lambda_f | \langle \sigma_f | V_j | \sigma_i \rangle e^{i\mathbf{QR}_j} | \lambda_i \rangle. \quad (\text{C.3.31})$$

Considering for the moment only the inner matrix element, we have

$$\begin{aligned}V_j|u\rangle &= (\hat{b}_j + c_j(I_x^j \sigma_x + I_y^j \sigma_y + I_z^j \sigma_z))|u\rangle \\ &= \hat{b}_j|u\rangle + c_j(I_x^j + iI_y^j)|v\rangle + c_j I_z^j|u\rangle.\end{aligned}\quad (\text{C.3.32})$$

$|u\rangle$ and $|v\rangle$ are orthonormal, so this leads to

$$\begin{aligned}\langle u | V_j | u \rangle &= \hat{b}_j + c_j I_z^j & \langle v | V_j | u \rangle &= c_j (I_x^j + iI_y^j) \\ \langle u | V_j | v \rangle &= c_j (I_x^j - iI_y^j) & \langle v | V_j | v \rangle &= \hat{b}_j - c_j I_z^j\end{aligned}\quad (\text{C.3.33})$$

As was discussed in A.2.2, apart from exceptional circumstances both the assignment of different isotopes to the atomic positions as well as the configuration of the nuclear spins will be completely random. Thus the matrix elements (C.3.33) pertaining to the neutron spin can be pulled out of the total matrix element, leading to an expression analogous to (C.3.25) with effective scattering lengths $b_j^{w_2, w_1} = \langle w_2 | V_j | w_1 \rangle$ that depend on the spins of incident and outgoing neutrons. In the following, the atomic indices j will be suppressed.

The average values of (C.3.33) are

$$\begin{aligned}\langle b^{u,u} \rangle_{\text{spin,iso}} &= \langle \hat{b} \rangle_{\text{iso}} & \langle b^{v,u} \rangle_{\text{spin,iso}} &= 0 \\ \langle b^{u,v} \rangle_{\text{spin,iso}} &= 0 & \langle b^{v,v} \rangle_{\text{spin,iso}} &= \langle \hat{b} \rangle_{\text{iso}},\end{aligned}\quad (\text{C.3.34})$$

as $\langle I_x \rangle_{\text{spin}} = \langle I_y \rangle_{\text{spin}} = \langle I_z \rangle_{\text{spin}} = 0$. Now the coherent scattering is sensitive only to this averaged scattering length, so it follows immediately that coherent scattering is purely in the non-spin-flip channel, and that the coherent scattering length $b_{\text{coh}} = \langle \hat{b} \rangle_{\text{iso}}$.

Consequently, in the non-magnetic case spin-flip scattering contributes only to incoherent scattering. As the incoherent cross section is proportional to the variance of the effective scattering lengths due to isotopic assignment and spin configuration, we compute the averages of the squared effective scattering lengths in the respective spin channels

$$\langle |b^{u,u}|^2 \rangle_{\text{spin,iso}} = \langle |b^{v,v}|^2 \rangle_{\text{spin,iso}} = \langle \hat{b}^2 \rangle_{\text{iso}} + \langle c^2 I_z^2 \rangle_{\text{spin,iso}} \quad (\text{C.3.35})$$

and

$$\langle |b_j^{v,u}|^2 \rangle_{\text{spin,iso}} = \langle |b_j^{u,v}|^2 \rangle_{\text{spin,iso}} = \langle c^2 I_x^2 \rangle_{\text{spin,iso}} + \langle c^2 I_y^2 \rangle_{\text{spin,iso}}. \quad (\text{C.3.36})$$

We know that the spin states are also eigenstates to the operator

$$\mathbf{I}^2 = I_x^2 + I_y^2 + I_z^2 \quad (\text{C.3.37})$$

with eigenvalue $I(I+1)$, thus for random nuclear spins we have

$$\langle I_x^2 \rangle_{\text{spin}} = \langle I_y^2 \rangle_{\text{spin}} = \langle I_z^2 \rangle_{\text{spin}} = \frac{1}{3}I(I+1). \quad (\text{C.3.38})$$

The contributions in the four spin channels are therefore

$$\sigma_{\text{inc}}^{u,u} = \sigma_{\text{inc}}^{v,v} = 4\pi \left(\langle \hat{b}^2 \rangle_{\text{iso}} - \langle \hat{b} \rangle_{\text{iso}}^2 + \frac{1}{3} \langle c^2 I(I+1) \rangle_{\text{iso}} \right) \quad (\text{C.3.39})$$

and

$$\sigma_{\text{inc}}^{u,v} = \sigma_{\text{inc}}^{v,u} = 4\pi \frac{2}{3} \langle c^2 I(I+1) \rangle_{\text{iso}}. \quad (\text{C.3.40})$$

Thus, we see that the incoherent cross section due to nuclear spin for non-spin-flip scattering is half of the value for spin-flip scattering, and that the incoherent cross section due to isotopic assignment is again only in the non-spin-flip channel. Thus, for instance in the case of natural Ni, which consists of a number of isotopes with nearly all having spin $I = 0$, the incoherent scattering is nearly exclusively non-spin-flip, while for V with essentially just one isotope, the incoherent scattering shows the 1 : 2 ratio of non-spin-flip to spin-flip scattering.

C.4 The van Hove formalism

The correlation functions as introduced by Léon van Hove (1954) establish a link between the dynamical behaviour of the nuclei in the sample and the double differential cross sections in quasi-elastic and inelastic scattering. Canonically, they are discussed with respect to a non-magnetic scattering system composed only of a single kind of element. How this formalism can be generalized to multi-component systems will be pointed out below.

C.4.1 Correlation functions

The starting point is to define a function $S(\mathbf{Q}, \omega)$ so that the coherent part of the double differential cross section (C.3.25), that is, where the scattering lengths b_j are replaced by their expected values, for an elemental system can be written as

$$\begin{aligned} \left(\frac{d^2\sigma}{d\Omega dE_f} \right)_{\text{coh}} &= \frac{\sigma_{\text{coh}}}{4\pi} \frac{k_f}{k_i} \frac{1}{2\pi\hbar} \int dt \sum_{j,j'} \langle e^{-i\mathbf{Q}\mathbf{R}_{j'}(0)} e^{i\mathbf{Q}\mathbf{R}_j(t)} \rangle e^{-i\omega t} \\ &= \frac{\sigma_{\text{coh}}}{4\pi} \frac{k_f}{k_i} N S(\mathbf{Q}, \omega), \end{aligned} \quad (\text{C.4.1})$$

with N the number of nuclei. Thus,

$$S(\mathbf{Q}, \omega) = \frac{1}{2\pi\hbar N} \int dt \sum_{j,j'} \langle e^{-i\mathbf{Q}\mathbf{R}_{j'}(0)} e^{i\mathbf{Q}\mathbf{R}_j(t)} \rangle e^{-i\omega t}. \quad (\text{C.4.2})$$

This function is called the (*coherent*) *scattering function* or *dynamical structure factor*.⁴ The (*coherent*) *intermediate scattering function* is its temporal Fourier transform (apart from a factor \hbar)

$$I(\mathbf{Q}, t) = \hbar \int d\omega S(\mathbf{Q}, \omega) e^{i\omega t} = \frac{1}{N} \sum_{j,j'} \langle e^{-i\mathbf{Q}\mathbf{R}_{j'}(0)} e^{i\mathbf{Q}\mathbf{R}_j(t)} \rangle, \quad (\text{C.4.3})$$

and the (*time-dependent*) *pair-correlation function* is in turn the spatial inverse Fourier transform of the intermediate scattering function

$$\begin{aligned} G(\mathbf{r}, t) &= \frac{1}{(2\pi)^3} \int d\mathbf{Q} I(\mathbf{Q}, t) e^{-i\mathbf{Q}\mathbf{r}} = \frac{\hbar}{(2\pi)^3} \int d\mathbf{Q} d\omega S(\mathbf{Q}, \omega) e^{-i\mathbf{Q}\mathbf{r} + i\omega t} \\ &= \frac{1}{(2\pi)^3 N} \int d\mathbf{Q} \sum_{j,j'} \langle e^{-i\mathbf{Q}\mathbf{R}_{j'}(0)} e^{i\mathbf{Q}\mathbf{R}_j(t)} \rangle e^{-i\mathbf{Q}\mathbf{r}}. \end{aligned} \quad (\text{C.4.4})$$

Analogously, the *incoherent scattering function*, *incoherent* or *self-intermediate scattering function* and the *self-correlation function* are defined analogously in terms of the incoherent part of the double differential cross section

$$\left(\frac{d^2\sigma}{d\Omega dE_f} \right)_{\text{inc}} = \frac{\sigma_{\text{inc}}}{4\pi} \frac{k_f}{k_i} N S_i(\mathbf{Q}, \omega), \quad (\text{C.4.5})$$

that is,

$$S_i(\mathbf{Q}, \omega) = \frac{1}{2\pi\hbar N} \int dt \sum_j \langle e^{-i\mathbf{Q}\mathbf{R}_j(0)} e^{i\mathbf{Q}\mathbf{R}_j(t)} \rangle e^{-i\omega t}, \quad (\text{C.4.6})$$

$$I_s(\mathbf{Q}, t) = \frac{1}{N} \sum_j \langle e^{-i\mathbf{Q}\mathbf{R}_j(0)} e^{i\mathbf{Q}\mathbf{R}_j(t)} \rangle, \quad (\text{C.4.7})$$

and

$$G_s(\mathbf{r}, t) = \frac{1}{(2\pi)^3 N} \int d\mathbf{Q} \sum_j \langle e^{-i\mathbf{Q}\mathbf{R}_j(0)} e^{i\mathbf{Q}\mathbf{R}_j(t)} \rangle e^{-i\mathbf{Q}\mathbf{r}}. \quad (\text{C.4.8})$$

To actually perform the inverse Fourier transform in the definition of $G(\mathbf{r}, t)$ and $G_s(\mathbf{r}, t)$ and to write these quantities only in terms of positional coordinates, the non-commuting of the position operators $\mathbf{R}_j(t)$ has to be respected. In order to separate one of the two out of the integral we first artificially insert another integral over a δ distribution and exchange the order of integration

$$\begin{aligned} \int d\mathbf{Q} e^{-i\mathbf{Q}\mathbf{R}_{j'}(0)} e^{i\mathbf{Q}\mathbf{R}_j(t)} e^{-i\mathbf{Q}\mathbf{r}} &= \int d\mathbf{Q} \int d\mathbf{r}' \delta(\mathbf{r}' - \mathbf{R}_{j'}(0)) e^{-i\mathbf{Q}\mathbf{r}'} e^{i\mathbf{Q}\mathbf{R}_j(t)} e^{-i\mathbf{Q}\mathbf{r}} \\ &= \int d\mathbf{r}' \delta(\mathbf{r}' - \mathbf{R}_{j'}(0)) \underbrace{\int d\mathbf{Q} e^{-i\mathbf{Q}(\mathbf{r}' - \mathbf{R}_j(t) + \mathbf{r})}}_{=(2\pi)^3 \delta(\mathbf{r}' - \mathbf{R}_j(t) + \mathbf{r})}. \end{aligned} \quad (\text{C.4.9})$$

⁴To quote Squires (1978): "It is also known as the *scattering law*, though why a function should be called a law is a mystery to the author." The present author shares this view.

Therefore

$$G(\mathbf{r}, t) = \frac{1}{N} \int d\mathbf{r}' \sum_{j,j'} \langle \delta(\mathbf{r}' - \mathbf{R}_{j'}(0)) \delta(\mathbf{r}' + \mathbf{r} - \mathbf{R}_j(t)) \rangle \quad (\text{C.4.10})$$

as well as

$$G_s(\mathbf{r}, t) = \frac{1}{N} \int d\mathbf{r}' \sum_j \langle \delta(\mathbf{r}' - \mathbf{R}_j(0)) \delta(\mathbf{r}' + \mathbf{r} - \mathbf{R}_j(t)) \rangle. \quad (\text{C.4.11})$$

Defining the *particle-density operator*

$$\rho(\mathbf{r}, t) = \sum_j \delta(\mathbf{r} - \mathbf{R}_j(t)) \quad (\text{C.4.12})$$

the pair-correlation function can further be written as

$$G(\mathbf{r}, t) = \frac{1}{N} \int d\mathbf{r}' \langle \rho(\mathbf{r}', 0) \rho(\mathbf{r}' + \mathbf{r}, t) \rangle, \quad (\text{C.4.13})$$

and the self-correlation function is given by

$$G_s(\mathbf{r}, t) = \int d\mathbf{r}' \langle \rho_s(\mathbf{r}', 0) \rho_s(\mathbf{r}' + \mathbf{r}, t) \rangle \quad (\text{C.4.14})$$

with

$$\rho_s(\mathbf{r}, t) = \delta(\mathbf{r} - \mathbf{R}_j(t)) \quad (\text{C.4.15})$$

the density operator of any specific particle j .

The generalization to multi-element systems is straight-forward: taking for instance (C.4.10), the double sum over the particles has to be split into $L \times L$ partial sums for an L -element system according to the species of the respective particles, giving partial pair-correlation functions $G^{\alpha,\beta}(\mathbf{r}, t)$ for the correlations between particles of elements α and β . Analogously partial intermediate scattering functions and dynamical structure factors can be defined, so that the coherent double differential cross section is given by the sum over the partial dynamical structure factors, weighted by the respective products of scattering lengths. In the same way, L element-specific self-correlation functions, incoherent intermediate scattering functions and incoherent scattering functions can be defined to write the incoherent double differential cross sections.

C.4.2 Properties of the correlation functions

Expression (C.3.13) shows that, as the Schrödinger operators \mathbf{R}_j are self-adjoint, the partial double differential cross sections for $\lambda_1 \rightarrow \lambda_2$ is the same as the one for $\lambda_2 \rightarrow \lambda_1$. Thus, the difference between $S(\mathbf{Q}, \omega)$, which is essentially these partial double differential cross sections summed over all initial and final states with a weighting proportional to the Boltzmann factor of the initial state, and $S(-\mathbf{Q}, -\omega)$, the double differential cross section for the reverse transitions, is just that in

the latter case the final states would determine the weighting. This leads to the relation

$$S(\mathbf{Q}, \omega) = e^{\hbar\omega/k_B T} S(-\mathbf{Q}, -\omega), \quad (\text{C.4.16})$$

which is known as the *principle of detailed balance*. In words, it means that, all other things being equal, the probability for the neutron to lose energy ($\omega > 0$) is larger than to gain energy. This principle is not restricted to neutron scattering, more generally in any system in thermal equilibrium the frequencies of back and forth transitions between any two states have to be equal, thus the rates have to vary inversely proportional to the respective weights of the initial states in the ensemble.

As the double differential cross section (C.4.1) is real (for real interaction potentials, that is, in the absence of absorption as is always assumed here), it immediately follows that $S(\mathbf{Q}, \omega)$ is real as well

$$S(\mathbf{Q}, \omega) = S^*(\mathbf{Q}, \omega). \quad (\text{C.4.17})$$

From this expression Fourier transformation gives

$$I(\mathbf{Q}, t) = I^*(\mathbf{Q}, -t) \quad (\text{C.4.18})$$

and

$$G(\mathbf{r}, t) = G^*(-\mathbf{r}, -t). \quad (\text{C.4.19})$$

Using (C.4.16) we obtain

$$\begin{aligned} I(\mathbf{Q}, t) &= \hbar \int d\omega S(\mathbf{Q}, \omega) e^{i\omega t} = \hbar \int d\omega S(-\mathbf{Q}, -\omega) e^{\hbar\omega/k_B T} e^{i\omega t} \\ &= \hbar \int d\omega S(-\mathbf{Q}, \omega) e^{-\hbar\omega/k_B T} e^{-i\omega t} = I(-\mathbf{Q}, -t + i\hbar/k_B T) \end{aligned} \quad (\text{C.4.20})$$

and analogously

$$G(\mathbf{r}, t) = G(-\mathbf{r}, -t + i\hbar/k_B T) = G^*(\mathbf{r}, t - i\hbar/k_B T). \quad (\text{C.4.21})$$

Thus, $G(\mathbf{r}, t)$ in general is complex. This is inherently a quantum-mechanical effect: in the classical limit with $\hbar \rightarrow 0$, the position operators and therefore also the particle-density operators commute also for different times. As a consequence we have in this case

$$\begin{aligned} G(\mathbf{r}, t) &= \frac{1}{N} \int d\mathbf{r}' \langle \rho(\mathbf{r}', 0) \rho(\mathbf{r}' + \mathbf{r}, t) \rangle = \frac{1}{N} \int d\mathbf{r}' \langle \rho(\mathbf{r}' + \mathbf{r}, t) \rho(\mathbf{r}', 0) \rangle \\ &= G(-\mathbf{r}, -t) = G^*(\mathbf{r}, t) \end{aligned} \quad (\text{C.4.22})$$

with the last equality due to (C.4.19).

C.4.3 Classical interpretation of the correlation functions

Interpreting $\mathbf{R}_j(t)$ in (C.4.10) as classical particle positions, the pair-correlation function $G^{\text{cl}}(\mathbf{r}, t)$ is just the probability density for the position $\mathbf{r}' + \mathbf{r}$ to be occupied

by an atom at time t if position \mathbf{r}' was occupied by any atom (either the same or a different one) at time 0. Analogously, the self-correlation function in the classical interpretation $G_s^{\text{cl}}(\mathbf{r}, t)$ is the probability density for the position $\mathbf{r}' + \mathbf{r}$ to be occupied by an atom at time t if position \mathbf{r}' was occupied by the same atom at time 0, or in other words, for an atom to move a distance \mathbf{r} within a time t . With the connection of the correlation functions to the scattering functions and thus to the experimentally accessible double differential cross sections, it would be very tempting to derive expressions for the correlation functions in a classical setting and compare them to the experiments, as in the general case full quantum-mechanical calculations become unfeasible.

In general, quantum-mechanical effects become negligible at large distances and long times, that is, for $\hbar^2 q^2/2m \ll k_B T$ and $\hbar\omega \ll k_B T$, with m the particle mass. At low temperatures, diffusive dynamics in the solid state can become arbitrarily slow, so that the classical approximation is valid. On the other hand, oscillatory dynamics belong clearly to the full quantum-mechanical regime, where the quantization of energies is reflected in the discreteness of neutron energy transfers as will be discussed in more detail below. Diffusive dynamics in the liquid state constitute a middle ground, and especially here the following issue is relevant:

Specifically, as has been pointed out already below, in the classical approximation the pair-correlation function is real. As a consequence, the resulting scattering function as essentially its Fourier transform has to be even, that is

$$S^{\text{cl}}(\mathbf{Q}, \omega) = S^{\text{cl}}(-\mathbf{Q}, -\omega), \quad (\text{C.4.23})$$

which obviously violates detailed balance. Thus, the classical form of the pair-correlation function has to be expected to be a poor approximation to the actual expression. Schofield (1960) has suggested that a better approximation is afforded by setting

$$G(\mathbf{r}, t) = G^{\text{cl}}(\mathbf{r}, t - i\hbar/2k_B T) \quad (\text{C.4.24})$$

or

$$S(\mathbf{Q}, \omega) = S^{\text{cl}}(\mathbf{Q}, \omega) e^{\hbar\omega/2k_B T}, \quad (\text{C.4.25})$$

thereby fulfilling detailed balance. This is the approach typically taken in interpreting neutron scattering data.

A case where the classical interpretation becomes valid is constituted for $t \rightarrow \infty$, so that the Heisenberg operators $\mathbf{R}_j(t)$ become ordinary random variables. Further, as all correlations decay for long times, we have

$$G(\mathbf{r}, \infty) = \frac{1}{N} \int d\mathbf{r}' \langle \rho(\mathbf{r}') \rangle \langle \rho(\mathbf{r}' + \mathbf{r}) \rangle. \quad (\text{C.4.26})$$

After a double (inverse) Fourier to $S(\mathbf{Q}, \omega)$, this gives a δ distribution in frequency, that is, an ideally perfectly sharp elastic line with a corresponding variation in intensity with \mathbf{Q} . Note that such elastic scattering exists only for crystals, where $\langle \rho(\mathbf{r}') \rangle$ shows modulations according to the temporally stable translational periodicity, while in a liquid the diffusive dynamics lead to a flat $\langle \rho(\mathbf{r}') \rangle$ and thus no elastically scattered intensity apart from the forward direction.

On the other hand, also for $t = 0$ the classical approximation is strictly valid. Here the operators in (C.4.10) do commute, resulting in

$$G(\mathbf{r}, 0) = \delta(\mathbf{r}) + g(\mathbf{r}) \quad (\text{C.4.27})$$

where

$$g(\mathbf{r}) = \frac{1}{N} \sum_{j \neq j'} \langle \delta(\mathbf{r} - \mathbf{R}_j + \mathbf{R}_{j'}) \rangle \quad (\text{C.4.28})$$

is the *static pair-distribution function*.

Transforming back to $S(\mathbf{Q}, \omega)$, the pair-correlation function evaluated at $t = 0$, that is, essentially $g(\mathbf{r})$, contributes equally for all ω , or otherwise, $G(\mathbf{r}, 0)$ is just $S(\mathbf{Q}, \omega)$ integrated over ω . It is tempting to identify this with the (single-)differential cross section $d\sigma/d\Omega$, that is, the case of diffraction where all neutrons scattered into a given direction irrespective of energy are counted. However, the catch is that the equivalence of direction and wavevector transfer is valid only for a given energy transfer. Assuming this correspondence is what constitutes the so-called *static approximation*. Specifically, in the static approximation the diffraction differential cross section evaluates as

$$\left(\frac{d\sigma}{d\Omega} \right)_{\text{coh}}^{\text{sa}} = \frac{\sigma_{\text{coh}}}{4\pi} NI(\mathbf{Q}, 0) \quad (\text{C.4.29})$$

with \mathbf{Q} corresponding to the considered outgoing direction. Of course, if there is only elastic scattering (which however is actually not even fulfilled at zero temperature due to quantum-mechanical zero-point motion), the above expression is exact.

The degree of validity of the static approximation depends on the characteristic energy transfers experienced during scattering relative to the energy of the probe. If the energy transfers are small ($\Delta E/E \ll 1$), the equivalence between directions and wavevector transfers holds, and the static approximation is valid. For X-rays, this is typically the case, and static pair-distribution functions $g(\mathbf{r})$ are routinely derived from diffraction patterns taken with diffractometers without energy analysis. On the other hand, for thermal neutrons this is in general not fulfilled, as their energies are comparable to typical excitation energies. Note, however, that luckily the important case of studying Bragg peak positions on a diffractometer is not affected by these issues, as the Bragg intensities are exclusively due to elastic scattering. In contrast, for studies of the diffuse intensity between the peaks either energy analysis has to be performed to extract the elastic intensity or the intensity at a given outgoing direction has to be modelled as an integral over $S(\mathbf{Q}, \omega)$ along the appropriate path through four-dimensional (\mathbf{Q}, ω) -space.

C.5 Fundamentals of magnetic scattering

Up to now, exclusively nuclear neutron scattering was considered, that is, only interactions with the sample due to the nuclear force. However, via its magnetic

moment a neutron experiences also electromagnetic interactions with the sample, specifically with the internal magnetic field resulting from both the magnetic moments and motions of the charged particles making up the sample. According to the different masses, for both mechanisms the effect of electrons is proportionally larger than of protons. The corresponding scattering contributions have the same order of magnitude as the nuclear contributions, so that neutron scattering is by far the most important experimental method to microscopically study magnetism. The fundamental results of the theory for the scattering of unpolarized neutron beams will be given here, where due to the complexity of the matter steps in the derivation will often be skipped.

C.5.1 The neutron-electron interaction

A given electron with magnetic dipole moment

$$\boldsymbol{\mu}_e = -2\mu_B \mathbf{s} \quad (\text{C.5.1})$$

with the origin chosen at the position of the electron, where \mathbf{s} is the electron's spin (operator),⁵ and momentum (operator) \mathbf{p} has an associated magnetic field of

$$\mathbf{B}(\mathbf{R}) = \frac{\mu_0}{4\pi} \left(\nabla \times \left(\frac{\boldsymbol{\mu}_e \times \mathbf{R}}{R^3} \right) - \frac{2\mu_B}{\hbar} \frac{\mathbf{p} \times \mathbf{R}}{R^3} \right), \quad (\text{C.5.2})$$

where the first term follows from the magnetic field of a dipole and the second from the Biot-Savart law with the current element due to the electron of

$$I d\mathbf{l} = -\frac{e}{m_e} \mathbf{p} = -\frac{2\mu_B}{\hbar} \mathbf{p}. \quad (\text{C.5.3})$$

With the potential energy of a dipole in a field

$$V = -\boldsymbol{\mu} \mathbf{B}, \quad (\text{C.5.4})$$

the potential felt by the neutron can be written as

$$V(\mathbf{R}; \boldsymbol{\sigma}) = -\mu_0 \gamma \mu_N 2\mu_B \boldsymbol{\sigma} \left(\underbrace{\frac{1}{4\pi} \nabla \times \left(\frac{\mathbf{s} \times \mathbf{R}}{R^3} \right)}_{\mathbf{w}_S} + \underbrace{\frac{1}{4\pi \hbar} \frac{\mathbf{p} \times \mathbf{R}}{R^3}}_{\mathbf{w}_L} \right), \quad (\text{C.5.5})$$

using

$$\boldsymbol{\mu}_n = -\gamma \mu_N \boldsymbol{\sigma} \quad (\text{C.5.6})$$

as the magnetic dipole moment of the neutron with the nuclear magneton

$$\mu_N = \frac{e\hbar}{2m_p} \quad (\text{C.5.7})$$

and the dimensionless factor $\gamma = 1.913$. This is the canonical notation in the neutron scattering community, but note that γ is not the gyromagnetic ratio (which has dimension $\text{s}^{-1}\text{T}^{-1}$), even though this is typically also denoted by γ , and neither it is the dimensionless g -factor (actually it is the negative of the half of the neutron's $g = -3.826$).

⁵Note that by accepted convention the electron spin \mathbf{s} is defined to have eigenvalues of $\pm \frac{1}{2}$, while in the neutron scattering community the operator $\boldsymbol{\sigma}$ defining the neutron's magnetic moment is represented by the Pauli operator and thus has eigenvalues of ± 1 , even though in both cases spin- $\frac{1}{2}$ particles are considered. Correctly, the neutron's spin would be $\boldsymbol{\sigma}/2$, but this distinction is typically neglected.

C.5.2 The partial differential scattering cross section due to electrons

Applying the generic expression for the partial cross section (C.3.10) to the case of electrons, the neutron spins have to be explicitly considered, giving

$$\left. \frac{d^2\sigma}{d\Omega dE_f} \right|_{\sigma_i, \lambda_i \rightarrow \sigma_f \lambda_f} = \frac{k_f}{k_i} \left(\frac{m_n}{2\pi\hbar^2} \right)^2 |\langle \mathbf{k}_f \sigma_f \lambda_f | V | \mathbf{k}_i \sigma_i \lambda_i \rangle|^2 \delta(\hbar\omega + E_{\lambda_i} - E_{\lambda_f}). \quad (\text{C.5.8})$$

Now the matrix elements of \mathbf{W}_S and \mathbf{W}_L , responsible for interaction with the spin and orbital components of the magnetization, with respect to the neutron spatial coordinates have to be computed. After some purely mathematical steps the results are

$$\langle \mathbf{k}_f | \mathbf{W}_{Sj} | \mathbf{k}_i \rangle = e^{i\mathbf{Q}\mathbf{r}_j} \frac{\mathbf{Q} \times \mathbf{s}_j \times \mathbf{Q}}{|\mathbf{Q}|^2} \quad (\text{C.5.9})$$

and

$$\langle \mathbf{k}_f | \mathbf{W}_{Lj} | \mathbf{k}_i \rangle = \frac{i}{\hbar} e^{i\mathbf{Q}\mathbf{r}_j} \frac{\mathbf{p}_j \times \mathbf{Q}}{|\mathbf{Q}|^2}, \quad (\text{C.5.10})$$

where \mathbf{r}_j is the position of electron j . Further, collecting the prefactors gives

$$\underbrace{\frac{\mu_0 \gamma \mu_N 2\mu_B}{\text{from (C.5.5)}}}_{\text{from (C.5.5)}} \times \underbrace{\frac{m_n}{2\pi\hbar^2}}_{\text{from (C.5.8)}} = \gamma \mu_0 \frac{e\hbar}{2m_p} 2 \frac{e\hbar}{2m_e} \frac{m_n}{2\pi\hbar^2} \approx \gamma \frac{\mu_0}{4\pi} \frac{e^2}{m_e} = \gamma r_0, \quad (\text{C.5.11})$$

where r_0 is the classical electron radius (also called Thomson scattering length) and neutron and proton masses have been equated.

Defining the operators

$$\hat{\mathbf{W}}_{\perp S} = \frac{1}{|\mathbf{Q}|^2} \sum_j e^{i\mathbf{Q}\mathbf{r}_j} (\mathbf{Q} \times \mathbf{s}_j \times \mathbf{Q}) \quad (\text{C.5.12})$$

and

$$\hat{\mathbf{W}}_{\perp L} = \frac{i}{\hbar |\mathbf{Q}|^2} \sum_j e^{i\mathbf{Q}\mathbf{r}_j} (\mathbf{p}_j \times \mathbf{Q}) \quad (\text{C.5.13})$$

the partial differential cross section reads

$$\left. \frac{d^2\sigma}{d\Omega dE_f} \right|_{\sigma_i, \lambda_i \rightarrow \sigma_f \lambda_f} = (\gamma r_0)^2 \frac{k_f}{k_i} |\langle \sigma_f \lambda_f | \sigma (\hat{\mathbf{W}}_{\perp S} + \hat{\mathbf{W}}_{\perp L}) | \sigma_i \lambda_i \rangle|^2 \delta(\hbar\omega + E_{\lambda_i} - E_{\lambda_f}). \quad (\text{C.5.14})$$

Defining further the electron spin density operator

$$\rho_S(\mathbf{r}) = \sum_j \delta(\mathbf{r} - \mathbf{R}_j) \mathbf{s}_j \quad (\text{C.5.15})$$

we see that we can write $\hat{\mathbf{W}}_{\perp S}$ as the component perpendicular to \mathbf{Q}

$$\hat{\mathbf{W}}_{\perp S} = \frac{1}{|\mathbf{Q}|^2} (\mathbf{Q} \times \hat{\mathbf{W}}_S \times \mathbf{Q}) \quad (\text{C.5.16})$$

of an operator

$$\hat{\mathbf{W}}_S = \sum_j e^{i\mathbf{Q}\cdot\mathbf{r}_j} \mathbf{s}_j \quad (\text{C.5.17})$$

that is the Fourier transform of the electron spin density operator. By more involved calculations a formally analogous result is obtained for the orbital component

$$\hat{\mathbf{W}}_{\perp L} = -\frac{1}{2\mu_B} \frac{1}{|\mathbf{Q}|^2} (\mathbf{Q} \times \hat{\mathbf{M}}_L(\mathbf{Q}) \times \mathbf{Q}) \quad (\text{C.5.18})$$

where $\hat{\mathbf{M}}_L(\mathbf{Q})$ is the Fourier transform of the magnetization due to the orbital magnetic moments. Indeed, by defining also a spin magnetization operator

$$\mathbf{M}_S(\mathbf{r}) = -2\mu_B \rho_S(\mathbf{r}) \quad (\text{C.5.19})$$

the analogy becomes complete, so that (C.5.14) can be written in terms of the Fourier transform of the total magnetization's component perpendicular to \mathbf{Q}

$$\left. \frac{d^2\sigma}{d\Omega dE_f} \right|_{\sigma_i, \lambda_i \rightarrow \sigma_f, \lambda_f} = \left(\frac{\gamma r_0}{2\mu_B} \right)^2 \frac{k_f}{k_i} |\langle \sigma_f \lambda_f | \sigma \hat{\mathbf{M}}_{\perp} | \sigma_i \lambda_i \rangle|^2 \delta(\hbar\omega + E_{\lambda_i} - E_{\lambda_f}). \quad (\text{C.5.20})$$

Thus, neutron scattering is sensitive always only on the *perpendicular* component of the sample magnetization.

C.5.3 The general double differential cross section

To now obtain the full double differential cross section, the same program as in Sect. C.3.1 has to be performed, that is, these partial differential cross sections have to be summed over all final states and averaged (with the correct weighting) over all initial states, where now also the neutron spin is explicitly considered. As the neutron spin does not affect the argument of the δ distribution, the summation with respect to it can be performed before the δ distribution is transformed. That is, we need to compute

$$\sum_{\sigma_i, \sigma_f} p_{\sigma_i} |\langle \sigma_f \lambda_f | \sigma \hat{\mathbf{M}}_{\perp} | \sigma_i \lambda_i \rangle|^2. \quad (\text{C.5.21})$$

The inner product $\sigma \hat{\mathbf{M}}_{\perp}$ is just the sum of the products of the components, and the neutron spin and the electron coordinates are independent degrees of freedom. Thus, these matrix elements are the product of matrix elements in the respective degrees of freedom

$$\langle \sigma_f \lambda_f | \sigma_{\alpha} \hat{M}_{\perp, \alpha} | \sigma_i \lambda_i \rangle = \langle \sigma_f | \sigma_{\alpha} | \sigma_i \rangle \langle \lambda_f | \hat{M}_{\perp, \alpha} | \lambda_i \rangle \quad (\text{C.5.22})$$

where α is a specific Cartesian coordinate axis. We treat for now only the first factor. Summing over the final neutron spin states gives

$$\sum_{\alpha, \beta} \sum_{\sigma_f} \langle \sigma_i | \sigma_{\alpha} | \sigma_f \rangle \langle \sigma_f | \sigma_{\beta} | \sigma_i \rangle = \sum_{\alpha, \beta} \langle \sigma_i | \sigma_{\alpha} \sigma_{\beta} | \sigma_i \rangle. \quad (\text{C.5.23})$$

Now we distinguish between $\alpha = \beta$ and $\alpha \neq \beta$. Due to the neutron's spin $\frac{1}{2}$ it has two spin states. With the expressions for the pertaining spin algebra (C.3.30) we have

$$\langle u | \sigma_\alpha^2 | u \rangle = \langle v | \sigma_\alpha^2 | v \rangle = 1 \quad (\text{C.5.24})$$

and for $\alpha \neq \beta$

$$\langle u | \sigma_\alpha \sigma_\beta | u \rangle = -\langle v | \sigma_\alpha \sigma_\beta | v \rangle = \pm i. \quad (\text{C.5.25})$$

With

$$p_u = p_v = \frac{1}{2} \quad (\text{C.5.26})$$

for unpolarized incident neutrons we get

$$\begin{aligned} \sum_{\sigma_i, \sigma_f} p_{\sigma_i} |\langle \sigma_f \lambda_f | \sigma \hat{\mathbf{M}}_\perp | \sigma_i \lambda_i \rangle|^2 &= \sum_{\alpha, \beta} \langle \lambda_i | \hat{\mathbf{M}}_{\perp, \beta}^* | \lambda_f \rangle \langle \lambda_f | \hat{\mathbf{M}}_{\perp, \alpha} | \lambda_i \rangle \underbrace{\sum_{\sigma_i} p_{\sigma_i} \langle \sigma_i | \sigma_\beta \sigma_\alpha | \sigma_i \rangle}_{=\delta_{\alpha, \beta}} \\ &= \sum_{\alpha} \langle \lambda_i | \hat{\mathbf{M}}_{\perp, \alpha}^* | \lambda_f \rangle \langle \lambda_f | \hat{\mathbf{M}}_{\perp, \alpha} | \lambda_i \rangle \end{aligned} \quad (\text{C.5.27})$$

Thus we get for the full double differential cross section

$$\begin{aligned} \frac{d^2 \sigma}{d\Omega dE_f} &= \left(\frac{\gamma r_0}{2\mu_B} \right)^2 \frac{k_f}{k_i} \sum_{\lambda_f, \lambda_i} p_{\lambda_i} \sum_{\alpha} \langle \lambda_i | \hat{\mathbf{M}}_{\perp, \alpha}^* | \lambda_f \rangle \langle \lambda_f | \hat{\mathbf{M}}_{\perp, \alpha} | \lambda_i \rangle \delta(\hbar\omega + E_{\lambda_i} - E_{\lambda_f}) \\ &= \left(\frac{\gamma r_0}{2\mu_B} \right)^2 \frac{k_f}{k_i} \sum_{\alpha, \beta} \left(\delta_{\alpha, \beta} - \frac{Q_\alpha Q_\beta}{|\mathbf{Q}|^2} \right) \\ &\quad \sum_{\lambda_f, \lambda_i} p_{\lambda_i} \langle \lambda_i | \hat{\mathbf{M}}_{\perp, \alpha}^* | \lambda_f \rangle \langle \lambda_f | \hat{\mathbf{M}}_{\perp, \beta} | \lambda_i \rangle \delta(\hbar\omega + E_{\lambda_i} - E_{\lambda_f}) \end{aligned} \quad (\text{C.5.28})$$

using the identity

$$\begin{aligned} \hat{\mathbf{M}}_\perp^* \hat{\mathbf{M}}_\perp &= \left(\hat{\mathbf{M}}^* - \frac{(\hat{\mathbf{M}}^* \mathbf{Q}) \mathbf{Q}}{|\mathbf{Q}|^2} \right) \left(\hat{\mathbf{M}} - \frac{(\hat{\mathbf{M}} \mathbf{Q}) \mathbf{Q}}{|\mathbf{Q}|^2} \right) = \hat{\mathbf{M}}^* \hat{\mathbf{M}} - \frac{(\hat{\mathbf{M}}^* \mathbf{Q})(\hat{\mathbf{M}} \mathbf{Q})}{|\mathbf{Q}|^2} \\ &= \sum_{\alpha, \beta} \left(\delta_{\alpha, \beta} - \frac{Q_\alpha Q_\beta}{|\mathbf{Q}|^2} \right) \hat{M}_\alpha^* \hat{M}_\beta \end{aligned} \quad (\text{C.5.29})$$

in the last step. Thus, we have arrived again at an expression where the properties of the sample are separated from the specifics of the scattering process.

C.5.4 Spin-only scattering and the magnetic form factor

An important special case given by scattering due to spin only, that is, where there is no orbital contribution to the magnetization. Further, we assume that the unpaired electrons are localized close to the nuclear positions, so that the concept of spin magnetization due to the single atoms is well-defined (this is known as the

Heitler-London model). Thus, the spin contribution due to the distinct electrons (C.5.17) can be reduced to an expression involving atoms

$$\hat{\mathbf{W}}_S = \sum_n e^{i\mathbf{Q}\mathbf{R}_n} \sum_{j_n} e^{i\mathbf{Q}\Delta\mathbf{r}_{j_n}} \mathbf{s}_{j_n} \quad (\text{C.5.30})$$

where \mathbf{R}_n are the atomic positions and $\Delta\mathbf{r}_{j_n}$ the positions of the respective electrons relative to the nucleus. Thus, the contribution to the matrix element due to atom n is

$$\langle \lambda_f | \hat{\mathbf{W}}_S | \lambda_i \rangle_n = \langle \lambda_f | e^{i\mathbf{Q}\mathbf{R}_n} \sum_{j_n} e^{i\mathbf{Q}\Delta\mathbf{r}_{j_n}} \mathbf{s}_{j_n} | \lambda_i \rangle. \quad (\text{C.5.31})$$

In the typical case where transitions of the orbital states of the electrons or of the spin quantum numbers of the ions are too high in energy to be either excitable by the incident neutron energies or to happen spontaneously as thermal excitations, the transitions involve only the orientations of the spins (or the nuclear positions as was treated in the previous sections). Thus, the frozen degrees of freedom can be pulled out of the matrix element, giving

$$\langle \lambda_f | \hat{\mathbf{W}}_S | \lambda_i \rangle_n = F_n(\mathbf{Q}) \langle \lambda_f | e^{i\mathbf{Q}\mathbf{R}_n} \mathbf{S}_n | \lambda_i \rangle, \quad (\text{C.5.32})$$

where \mathbf{S}_n is the atomic spin vector. The Fourier transform of the normalized density of the unpaired electrons belonging to a given atom

$$F_n(\mathbf{Q}) = \frac{\int d\mathbf{r} \rho_n(\mathbf{r}) e^{i\mathbf{Q}\mathbf{r}}}{\int d\mathbf{r} \rho_n(\mathbf{r})} \quad (\text{C.5.33})$$

is known as the *magnetic form factor* of the atom. This gives the expression for the double differential cross section

$$\begin{aligned} \frac{d^2\sigma}{d\Omega dE_f} &= (\gamma r_0)^2 \frac{k_f}{k_i} \sum_{\alpha, \beta} \left(\delta_{\alpha, \beta} - \frac{Q_\alpha Q_\beta}{|\mathbf{Q}|^2} \right) \sum_{n, n'} F_n^*(\mathbf{Q}) F_n(\mathbf{Q}) \\ &\quad \sum_{\lambda_f, \lambda_i} p_{\lambda_i} \langle \lambda_i | e^{-i\mathbf{Q}\mathbf{R}_{n'}} S_{n'}^\alpha | \lambda_f \rangle \langle \lambda_f | e^{i\mathbf{Q}\mathbf{R}_n} S_n^\beta | \lambda_i \rangle \delta(\hbar\omega + E_{\lambda_i} - E_{\lambda_f}) \end{aligned} \quad (\text{C.5.34})$$

where S_n^α is the operator corresponding to the component α of the spin of atom n .

Due to the normalization in (C.5.33)

$$F_n(\mathbf{0}) = 1. \quad (\text{C.5.35})$$

As the unpaired spin density for typical cases is essentially non-negative, for $\mathbf{Q} \neq \mathbf{0}$ it decays towards zero. Thus, its behaviour (and also the effect on the intensity of magnetic scattering as we will see below) is perfectly analogous to the conventional atomic form factor relevant for X-ray scattering, which is the Fourier transform of the non-spin-resolved atomic electron density. However, while apart from the very lightest elements the majority of an atom's electrons is in deeper shells and thus close to the nucleus, the unpaired spin density is due to partially filled outer shells. As a consequence, the magnetic form factor decays much faster with \mathbf{Q} than the conventional form factor, so that magnetic scattering is only visible in the innermost Brillouin zones. The magnetic form factor is in principle transferable between different structures as long as the ionization state of the respective atoms is the same. Parametrizations of the magnetic form factors of the elements in the relevant ionization states are available in tabulated form. This decay with \mathbf{Q} can for instance be used to separate nuclear from magnetic diffraction peaks.

C.5.5 The magnetic case of van Hove theory

To repeat, the assumptions introduced in the previous section implied that the degrees of freedom of a system accessible by neutron scattering, which previously comprised only the nuclear positions, are augmented by the orientations of the atomic spins. The nuclei have no accessible additional internal structure, and analogously the atomic spins can only rigidly rotate their orientations.

Those two qualitatively different independent degrees of freedom give in the full theory four kinds of scattering: When neither nuclear positions nor spin orientations change, the scattering is elastic. When the spin configuration does not change but the nuclear arrangement does, for instance by phonon excitation or de-excitation, the scattering is inelastic in the phonon system. This kind of scattering is known as *magnetovibrational scattering*. Both cases in principle correspond to phenomena treated already in the nuclear case, but here the interaction is rather mediated by the unpaired electron densities that are rigidly fixed to the nuclear positions, giving possibilities to separate these contributions via polarization analysis and via the effect of the orientation of the magnetization with respect to the wavevector transfer. Further, there is the converse case where the scattering is elastic with respect to the nuclear positions but inelastic with respect to the spin orientations, and finally the case where both nuclear position and spin orientation states change.

Here the third case shall be considered in more detail, where the nuclear configuration is frozen but the spin configuration changes. We can expect this to formally parallel the case of inelastic non-magnetic scattering, where it turned out that the double differential cross section is essentially the dynamical structure factor $S(\mathbf{Q}, \omega)$, which has in the classical view an immediate interpretation as the Fourier transform of correlation functions. Indeed, for a system composed of magnetically equivalent atoms considered for simplicity the double differential cross section can be written as

$$\frac{d^2\sigma}{d\Omega dE_f} = (\gamma r_0)^2 \frac{k_f}{k_i} F^2(\mathbf{Q}) e^{-2W(\mathbf{Q})} \sum_{\alpha, \beta} \left(\delta_{\alpha, \beta} - \frac{Q_\alpha Q_\beta}{|\mathbf{Q}|^2} \right) S^{\alpha, \beta}(\mathbf{Q}, \omega) \quad (\text{C.5.36})$$

with the magnetic dynamical structure factor

$$S^{\alpha, \beta}(\mathbf{Q}, \omega) = \sum_{n, n'} e^{i\mathbf{Q}(\mathbf{R}_n - \mathbf{R}_{n'})} \sum_{\lambda_f, \lambda_i} p_{\lambda_i} \langle \lambda_i | S_{n'}^\alpha | \lambda_f \rangle \langle \lambda_f | S_n^\beta | \lambda_i \rangle \delta(\hbar\omega + E_{\lambda_i} - E_{\lambda_f}). \quad (\text{C.5.37})$$

As the nuclear positions \mathbf{R}_n are assumed to be not affected by the scattering event, they are just classical quantities and can be pulled out of the matrix elements. The Debye-Waller factor $e^{-2W(\mathbf{Q})}$ introduced here takes into account the random displacements of the nuclei from their ideal positions and will be discussed in more detail later.

By an approach analogous to the one taken in Sect. C.3.1 the magnetic dynamical structure factor can be transformed to

$$S^{\alpha, \beta}(\mathbf{Q}, \omega) = \frac{1}{2\pi\hbar N} \sum_{n, n'} e^{i\mathbf{Q}(\mathbf{R}_n - \mathbf{R}_{n'})} \int dt \langle S_{n'}^\alpha(0) S_n^\beta(t) \rangle e^{-i\omega t}, \quad (\text{C.5.38})$$

where $\langle S_{n'}^\alpha(0) S_n^\beta(t) \rangle$ is essentially the van Hove pair-correlation function for the components of the spins. It has the same qualitative features as the nuclear

analogon, specifically it is accessible to a classical interpretation only under qualifications, but in this case it gives the probability for the spin of atom n to point along β at time $t' + t$ if the spin of atom n' was pointing along α at time t' .

C.5.6 The fluctuation-dissipation theorem for magnetism

In general, a *fluctuation-dissipation theorem* relates the first-order response to some perturbation of a statistical system in equilibrium to the equilibrium fluctuations of the system in the corresponding degrees of freedom. Specifically for the case of neutron scattering on magnetic systems, it reads

$$S^{\alpha,\beta}(\mathbf{Q}, \omega) = \frac{\hbar}{\pi} \frac{1}{1 - e^{-\hbar\omega/k_B T}} \text{Im}(\chi^{\alpha,\beta}(\mathbf{Q}, \omega)). \quad (\text{C.5.39})$$

$\chi^{\alpha,\beta}(\mathbf{Q}, \omega)$ is the generalized magnetic susceptibility tensor defined by how the magnetization of a sample reacts to frequency- and wavevector-dependent magnetic field in first order (that is, for low fields)

$$M^\alpha(\mathbf{Q}, \omega) = \chi^{\alpha,\beta}(\mathbf{Q}, \omega) H^\beta(\mathbf{Q}, \omega). \quad (\text{C.5.40})$$

The neutron can be understood as establishing this magnetic field due to its magnetic moment and at the same time detecting its response, all in the regime of validity of first-order perturbations as long as the conditions of kinematic scattering are fulfilled. That is, with neutron scattering not only the intrinsic frequencies of atomic spins are accessible (where with macroscopic magnetization measurements only much longer timescales are accessible, corresponding rather to the dynamics of magnetic domains) or the spatial scale of the moments is accessible (which is completely unfeasible with macroscopic measurements), but all this is achieved in the perfect low-field limit, which also is experimentally not achievable with macroscopic methods. Due to these aspects, the potential of neutron scattering for studying magnetism on its fundamental scale is and probably will remain unattainable for other experimental methods.

Chapter D

Applications

The subject of this final chapter will be the application of both the theoretical results as well as the experimental techniques presented in the previous chapters to probe the properties of specific physical systems, predominantly in the solid state.

D.1 Diffraction

Diffraction, which implies recording the scattered neutron intensity only with respect to the outgoing direction (and the time of flight in the case of a pulsed incident beam) without sensitivity to possible energy transfers at the sample (and typically interpreting the data only in terms of elastic scattering, assuming all inelastic intensity to contribute only to the background), is concerned with the structural arrangements of the scatterers in the sample. Often, these scatterers are in fact single atoms, but in the case of small-angle scattering larger scales are probed.

D.1.1 Single-crystal diffraction

As was derived in Sect. C.1.4, the defining feature of elastic scattering from single crystals is the appearance of sharp peaks of intensity as a function of wavevector transfer \mathbf{Q} , the Bragg peaks.¹ Their positions coincide with the positions of the reciprocal lattice.

However, when first mounting a single crystal in a general orientation in a monochromatic beam, in the general case there will be no scattered intensity to be detected. A very helpful device for understanding this issue is given by the so-called *Ewald sphere*: For a given incident beam direction and energy, the incident wavevector \mathbf{k}_i is fixed. In the case of elastic scattering, also the length

¹We will leave the discussion of studies of the diffuse intensity for later.

of the outgoing wavevector is fixed, with the direction of detection corresponding to the orientation of \mathbf{k}_f . This results in the accessible wavevector transfers \mathbf{Q} lying on a sphere of radius $|\mathbf{k}_i|$, the above-mentioned Ewald sphere. Positions on a two-dimensional detector thus directly correspond to points on the Ewald sphere in reciprocal space. Note that this sphere is not centered around the origin of reciprocal space but rather around \mathbf{k}_i , with the origin actually lying on the Ewald sphere, corresponding to vanishing wavevector transfer for the case of forward scattering. For a general orientation of the single-crystalline sample not a single one of the finitely many accessible Bragg peaks (those with $|\mathbf{G}| \leq Q_{\max} = 2|\mathbf{k}_i|$, which is realized for backscattering) will lie on the Ewald sphere, being a two-dimensional manifold in three-dimensional space.

Note that in the actual experimental case, the Ewald sphere is best imagined to be somewhat diffuse. This is due, first, to a finite monochromaticity of the incident beam, giving a sheaf of spheres with different radii (and also centers, lined up along the incident beam), but still all coinciding at the origin, and, second, a finite divergence of the incident beam, leading to a sheaf of spheres with same radii but centers distributed perpendicular to the incident beam. Thus, intensity will be recorded also when a peak is some distance off the ideal Ewald sphere.

A classical method of single-crystal diffraction is the *rotating crystal method*. In the original implementation a photographic film functions as a two-dimensional integrating detector, covering a given part of the Ewald sphere. When now the sample and thus the crystal lattice is rotated in real space, the reciprocal lattice rotates along, with the reciprocal lattice vectors moving along circular paths around the rotation axis (typically oriented vertically, perpendicular to the incident beam). Every time a reciprocal lattice vector passes through the Ewald sphere, the diffraction condition is fulfilled and intensity is recorded on the film. After a full rotation, a characteristic pattern results on the detecting film, allowing to determine the crystal symmetry as well as the lattice constants.

In addition, such a measurement yields also quite accurate peak strengths, defined as the three-dimensional integral over the immediate vicinity of the reciprocal lattice vector in reciprocal space (that is, covering all intensity even for peaks with finite widths). For the proportionality constant between measured intensity and inherent peak strengths here already geometric effects appear that are more prominently known from the Lorentz factor of powder diffraction, for which a qualitative expression will be derived in Sect. D.1.3. Specifically, the intensity value at a given point on the film is proportional to the average value over the intensity in three-dimensional reciprocal space along the circular path corresponding to this detector position. Assuming that only one peak contributes at this detector position, for a given peak strength the detected intensity is thus the higher the shorter the path length is.

The second factor concerns the angle between the Ewald sphere and the path at the crossing point. If this angle is large, the peak crossing happens fast, giving a lower intensity than for small crossing angles. This also affects the achievable resolution: for a given peak width in three-dimensional space, a low-angle crossing will lead to a broad signal on the detector. Thus, for given incident collimations and detector resolutions the intrinsic peak width can be optimally resolved for low-angle crossings, that is, near back-scattering.

With today's detectors with immediate read-out, rocking scans can be performed, giving access to information beyond the rotating crystal method. Here the crystal is oriented so that the diffraction condition is nearly fulfilled, and then it is slowly rotated through the diffraction condition. With a two-dimensional detector, the resulting frames correspond to successive parallel cuts through three-dimensional reciprocal space, giving the complete three-dimensional shape of the considered peak.

As mentioned above, with single-crystal diffraction the crystal structure of a system as well as the intensity of the different peaks can be studied. However, the former is a very fundamental question and thus typically needs to be solved before any single crystals are available, and also for studying the latter problem powder diffraction is a very successive method, as will be discussed below. The main selling point of single-crystal diffraction is thus its ability to study the full three-dimensional peak shapes. The two principal aspects that are accessible in this way are on the one hand the mosaicity, that is, a distribution of local crystal orientations in a nominal single crystal due to small-angle grain boundaries, and on the other hand finite peak widths with specifically anisotropic peak shapes due to lattice defects and the associated strain fields.

D.1.2 Diffraction on polycrystals

A sample of solid matter prepared without following any special protocols, in the simplest case obtained by casting a melt, will in general be in the polycrystalline state. That is, while on the microscopic scale it has the crystalline structure corresponding to its stable (or possibly meta-stable) phase, the specific orientation of the crystal lattice does not extend through the whole piece of material as in the case of a single crystal. Rather, a polycrystal has a microstructure of grains, corresponding to crystallites that are rotated with respect to each other.

On the one hand, diffraction on such a polycrystal can be done as substitute for powder diffraction (see below) when powders of the sample in the desired state cannot be obtained, for instance due to too high ductility or reactivity with the atmosphere. However, the effects of the polycrystalline structure on the diffraction pattern as discussed in the following can have a significant impact on the interpretation, thus care has to be taken with this approach.

The main case for performing diffraction measurements on polycrystals thus lies in engineering, where effects due to the microstructure of samples prepared in the same way as in the actual industrial application can be studied. While, as is often the case, X-ray and neutron scattering can in principle probe the same aspects of the system, here using neutrons has a significant advantage, as their large penetration length allows often to study mechanical parts in their actual shape, while for X-ray scattering sections have to be prepared, which can affect the properties to be studied, specifically for the case of residual stress analysis.

Compared to the case of single-crystal diffraction, the concept of the Ewald sphere holds without modification. However, when a number of crystallite grains are in the beam, each of those will lead to its own reciprocal lattice of diffraction peaks,

with weights that vary according to the grain volume. With typical resolutions between 10^{-2} and 10^{-3} , the probability of a given reflection to cut through the Ewald sphere varies on the same order of magnitude. Thus, as soon as a sufficient number of crystallites is in the illuminated volume, there will be diffracted intensity for any orientation of the sample.

The diffracted intensity will form the so-called *Debye-Scherrer rings* on the detector: as for arbitrary orientation of the crystallites the length of the reciprocal lattice vectors is still fixed, so is the length of \mathbf{Q} and thus the scattering angle. A given reflection thus corresponds to a *Debye-Scherrer cone* of outgoing intensity with some opening angle, and the intersection with the Ewald sphere gives rings of intensity on a flat detector. For not too fine microstructures, these rings will display an appreciable graininess, where each grain of intensity on the detector corresponds to an actual crystallite grain that fulfills the diffraction condition for the specific \mathbf{k}_f . Thus, for the evaluation of such data there is a contribution to the statistical uncertainty in addition to the conventional neutron counting statistics to consider, corresponding to the limited number of grains fulfilling the diffraction condition. When statistically better-defined Debye-Scherrer ring profiles are desirable, the polycrystal can in addition be rotated during the measurement, so that more grains contribute to the recorded intensity (but see the following discussion for orientational dependence even in the case of a polycrystal).

Apart from instrumental effects such as finite collimation or monochromatization/energy resolution, there are two principal effects that give rise to finite widths of the Debye-Scherrer rings. On the one hand, this can be due to finite sizes of the diffracting grains, called *size broadening*. Qualitatively, this can be easily understood: when for a given grain and a given reflection N lattice planes are contributing to the diffracted intensity, the reflection will have a relative width in reciprocal space on the order of $1/N$, as for this deviation the uppermost and lowermost planes will get out of phase. Translated into an angular width for monochromatic radiation, a quantitative expression is given by the *Scherrer equation*

$$L = \frac{K\lambda}{B(2\theta)\cos(2\theta/2)} \quad (\text{D.1.1})$$

where B is the angular full width at half maximum of the diffraction peak (in radians), 2θ is the scattering angle, and L is the corresponding crystallite size. The numerical value of the dimensionless constant K depends on the assumed grain morphology and the associated definition of the grain size, typically and has a value of $K = 0.89$ for a flat crystallite platelet oriented perpendicular to \mathbf{Q} .

Further, also locally varying lattice constants will give rise to finite intrinsic peak widths. These can be due to chemical inhomogeneities such as due to *Seigerung* effects in casting without subsequent solution annealings, or intrinsic strains, where the phenomenon is known as *strain broadening*. Of course, in this case a given distribution relative local strains means a corresponding distribution of local lattice parameters, and thus a corresponding relative width of the peak in reciprocal space. Given the elasticity tensor, the intrinsic strains can be converted to residual stresses, that is, the stresses that remain even for no external load on the sample. Size and strain broadening can be separated by their variation with the order of the reflection: for size broadening, the absolute width of a peak

is independent of $|\mathbf{Q}|$ (and the variation according to the Scherrer equation is just due to the correspondence between scattering angle and wavevector transfer), while strain broadening gives constant *relative* peak widths.

Finally, polycrystals will typically display *texture*, which means preferred orientations of the crystallite grains. This can result both from directional solidification in standard casting sample preparation as well as from further sample treatments, which in general are not isotropic, for instance rolling or cutting. It is quantified in the so-called pole figures, which are density plots of the intensity of given diffraction peaks as function of direction. The distributions of two non-parallel peaks are necessary for a full specification of the three-dimensional orientation distribution. Texture is the main reason why normally powder diffraction as discussed below is the preferred method for determining structural properties of unperturbed systems.

Thus, diffraction on polycrystals is a very attractive method for engineering applications as it allows to determine preferred grain orientations as well as residual stresses, which are hard to obtain quantitatively by microscopy methods. By using collimators on the incident and outgoing paths, this can even be done non-destructively with three-dimensional spatial resolution, which is known under the term strain scanning.

D.1.3 Powder diffraction

Powder diffraction is closely related to diffraction from a polycrystalline sample. However, assuming that the powder grains either grow themselves or have been milled to roughly spheroid shapes (that is, that they have neither plate- nor needle-like morphology), they will be oriented perfectly randomly. Further, as gravitation can be neglected in this respect, they will also be in a stress-free state on the scale of the grains (however, on smaller scales there can be stresses, such as due to dislocations within the grains). Thus, the main effects that have been of engineering interest in the polycrystalline case discussed above do not apply here, and ground-state aspects of the system can be studied more directly.

Due to the absence of preferred orientations, the fundamental experimental results are one-dimensional diffraction patterns, to which the experimental data are reduced beforehand (possibly to sets of spectra with different instrumental resolutions for data taken with area detectors or in time-of-flight mode). Within these patterns, the interest lies on the diffraction peaks, specifically their positions, intensities (peak area) and widths (in contrast, non-trivial peak shapes are typically due to instrumental resolution effects as opposed to intrinsic effects), while the background due to incoherent and inelastic scattering is typically phenomenologically modelled and subtracted. For the case of simple crystal structures and reasonable resolutions, the peaks will be clearly separated, and so their intensities and widths can be fitted independently and modelled successively. For more complicated structures with large real-space lattice constants and low crystalline symmetries, the number of peaks in the diffraction pattern increases greatly, which can prohibit this approach from being followed due to peak overlap. The solution to this problem in the form of whole-pattern refinement will be given

below.

Assuming the kinematical theory of diffraction to be valid and neglecting absorption, apart from the structure factor S_{hkl} the strength of a given peak will depend essentially on three further factors

$$I_{hkl} = M_{hkl} D(\mathbf{Q}) L(2\theta) |S_{hkl}|^2. \quad (\text{D.1.2})$$

The most obvious one is the *multiplicity factor* M_{hkl} . For instance in an fcc system, there are 24 reflections of the kind $\{3, 1, 1\}$ and 8 of the kind $\{2, 2, 2\}$ arranged over three-dimensional reciprocal space. The intensity in the diffractogram for a given wavevector transfer is proportional to the average over the corresponding spheres in reciprocal space, so it scales with M_{hkl} , the number of equivalent reflections.

Next, there is the Lorentz factor L that depends only on the scattering angle 2θ . It is due to the geometric aspects of the scattering process that have been discussed qualitatively already in Sect. D.1.1. Specifically, as the intensity detected for a given scattering angle is the average over the corresponding sphere in reciprocal space, the surface of which scales with $Q^2 \propto \sin(2\theta/2)^2$, the intensity decreases with the scattering angle with $\sin(2\theta/2)^{-2}$, all else being equal (this effect can also be understood as the probability of a given grain in arbitrary orientation fulfilling the diffraction condition for a given reflection). Further, there is no linear relation between wavevector transfer and scattering angle, but rather

$$Q = 2Q_0 \sin\left(\frac{2\theta}{2}\right). \quad (\text{D.1.3})$$

Therefore, for fixed wavelength (and thus Q_0) we have

$$dQ \propto \cos(2\theta/2) d2\theta. \quad (\text{D.1.4})$$

This means that in the vicinity of backscattering the wavevector transfer does not vary much with scattering angle, so these regions in reciprocal space are sampled with correspondingly more weight. Summarizing these two geometrical effects into the *Lorentz factor* gives

$$L(2\theta) \propto \frac{1}{\sin(2\theta/2)^2 \cos(2\theta/2)} \propto \frac{1}{\sin(2\theta) \sin(\theta)}. \quad (\text{D.1.5})$$

The third factor is the *Debye-Waller factor* $D(\mathbf{Q})$. This is a function that decays monotonously from 1 to 0 as Q increases and is due to deviations of the atoms from their ideal positions, which leads to phase shifts and thus destructive interferences. Such deviations necessarily results from zero-point motion as well as phononic excitations with temperature. Due to the latter effect, the decay with Q is more drastic at higher temperatures. Further, also static displacements due to chemical disorder can contribute. The displacements can be modelled as a spatial distribution of the nuclear positions around the ideal sites, from which the Debye-Waller factor results just as the magnetic form-factor for neutrons or the atomic form-factor for X-rays. The dynamic contributions are due to phonons, the amplitudes of which do not interact in the harmonic approximation. Thus, by the central limit theorem the corresponding probability density is a three-dimensional

Gaussian distribution, which in the case of cubic symmetry is defined by just one parameter

$$\rho(\mathbf{u}) \propto e^{-|\mathbf{u}|^2/2\sigma^2}. \quad (\text{D.1.6})$$

The scattering amplitude is proportional to the Fourier transform of this distribution evaluated at the respective \mathbf{Q} , and the intensity its absolute square. Thus, for a cubic Bravais lattice system we obtain

$$D(\mathbf{Q}) = e^{-2W(|\mathbf{Q}|)} = e^{-|\mathbf{Q}|^2 \langle u^2 \rangle / 3}. \quad (\text{D.1.7})$$

Thermal values of $\sqrt{\langle u^2 \rangle}$ can reach a few tens of Ångströms, so that an appreciable decrease of peak strengths is observed already over the first few reflections, and static contributions can increase this even further. For structures with inequivalent sublattices, each sublattice can in principle have its own distribution of displacements. In this case, Eq. (D.1.2) is not strictly applicable, and the effect has rather to be modelled within the structure factor, as it is the case with atomic form factors.

As noted above, the obvious procedure of first determining peak positions and intensities and in a second step finding a structure with internal parameters that reproduces this list of values, which historically seemed like the only possible approach due to the limited computing capacities, becomes impossible to do unambiguously due to peak overlap. In 1969, Hugo Rietveld proposed to abandon the above-sketched two-step procedure in favour of a direct modelling of the full diffraction pattern by a set of parameters describing both the structure of the sample as well as the behaviour of the instrument (such as instrument resolution functions). In the meantime, this has become one of the most productive methods in the whole of physics. At the time of its introduction, this was a quite demanding method in terms of computing power, and its successful execution inspired admiration and led to it being considered the gold standard of powder diffraction data analysis. However, with today's increased computing capacities such seeming brute-force direct modelling approaches with their obvious advantages are generally becoming more common-place, and the singularity of the Rietveld method is gradually reducing. Note that this method specifically is concerned with refining, that is, a continuous optimization of the structural parameters to fit the data. In contrast, the determination of the unit cell and space group is the domain of crystallography, a whole scientific discipline outside of physics, and structure solution, that is, finding a plausible real-space model within the constraints of the unit cell and space group, is rather a problem of chemistry.

D.1.4 Diffuse scattering

How the diffuse scattering (the intensity between the Bragg peaks) from a single crystal is connected to correlations in the arrangements of chemically inequivalent atoms was already treated in Sect. C.1.6. Here additional aspects shall be commented on.

In C.1.6, the diffuse scattered intensity was related to a correlation function. Also the differential cross sections that were derived in Sect. C.3 have always

been assumed to be directly accessible in a scattering experiment. However, this corresponds to equating the actually measured intensities with their expected value, and it is not trivial to see why this should be valid.

Indeed, in the ideal case, where the incident radiation is assumed to be perfectly monochromatic and non-divergent, and the sample is for simplicity assumed to be a static classical system, the scattered intensity is strictly the absolute square of the Fourier transform of the scattering length density evaluated at the corresponding \mathbf{Q} . Chemical disorder in the sample will give random interferences, and so the intensity in the diffuse regime will be a random variable (with an exponential distribution, being the absolute square of the amplitude, which shows a normal distribution due to the central limit theorem) with an expected value that is related to the static pair-distribution function.

The point is now that the scale of these fluctuations in scattered intensity over reciprocal space is the inverse of the dimensions of the illuminated volume.² Assuming the scattering to sample atomic scales, the relative size of these fluctuations therefore goes with $1/N$, the typical number of interfering atoms per dimensions, which for neutrons is about 10^8 . Thus it transpires that the scattering experiment is self-averaging in the sense that experimentally realizable monochromatizations and divergences correspond to distributions of wavevector transfers sampled at a given detector position, which washes out the fluctuations.

Only the high brilliance of synchrotron beams allows to collimate and monochromatize the beam to a point (together with the smaller sample dimensions in X-ray scattering) where the ideal situation is approached and the fluctuations become visible. This is then called *coherent illumination* (which should not be confused with the distinction between coherent and incoherent scattering in the case of neutrons), where the actual sample microstates are accessible. The observed graininess of the diffuse intensity is called *speckles*, and is more familiar from the optical regime, where lasers provide coherent illumination with much less effort.

A variation of the diffuse scattering over reciprocal space corresponds to a preference for specific local configurations of chemically distinct atoms due to interactions, which is known as *short-range order*. On the pair level, such local correlations are quantified by the *Warren-Cowley short-range order parameters*. Consider a binary system with composition c (i.e. the concentration of element A is c and the concentration of element B is $1 - c$), for simplicity on a Bravais lattice. For a given lattice vector \mathbf{r} let $P_{\mathbf{r}}^{A,B}$ be the probability for site \mathbf{x} to be occupied by A and site $\mathbf{x} + \mathbf{r}$ by B, averaged over all \mathbf{x} (i.e. it is half the probability for a pair of sites related by a vector \mathbf{r} to be occupied by distinct elements). The short-range order parameters are then given by

$$\alpha_{\mathbf{r}} = 1 - \frac{P_{\mathbf{r}}^{A,B}}{c(1-c)}. \quad (\text{D.1.8})$$

Note that in the absence of correlations (that is for very high temperature or large \mathbf{r}) $P_{\mathbf{r}}^{A,B} = c(1-c)$, therefore $\alpha_{\mathbf{r}} = 0$ in this case. Negative values of $\alpha_{\mathbf{r}}$ correspond to negative correlations, that is preferred unlike pairs, while positive values correspond to like pairs. In the extreme case where an atom A at \mathbf{x} implies also

²Note that this equally pertains to the intrinsic width of Bragg peaks in the kinematic theory.

an atom A at $\mathbf{x} + \mathbf{r}$ (equivalently for B), $\alpha_{\mathbf{r}}$ equals one (which is trivially fulfilled for $\mathbf{r} = \mathbf{0}$).

As was discussed with respect to the static approximation in Sect. C.4.3, the fact that a neutron can experience significant energy transfers at the sample compared to thermal neutron energies would lead to neutrons of different \mathbf{Q} being detected at a given detector position in the diffuse regime without energy analysis. Thus, energy analysis has to be done for meaningful studies of the diffuse intensity, so that only the elastic intensity is detected. In the kinematical theory, the elastic part of the intensity is the Fourier transform of the pair-distribution function of the time-averaged configuration. On the other hand, for X-ray scattering energy transfers do not appreciably change the wavevector transfer, and so no energy analysis is done for studies of the diffuse intensity (that is, no analysis with respect to phonon or magnon transitions — Compton scattering or fluorescence photons are typically discriminated against if the intrinsic energy resolution of the detector allows it). As a consequence, in this case the Fourier transform of the pair-distribution function corresponding to instantaneous configurations is probed, including all dynamic displacements in the positions.

D.1.5 Small-angle scattering

Small-angle scattering is concerned with length scales on the order of nanometers to hundreds of nanometers. While there are solid-state crystals which lattice constants in this regime (silver behenate with $c = 58.380 \text{ \AA}$ is an example, being a popular calibration sample for small-angle instruments), and also for instance some micelles can order in a regular arrangement and give rise to diffraction peaks in this regime, small-angle scattering in the proper sense is concerned with non-regular arrangements that give rise to a smoothly varying, typically isotropic scattering signal around the forward direction. In any case, on these scales the atomicity of matter is not resolvable and modelling is done in terms of continuous scattering length densities.

The fact that the incident beam has necessarily some divergence limits the accessible \mathbf{Q} towards small values, and the contribution due to the tails of the direct beam has to be known accurately to recover the scattered contribution from the detected signal. This pertains both to measurements of the beam profile with empty sample holders as well as the transmission of the sample. Further, with the constructive interference of potentially large scattering entities in real space at small \mathbf{Q} and the fact that the scattered intensity is the absolute square of the amplitude and thus the Fourier transform of the scatterer density, the problem of multiple scattering is more severe for small-angle scattering than for wide-angle scattering. In other words, the probability for a given neutron or photon to experience a scattering event by a small angle in a sample with spatial inhomogeneities on the corresponding scale is much larger than the probability for scattering events by larger angles. Thus, what with the resolution of wide-angle experiments still looks like the direct beam can actually have already experienced a number of small-angle scattering events.

A typical case of small-angle scattering is to study the shape of particles in

suspension. Specifically for small-angle neutron scattering, the technique of *contrast matching* is very potent. What it means is that the scattering length density of the solvent can be adjusted by isotope substitution without changing the chemical behaviour, where deuteration, that is substituting ^1H by ^2D , is the dominating case — its converse is called protonation. For instance when the particles have a core-shell structure, by choosing the scattering length density of the solvent equal to one of the parts, the scattered signal is exclusively due to the other part.

For back-of-the-envelope calculations, the so-called *small-angle approximation* is often used, which consists in equating the sine with its argument (measured in radians), giving

$$|\mathbf{Q}| = 2|\mathbf{Q}_0| \sin(2\theta/2) \approx |\mathbf{Q}_0|2\theta \quad (\text{D.1.9})$$

with an error in third order of 2θ . Also, the Ewald sphere can be assumed to be flat with the same relative accuracy, but for the typical case of isotropical systems the direction of \mathbf{Q} makes no difference anyway.

For the above-mentioned case of the system consisting of well-defined particles with some distribution of shapes and sizes that are arranged in some more or less random way, the resulting small-angle scattering signal can conceptually be understood as the product of a *particle form factor*, which is only due to the size and shape distribution of the particles, and an *interparticle structure factor*, which quantifies the correlations in the particles' positions. Specifically for concentrated systems, the structure factor will show an increase from small \mathbf{Q} up to a maximum, which corresponds in some sense to the most frequent nearest-neighbour distances, and which is due to the particles not being able to intersect. As will be discussed below, on these scales the particle form factor is flat, while it decays at higher \mathbf{Q} . Thus, the small-angle signal often has the form of a ring of intensity.

The most simple shape to consider is a sphere. The corresponding scattering intensity, that is, the absolute square of its Fourier transform, can easily be calculated in spherical coordinates and evaluates as

$$I(\mathbf{Q}) = \rho^2 V^2 \underbrace{\left(\frac{3(\sin(QR) - QR \cos(QR))}{(QR)^3} \right)^2}_{P(Q)} \quad (\text{D.1.10})$$

where ρ is the contrast in scattering length density between the particle and the solvent, V is the particle volume, R the radius, and $P(Q)$ is the dimensionless form factor (with $P(0) = 1$). $P(Q)$ has characteristic zeros close to $QR = \pi(n + 1/2)$ for $n \geq 1$. In reality, the particles will have some polydispersity, that is, some distribution of radii, which will smoothen the distribution and lift the zeros, but, as evidenced by the plot in Fig. D.1, at a relative standard deviation of 8% still the first four minima are clearly discernible.

$P(Q)$ is a function that is positive everywhere (apart from the artificial example of a perfect sphere) and decays outwards (see below), so for general $P(Q)$ we can write

$$P(Q) = e^{F(Q)}, \quad (\text{D.1.11})$$

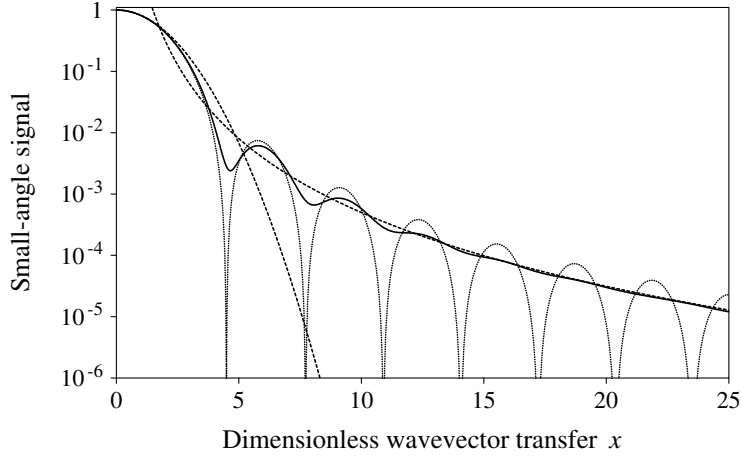


Figure D.1: Illustration of models for small-angle scattering curves. Dotted: spherical particle with unity radius, solid: spherical particles with Gaussian distribution of radii ($\sigma/R = 0.08$), dashed lines: Guinier model (parabola at small x) and Porod law (power-law decay at large x).

where $F(0) = 0$, $F(Q) \rightarrow -\infty$ for $Q \rightarrow \infty$, and $F(Q)$ is symmetric with respect to Q as the same applies for $P(Q)$. Assuming $P(Q)$ to be analytic, we can expand $F(Q)$ as a Taylor series where due to symmetry only even orders appear. This is the technique of cumulant expansion, specifically we have for the second-order coefficient

$$F_2 = -(\langle z^2 \rangle - \langle z \rangle^2), \quad (\text{D.1.12})$$

the normalized central second moment of the scattering length density along some direction z . Performing the orientation average explicitly, the *radius of gyration* can be defined

$$R_g^2 = \frac{\int d\mathbf{r} \rho(\mathbf{r}) r^2}{\int d\mathbf{r} \rho(\mathbf{r})} \quad (\text{D.1.13})$$

assuming the center of mass of the scattering length density to be at the origin, which allows to write

$$P(Q) = e^{-R_g^2 Q^2/3}. \quad (\text{D.1.14})$$

This expression corresponds to the *Guinier approximation* and is valid for not too large Q (Fig. D.1). For the special case of spheres, the radius of gyration is related to the actual radius according to

$$R_g^2 = \frac{3}{5} R^2. \quad (\text{D.1.15})$$

When analyzing scattering signals for obtaining the radius of gyration of the particles, the effect of the interparticle structure factor has to be considered.

Apart from the regularly arranged zeros, Eq. (D.1.10) shows a decay with Q^{-4} for large Q . Such a behaviour is not specific to spherical particles, but holds

whenever the scattering volume is separated by a sharp interface into regions of two different scattering length densities (termed two phases from now on).³ This is the so-called *Porod law*, which is also illustrated in Fig. D.1. In this case, the pair-correlation function for small separations \mathbf{r} decays linearly with $|\mathbf{r}|$ with a decay constant equal to the interface area density (that is, the probability for two random points to be in different phases is for small separations and well-defined phase boundaries just the probability for a phase boundary to be found anywhere on the connecting line, which is the distance times the interface area per volume). The Fourier transform over the resulting cusp at $\mathbf{r} = \mathbf{0}$ can be done directly in spherical coordinates, indeed giving a contribution proportional to Q^{-4} from the lower integration boundary, where the upper boundary drops out with an argument as given in Sect. C.2.1. In a quantitative calculation, the proportionality factor gives a direct handle on the interface area density. The transition between the Guinier and the Porod regime is where Q becomes larger than the typical radius of curvature of the interface.

D.1.6 Diffraction on magnetic structures

The study of magnetic structures, that is, how the spins sitting on the distinct atoms are arranged,⁴ is one of the most important applications of neutron diffraction. Here the different cases will be presented in a qualitative way. The relevant principles as derived in Sects. C.5 and C.3.2 common to all these cases are the decay of all magnetic scattering towards large Q with the magnetic form factor, the sensitivity to magnetization only perpendicular to \mathbf{Q} , and for polarized neutron scattering the neutron spin flipping due to sample magnetizations perpendicular to the neutron polarization axis.

The easiest case to consider is a paramagnet. In the limit of infinite temperatures, the atomic spins are perfectly uncorrelated. Thus, the case is equivalent to uncorrelated nuclear spins, which was found in Sect. C.3.2 to give incoherent scattering. Determining this scattering contribution quantitatively allows to conclude on the sizes of the fluctuating spins. At lower temperatures, the atomic spins will start to display correlations. As a consequence, the previously perfectly flat incoherent scattering (apart from the decay with Q due to the magnetic form factor) will evolve modulations. Qualitatively, the interpretation of this magnetic diffuse scattering is equivalent to nuclear diffuse scattering, specifically a parallel ordering tendency will give higher intensity around the Bragg peaks (as for nuclear clustering), while an antiparallel tendency will give intensity between the peaks (as for nuclear ordering). Of course, as the spin configurations are dynamic, the scattering will be subject to energy transfers, specifically it constitutes a case of quasi-elastic scattering with no purely elastic peak as will be discussed in Sect. D.2, because the time-averaged magnetic scattering length is zero.

At still lower temperatures, a paramagnet will show a phase transition towards an ordered state. If parallel ordering tendencies are dominating, a ferromagnet results. At a sufficient external field, when the sample is fully magnetized, all

³Also Eq. (C.2.26) can be understood as an instance of this fact.

⁴For reasons of economy of prose, only spin magnetization will be explicitly considered, but note that the case for orbital magnetization is largely equivalent as was pointed out in Sect. C.5.

spins will be pointing in the same direction. Thus, for given \mathbf{Q} , the nuclear scattering length of each atom will be modified due to the interaction of the neutrons with the atomic spin, which is equal for all atoms. As a consequence, the Bragg peak intensities will change as well compared to the non-magnetic case, while the magnetic diffuse scattering will vanish. The magnetic contribution can be determined by varying the angle between the external field and \mathbf{Q} . On the other hand, under zero external field a soft magnet will have a vanishing net magnetization. In this case, there will still be a magnetic contribution to the peak intensities, but its effect will be comparatively small. To be precise, the finite correlation lengths in this case due to Weiss' domains will lead to the magnetic contributions being slightly broadened compared to the nuclear peaks. This pertains also to the $(0,0,0)$ -peak, so that this effect can be studied as small-angle scattering.

In the converse case of dominating antiparallel interactions between the spins, an antiferromagnet will result. Typically (but not always), this will result in an enlargement of the unit cell and thus in the appearance of additional peaks. These peaks are purely of magnetic origin, and thus can be easily identified by their decay with the magnetic form factor.

Actually, ferro- and antiferromagnets are just special cases of *spin spiral* structures: such arrangements are described by a magnetic ordering wavevector \mathbf{q} and a (possibly complex) amplitude μ^0 so that the magnetic moment of atom i is given by

$$\boldsymbol{\mu}_i = \text{Re}(\mu^0 e^{i\mathbf{q}\mathbf{R}_i}), \quad (\text{D.1.16})$$

where \mathbf{R}_i is its position. A ferromagnet has $\mathbf{q} = \mathbf{0}$, while for instance $\mathbf{q} = \pi(1, 1, 1)$ gives an antiferromagnet on the simple cubic lattice. A pure modulation is given if all entries of μ^0 have the same complex phase angle, while a spin spiral in the proper sense of the word (where all spins have the same length but rotate in space) results when $\text{Re}(\mu^0)$ and $\text{Im}(\mu^0)$ have the same length and are perpendicular. The special cases when the $\boldsymbol{\mu}_i$ turn within the plane perpendicular to \mathbf{q} (that is, when $\text{Re}(\mu^0)$ and $\text{Im}(\mu^0)$ are perpendicular to \mathbf{q}) is called a *helical* spin spiral, and the case of \mathbf{q} lying in the plane of rotation is called *cycloidal*. Note that the most general long-range ordered spin configurations can need a number of pairs of ordering wavevectors and amplitudes for their description. An example would be a cone spiral, which is a spin helix with an additional constant contribution parallel to \mathbf{q} .

Spin spirals can be classified into having commensurate modulations, where \mathbf{q} is an integer fraction of some reciprocal lattice vector, and incommensurate modulations. In the latter case, a given local configuration never repeats along \mathbf{q} in the strict sense. Practically, high-index commensurate and incommensurate modulations cannot be distinguished, but it is expected that due to spin-orbit coupling, which leads to preferred orientations of single spins with respect to the lattice, incommensurate modulations eventually lock in to some high-index commensurate modulation.

The signature of spin spirals in neutron diffraction is the appearance of magnetic satellite peaks at positions $\pm\mathbf{q}$ relative to the nuclear peaks.

As noted already above, magnetic peaks can be identified indirectly by their decay with Q according to the magnetic form factor, by their disappearance at the magnetic phase transition temperature, and by the effect of turning the sample magnetization with respect to \mathbf{Q} . However, the most detailed information on the magnetic structure can be gained by controlling and analyzing the neutrons' spin before and after the scattering. The corresponding methods are called *uniaxial polarization analysis*, when only the spin quantization along one axis is considered, and *spherical* or *3D polarimetry* in the general case.

A quantitative statement of the pertinent theories is too complicated to give in detail here, specifically for the three-dimensional case (which is also experimentally a very demanding method), thus only the results of Sect. C.3.2 for the uniaxial case will be quoted here: scattering on magnetization components parallel to the neutron polarization axis conserves the neutron spin, while the perpendicular components give spin-flip scattering. A main quantity to study here is the *flipping ratio*, that is, the ratio between spin-flip and non-spin-flip intensities, which has the advantage that it is independent, e.g., of Debye-Waller factors or magnetic form factors. For instance, uniaxial polarization analysis can be used to separate paramagnetic incoherent from nuclear spin incoherent scattering, as for the former the intensities in the spin channels vary in a known way with the orientation of the polarization axis to \mathbf{Q} , while the latter is insensitive to it.

D.2 Quasi-elastic scattering

Quasi-elastic scattering has two meanings: used in a quantitative sense, it just denotes the scattering of intensity at small energy transfers, such as below 1 meV. However, used as a qualitative distinction (which will be followed here) it denotes situations where the elastic peak itself is broadened in energy, as opposed to the case where energy transfers well separated from the elastic line appear, such as for instance for the phonon peaks to be discussed below under inelastic scattering.

Quasi-elastic scattering is observed whenever the self- or pair-correlation function becomes flat at infinite times, that is, when the system does not stay within some bounded region in phase space, which corresponds to *diffusive dynamics*. This applies for instance to liquids, which have no elastic peak as discussed in Sect. C.4.3, for soft condensed matter, which are a major case for quasi-elastic neutron scattering due to the strong incoherent scattering from hydrogen, or for paramagnetic fluctuations.

Here specifically solid-state diffusion shall be considered. For being accessible to neutron scattering, the dynamics have to be comparatively fast (so as to give appreciable energy transfers). This is realized for intermetallic systems, but most prominently again for the interstitial diffusion of hydrogen in metals.

For diffusion in a lattice (for simplicity assumed to be a Bravais lattice here), the pertinent correlation function (for hydrogen with its predominantly incoherent scattering this is the self-correlation function) in the classical approximation

fulfills the partial differential-difference equation

$$\frac{\partial}{\partial t}G(\mathbf{r}, t) = \sum_{\Delta\mathbf{r}} v_{\Delta\mathbf{r}}(G(\mathbf{r} - \Delta\mathbf{r}, t) - G(\mathbf{r}, t)), \quad (\text{D.2.1})$$

where $v_{\Delta\mathbf{r}}$ denotes the jump rate for jumps over distance vectors $\Delta\mathbf{r}$. For the intermediate scattering function this implies

$$\frac{\partial}{\partial t}I(\mathbf{Q}, t) = -I(\mathbf{Q}, t)\Gamma(\mathbf{Q}), \quad (\text{D.2.2})$$

where $\Gamma(\mathbf{Q})$ is the negative Fourier transform of the *diffusion kernel*

$$K(\mathbf{r}) = \sum_{\Delta\mathbf{r}} v_{\Delta\mathbf{r}}(\delta(\mathbf{r} - \Delta\mathbf{r}) - \delta(\mathbf{r})), \quad (\text{D.2.3})$$

that is

$$\Gamma(\mathbf{Q}) = \sum_{\Delta\mathbf{r}} v_{\Delta\mathbf{r}}(e^{i\mathbf{Q}\Delta\mathbf{r}} - 1). \quad (\text{D.2.4})$$

$\Gamma(\mathbf{Q})$ is called the *linewidth*. This becomes clear by solving the intermediate scattering function as

$$I(\mathbf{Q}, t) = I(\mathbf{Q}, 0)e^{-\Gamma(\mathbf{Q})t}, \quad (\text{D.2.5})$$

with $I(\mathbf{Q}, 0) = 1$ specifically for incoherent scattering. For the dynamical structure factor this yields a Lorentzian shape

$$S_i(\mathbf{Q}, \omega) = \frac{1}{\pi\hbar} \frac{\Gamma(\mathbf{Q})}{\omega^2 + \Gamma(\mathbf{Q})^2}, \quad (\text{D.2.6})$$

with $\Gamma(\mathbf{Q})$ being the half width at half maximum.

On the other hand, the long-time behaviour of $G(\mathbf{r}, t)$ is determined by the diffusion constant D (for cubic symmetry or isotropy, while in the general case it would be a second-order diffusion tensor), which allows to identify

$$\Gamma(\mathbf{Q}) = D\mathbf{Q}^2 \quad (\text{D.2.7})$$

in the limit of small Q (where again for the incoherent case D is the self-diffusion constant), which is the so-called *hydrodynamic limit*. For liquids, this theory of diffusion on a lattice can be adapted by radially averaging the diffusion kernel and thus the linewidth, corresponding to uncorrelated jumps over a given distance but random orientations.

Indeed, quasi-elastic neutron scattering can for example determine the diffusion constants in levitated droplets of metallic melts, without being subject to complications such as convection. However, the main advantage of such measurements lies in the sensitivity to the fundamental scale of the diffusional jumps, which allows to directly distinguish between different diffusion models as opposed to only indirect evidence given by macroscopic diffusion measurements.

There exist also intermediate states between statics and diffusive dynamics. This applies for instance for the diffusion of atoms in a cage such as for a bound

pair of a mobile and an immobile impurity in a host material, or for rotational dynamics of a molecule bound to its place in a crystal. Here the self-correlation function evolves from a single peak at $t = 0$ to a finite number of peaks at $t = \infty$, corresponding to the autocorrelation of the possible positions. For the dynamical structure factor, this gives a sum of a δ distribution in ω , corresponding to a purely elastic sharp peak, and a Lorentzian function, corresponding to quasi-elastic scattering. Apart from the timescale of the diffusive motion given by the width of the quasi-elastic signal, the geometry of such diffusive motion within a fixed volume is captured by the *elastic incoherent structure factor*, the ratio of elastic intensity to total intensity, which is determined from the measurements and fitted by the expressions corresponding to plausible models.

D.3 Inelastic scattering

In contrast to the broadening of the elastic line for diffusive dynamics discussed above, inelastic scattering refers to situations with well-separated energy transfers. This is the domain of *oscillatory dynamics*. In the easiest case, the considered degrees of freedom are subject to a quadratic potential. Indeed, this *harmonic approximation* is the correct low-temperature limit and will in general be assumed below. Classically, the resulting temporal evolution of the degrees of freedom will correspond to an oscillatory motion with some amplitude and a well-defined angular frequency ω . However, according to quantum mechanics the eigenstates of the system are quantized, with separations in energy equal to $\hbar\omega$. During a neutron scattering event, the sample can experience a transition between such states, leading to the corresponding neutron energy transfers.

A simple example of the general concepts sketched above lies in the vibrational dynamics of molecules. Here in principle equivalent information as by Raman scattering can be obtained, but with different selection rules. More typical examples for inelastic neutron scattering involve however degrees of freedom in crystals, specifically the nuclear positions and magnetic spins. The corresponding excitations are called *phonons* and *magnons*, respectively, with the names indicating their nature as quasi-particles. In a more general setting, these excitations are the massless *Goldstone bosons* due to the spontaneous breaking of the symmetries of the vacuum. These excitations are many-body effects, the theory of which becomes tractable due to the regular arrangements in crystals (allowing a concise description in reciprocal space) and the harmonic assumption.

D.3.1 Vibrational dynamics in crystals

The restoring force due to the displacement of an atom is given by interactions with its neighbouring atoms. Thus, the classical equations of motion are coupled differential equations in the positions of all atoms in the crystal. However, these interactions obey the discrete translation symmetry of the crystal, and with the forces being linear in the displacements in the harmonic approximation, the effect of the neighbouring atoms' displacements mathematically is a convolution. Writing the displacements as a Fourier sum, only the 3Λ equations for a given

\mathbf{q} remain coupled, where Λ is the number of atoms per unit cell. Solving the corresponding sets of linear equations gives 3Λ *normal modes* for each \mathbf{q} described by the *polarization vectors* $\mathbf{e}_s(\mathbf{q})$ and associated angular frequencies $\omega_s(\mathbf{q})$. For a given \mathbf{q} , the polarization vectors of the different modes, being eigenvectors of the Hermitian *dynamical matrix* (essentially the Fourier-transformed coupling constant matrix), are orthogonal and are generally chosen to be normalized. Thus, the classical temporal evolution of the positions of the atoms of the crystal would be given by

$$\mathbf{u}_{\lambda,i}(t) = \sum_{\mathbf{q},s} a_s(\mathbf{q}) (\mathbf{e}_s(\mathbf{q}))_{\lambda} e^{i\mathbf{q}\mathbf{r}_{\lambda,i}} e^{i\omega_s(\mathbf{q})t}, \quad (\text{D.3.1})$$

where $\mathbf{u}_{\lambda,i}$ is the displacement of atom i on sublattice λ from its equilibrium position at $\mathbf{r}_{\lambda,i}$, $a_s(\mathbf{q})$ are the complex amplitudes of the distinct normal modes (which are the degrees of freedom and specify the states of the system for all times) and the sum goes over the Brillouin zone and the different normal modes at given \mathbf{q} .

By construction, the time-dependent amplitudes in the distinct normal modes do not interact, which means that they correspond to uncoupled degrees of freedom subject to a harmonic potential. Thus, the standard problem of the quantum-mechanical harmonic oscillator applies, giving rise to the concept of phonons, that is, the image of the state of the system being described by how many phonons (each corresponding to a transition to the next energy level) are in each normal mode as sketched above. Starting from Eq. (C.3.25), writing the displacements in terms of phonon creation and annihilation operators along with further elementary manipulations, and performing a further Taylor expansion of the scattering phases of the displaced atoms leads to a series of differential cross sections, the so-called *phonon expansion*. Its terms correspond to scattering processes where a distinct number of phonon transitions happen. That is, the zeroth-order term is just the elastic cross section, which is essentially Eq. (C.3.25) with the Heisenberg operators $\mathbf{R}_j(t)$ being replaced by the static undisplaced atomic positions and additionally being multiplied by the Debye-Waller factor.

The coherent one-phonon differential cross section per atom, for simplicity for the case of a Bravais lattice with $\Lambda = 1$, results as

$$\begin{aligned} \left(\frac{d^2\sigma}{d\Omega dE_f} \right)^{\text{one ph.}} &= \frac{\sigma_{\text{coh}}}{4\pi} \frac{k_f}{k_i} \frac{V_{\text{BZ}}}{2m} D(\mathbf{Q}) \sum_{s,\mathbf{G},\mathbf{q}} \frac{(\mathbf{Q} \cdot \mathbf{e}_s(\mathbf{q}))^2}{\omega_s(\mathbf{q})} \\ &\times \left(\langle n_s(\mathbf{q}) + 1 \rangle \delta(\omega - \omega_s(\mathbf{q})) \delta(\mathbf{Q} - \mathbf{q} - \mathbf{G}) \right. \\ &\quad \left. + \langle n_s(\mathbf{q}) \rangle \delta(\omega + \omega_s(\mathbf{q})) \delta(\mathbf{Q} + \mathbf{q} - \mathbf{G}) \right). \end{aligned} \quad (\text{D.3.2})$$

Here V_{BZ} is the volume of the Brillouin zone, m is the atomic mass, and \mathbf{G} are the reciprocal lattice vectors. As the $\omega_s(\mathbf{q})$ are chosen as positive, the first term in the sum corresponds to an energy loss of the neutron ($\omega > 0$) due to the creation of a phonon (phonon emission), and the second term to an energy gain for phonon absorption. The second δ factor in both terms corresponds to crystal momentum conservation, restricting neutron wavevector \mathbf{Q} and phonon wavevector \mathbf{q} to be equal up to a reciprocal lattice vector. This is only to underline the point, but as \mathbf{e}_s , ω_s and n_s have the reciprocal lattice periodicity, they could equivalently be

evaluated at \mathbf{Q} and the explicit crystal momentum conservation condition could be dropped.

The expected value for the phonon number per mode according to Bose-Einstein statistics is given by

$$\langle n_s(\mathbf{q}) \rangle = \frac{1}{e^{\hbar\omega_s(\mathbf{q})/k_B T} - 1}. \quad (\text{D.3.3})$$

As

$$\frac{\langle n_s(\mathbf{q}) \rangle}{\langle n_s(\mathbf{q}) + 1 \rangle} = e^{-\hbar\omega_s(\mathbf{q})/k_B T} \quad (\text{D.3.4})$$

the detailed balance condition (C.4.16) is fulfilled, that is, specifically for low energies the energy-loss scattering will be much stronger than the energy-gain scattering.

The fact that in the one-phonon expression at a given \mathbf{Q} only phonons with the corresponding \mathbf{q} are emitted or absorbed, of which there are in the general case 3Λ possibilities for the different normal modes, gives a corresponding number of *dispersion branches*, that is, curves of $\omega_s(\mathbf{q})$, which can for high-symmetry directions be degenerate. In other words, where coherent elastic scattering on crystals gives intensity just on points (the Bragg peaks), that is, zero-dimensional manifolds in four-dimensional (\mathbf{Q}, ω) -space, one-phonon scattering gives three-dimensional hypersurfaces. Thus, without energy analysis there is intensity at all points in three-dimensional \mathbf{Q} -space, which is nothing else than thermal diffuse scattering.

For $\Lambda > 1$, one distinguishes between the three *acoustic* branches, where the displacements of the different sites are largely in phase (apart from the modulation of phase with $e^{i\mathbf{q}\cdot\mathbf{r}_{\lambda,i}}$), that is, where the polarization vector entries of the different sites are largely parallel, and the $3\Lambda - 3$ *optical* branches, where the displacements are out of phase. In the limit of small \mathbf{q} , acoustic modes correspond to macroscopic strain waves, while optical modes correspond to the oscillations of the entire sublattices against each other. Long-wavelength acoustic modes experience only small restoring forces (as the displacements with respect to their neighbours is small), so their frequencies and energies are small as well (and specifically go linearly to zero with $\mathbf{q} \rightarrow \mathbf{0}$). Thus, thermal diffuse scattering increases towards the Bragg peaks as the occupation numbers increase.

On the other hand, performing an experiment without \mathbf{Q} -resolution, such as on a polycrystal with an additional average over the scattering angle, or inherently in the case of incoherent scattering, gives a distribution of energy transfers, corresponding to the phonon *density of states*. Actually, for calculating thermodynamic quantities, the density of states incorporates all necessary information. As the phonon dispersions are smooth,⁵ in three dimensions the densities of states are

⁵When the interactions between the atoms are short-range, that is, fall sufficiently fast with distance, the phonon frequencies are necessarily smooth. However, interactions mediated by conduction electron can be non-local, with the most prominent consequence being the *Kohn anomalies* due to a jump in the generalized susceptibility at the Fermi level. This gives in turn a jump in the phonon dispersion, but such effects are typically small and, with finite experimental resolution, often not obvious.

continuous. However, stationary points of $\omega_s(\mathbf{q})$, where the gradient with respect to \mathbf{q} vanishes, give the so-called *van Hove singularities* in the densities of states, which locally have a square-root shape in three dimensions. For non-Bravais systems, the correspondence between the incoherent energy-resolved differential cross section and the density of states is more complicated, for instance due to different scattering lengths and different Debye-Waller factors for the respective sublattices.

In the two-phonon cross section (and analogously in the higher-order terms), phonons with different wavevectors \mathbf{q}_1 and \mathbf{q}_2 can participate, where we again have the condition

$$\mathbf{Q} = \mathbf{q}_1 + \mathbf{q}_2 + \mathbf{G} \quad (\text{D.3.5})$$

and analogously for the energy conservation. However, due to the higher number of degrees of freedom now for general \mathbf{Q} and ω the two conditions can be fulfilled, so that higher-order phonon terms give a diffuse background in (\mathbf{Q}, ω) -space. Experimentally, this is typically undesirable, as it is much harder to model than the sharp one-phonon dispersions and does not incorporate relevant information beyond the one-phonon behaviour.

Of course, the probability for multi-phonon processes rises with the phonon occupations numbers, that is with temperature. As the phonon expansion corresponds to the Taylor expansion of the scattering phases, the relative importance of higher-order processes increases with $\mathbf{Q}\mathbf{u}$, where \mathbf{u} is the typical thermal displacement. Another effect with an analogous behaviour is *anharmonicity*: in fact, also the harmonic assumption is just an approximation, and for large displacements higher-order terms in the interactions will appear. This now pertains to the dynamics of the crystal itself, leading to phonon-phonon scattering processes (where in the simplest case one phonon decays to two phonons or vice versa) and thus finite phonon lifetimes. As a consequence, the Fourier transform of the time-dependent amplitude in a given normal mode shows some width in ω , which directly translates to an intrinsic finite width of the measured dispersions. Quantitatively, this can be described by perturbation theory of the harmonic behaviour due to higher-order terms in the potential, and the resulting spectral functions have the expressions as for a damped harmonic oscillator.

The freedom of the experimenter when measuring phonon dispersion lies in the choice of the energy-gain or -loss side, in which Brillouin zone to measure, and, for high-symmetry structures, on which of a number of equivalent positions within the Brillouin zone, that is, those that correspond to \mathbf{q} that are related by point symmetry operations. As mentioned above, the energy-loss peaks have higher intensity, but due to aspects of focussing as discussed in Sect. B.2.5 also measuring on the energy-gain side can be advantageous, specifically at higher temperatures. As regards the other options, in the expression for the differential cross section (D.3.2) both the Debye-Waller factor and the inner product $(\mathbf{Q} \cdot \mathbf{e}_s(\mathbf{q}))^2$ depend explicitly on \mathbf{Q} . As the Debye-Waller factor (D.1.7) decays faster than exponentially with \mathbf{Q} while the inner product increases with a power law, there is some optimal value of $|\mathbf{Q}|$ in terms of scattered intensity. However, this is not necessarily the best choice, as the multi-phonon background increases even stronger with $|\mathbf{Q}|$, and also the resolution of the spectrometer will decrease.

A very important consequence of the choice of \mathbf{Q} lies in the weighting of the different modes according to the inner product. For instance, in a simple cubic system the reciprocal-space positions $\mathbf{Q}_1 = (1+q, 0, 0)$ and $\mathbf{Q}_2 = (1, q, 0)$ correspond to values of \mathbf{q} that are related by symmetry. However, at \mathbf{Q}_1 strictly only longitudinal modes contribute, while at \mathbf{Q}_2 transversal modes dominate, the more so as q becomes small. Note that in the first Brillouin zone in principle only longitudinal modes are accessible. These selection rules allow to distinguish the peaks belonging to different branches, which is specifically relevant near branch crossings. For the general case of non-Bravais structures, in an analogous way choosing the Brillouin zone one measures in determines whether the acoustic or the optical (and which of those) dispersions dominate.

D.3.2 Collective magnetic dynamics

In principle, the inelastic scattering from dynamic spin configurations is qualitatively equivalent to the above-treated nuclear case. The case of paramagnetic scattering would thus correspond to quasi-elastic scattering from a liquid as discussed in Sect. D.1.6, while the magnetic excitations of ordered arrangements are collective modes perfectly analogous to phonons, and are called *magnons*.

Specifically, the simplest approximation to the case of spin-only magnetization with local moments is given by the *Heisenberg model*, where the spins are assumed to have constant length but arbitrary orientation, and the Hamiltonian is given by

$$H = - \sum_{i,j} J_{i,j} \mathbf{S}_i \cdot \mathbf{S}_j, \quad (\text{D.3.6})$$

where \mathbf{S}_i is the atomic spin of the atom at site i and the exchange parameter $J_{i,j}$ depends on the relative distance between the sites i and j (and of course the respective sublattices in case of a non-Bravais structure). Further, this interaction between the moments can be augmented by a Zeeman term due to an external field (which typically is a few orders of magnitude weaker than the ion-ion interaction), and a single-ion anisotropy term due to spin orbit coupling that favours distinct orientations of the atomic spins with respect to the crystal lattice (and is typically still weaker). Even though the Heisenberg model is natural only for the case of localized moments, it can also describe more itinerant systems surprisingly well.

For a ferromagnet in the *linear spin-wave theory* (which in some sense neglects the fact that, different from the phonon case, the deviation of a spin approaches again the undisplaced value when one keeps adding magnons in a given mode), the cross section due to spin-wave inelastic scattering reads

$$\begin{aligned} \left(\frac{d^2\sigma}{d\Omega dE_f} \right)^{\text{one mag.}} &= (\gamma r_0)^2 \frac{k_f}{k_i} V_{\text{BZ}} \frac{S}{2} F^2(\mathbf{Q}) D(\mathbf{Q}) \left(1 + \frac{Q_z^2}{Q^2} \right) \\ &\times \sum_{\mathbf{G}, \mathbf{q}} \left(\langle n(\mathbf{q}) + 1 \rangle \delta(\omega - \omega(\mathbf{q})) \delta(\mathbf{Q} - \mathbf{q} - \mathbf{G}) \right. \\ &\quad \left. + \langle n(\mathbf{q}) \rangle \delta(\omega + \omega(\mathbf{q})) \delta(\mathbf{Q} + \mathbf{q} - \mathbf{G}) \right) \end{aligned} \quad (\text{D.3.7})$$

for magnetization in the z -direction. In fact, in the linear approximation there is only the elastic zero-magnon term and the one-magnon term.

In the Heisenberg model, spins are assumed to have constant length. The excitations of the ferromagnetic ground-state are thus transversal reorientations, with the physical picture of a spin wave corresponding to the precession of the spins around a cone, centered about the direction of magnetization, and proceeding as one goes along \mathbf{q} . The fixed length of the spins is in reality typically obeyed to a good approximation, so that there are no measurable longitudinal excitations (there are exceptions, however, when the system is undecided about the preferred value of the spin). As a consequence, a ferromagnet has just one magnon branch, because there is just one complex-valued degree of freedom per atom, the amplitude and phase of the precession around the magnetization as sketched above.

The magneto-crystalline anisotropy term due to spin-orbit coupling gives non-vanishing restoring forces also in the limit of $\mathbf{q} \rightarrow \mathbf{0}$, which results in the *anisotropy gap*, that is, $\omega(\mathbf{q})$ does not go to zero for small \mathbf{q} , in contrast to the phonon case. Further, even in the absence of this effect the dispersion is quadratic around $\mathbf{q} = \mathbf{0}$, because the interaction energy increases only quadratically with small differences in the orientations of neighbouring spins according to Eq. (D.3.6), again different from the linear behaviour of phonons.

In an antiferromagnet, additionally optical magnon branches appear. However, the corresponding energies can be quite high, which also applies to the acoustic branch for \mathbf{q} towards the Brillouin zone boundary. With thermal and even more so with cold triple-axis spectrometers, too high energy transfers cannot be measured, as magnon dispersions are generally measured on the energy-loss side (low temperatures are needed for sharp dispersions, giving very small probabilities for energy-gain transitions due to the Bose-Einstein occupation numbers). Thus, the measurement of magnon dispersions over the whole Brillouin zone is the domain of hot triple-axis spectrometers, or even time-of-flight spectrometers at pulsed sources using undermoderated neutrons.

Different from phonons, magnon scattering, as always for magnetic scattering, sees magnetization components perpendicular to \mathbf{Q} . This explains the fact that the magnon intensity is highest if the magnetization is parallel to \mathbf{Q} according to the factor $(1 + Q_z^2/Q^2)$ in Eq. (D.3.7), as in this case the modulations are purely perpendicular according to the picture of the spin wave sketched above. This can also be used to distinguish magnon from phonon branches by studying the effect of rotating the sample magnetization with respect to \mathbf{Q} on the intensities.